Multi-Objective Building Energy Management Optimization with Model Predictive Control

Vom Fachbereich
Elektrotechnik und Informationstechnik
der Technischen Universität Darmstadt
zur Erlangung des akademischen Grades
eines Doktor-Ingenieurs (Dr.-Ing.)
genehmigte Dissertation

von

M. Sc. Thomas Schmitt

geboren am 04. Juni 1991 in Frankfurt am Main

Referent:	Prof. Dr.-Ing. J. Adamy
Korreferent:	Prof. Dr. rer. nat. B. Sendhoff
Tag der Einreichung:	31. Januar 2022
Tag der mündlichen Prüfung:	23. Mai 2022

D17
Darmstadt 2022

Schmitt, Thomas: Multi-Objective Building Energy Management Optimization with Model Predictive Control
Darmstadt, Technische Universität Darmstadt
Jahr der Veröffentlichung auf TUprints: 2022
URN: urn:nbn:de:tuda-tuprints-223443
Tag der mündlichen Prüfung: 23.05.2022

Veröffentlicht unter CC BY-NC-ND 4.0 International
https://creativecommons.org/licenses/by-nc-nd/4.0/

Danksagung

Die vorliegende Dissertation entstand während meiner Zeit als wissenschaftlicher Mitarbeiter am Fachgebiet für Regelungsmethoden und Robotik (RMR) der Technischen Universität Darmstadt von 2018 bis 2022.

Zunächst möchte ich Prof. Dr.-Ing. Adamy für die Möglichkeit zur Promotion am RMR danken. Ich konnte mich von dem Moment, in dem er mir per Handschlag das Angebot dazu machte, bis zur Disputation selbst stets auf seine Unterstützung verlassen. Gleichzeitig hatte ich bezüglich meiner Forschung alle Freiheiten, die ich mir wünschen konnte. Des Weiteren bedanke ich mich bei Prof. Sendhoff für die Übernahme des Korreferats, hilfreiche Diskussionen und natürlich die Drittmittelfinanzierung durch das Honda Research Institute Europe GmbH.

Ein besonderer Dank gilt meinem Betreuer Dr. Tobias Rodemann für die vielen anregenden Diskussionen, die eingeräumte (und eingeforderte) Selbstständigkeit und die wertvollen Erkenntnisse, wie man sich durch die politischen Landschaften in der Wissenschaft navigiert. Mein Dank gilt ebenfalls Dr. Malte Probst für seine Rolle als Advisor und die wertvollen Hinweise in den halbjährlichen Meetings.

Während meiner Promotionszeit am Fachgebiet gab es – wie üblich – einige Rückschläge und Momente, in denen man kurzfristig das gesamte Unterfangen hinterfragt. Glücklicherweise gab es jedoch noch mehr positive Erlebnisse; von Kaffeerunden und angeregten Diskussionen bis zu den ausgelassenen Sommerfesten und Weihnachtsfeiern. Dafür und für alle weitere Unterstützung bedanke ich mich bei meinen ehemaligen Kollegen. Hervorzuheben sind Birgit Heid und Susanne Muntermann im Sekretariat, Jan Zimmermann für die vielen fachlichen Diskussionen als mein langzeitiger Büronachbar (bis ich für einen höhenverstellbaren Schreibtisch eingetauscht wurde), Dr.-Ing. Yury Furletov (unter anderem für die langen gemeinsamen Reparaturen meines geliebten 2002er Opel Astra) und Karsten Kreutz. Florian Meiners und Nikolas Hohmann danke ich besonders für das Korrekturlesen dieser Dissertation.

Außerdem danke ich meinen Studenten, insbesondere Jens Engel und Matthias Hoffmann, deren Arbeiten ein wertvoller Beitrag zum Gelingen dieser Dissertation waren. Zusammen mit ihnen hatte ich zumindest zeitweise meine eigene kleine Forschungsgruppe, die in der intensiven Entwicklung unseres Frameworks PARODIS ihren Höhepunkt hatte. Ich hoffe, dass sie in ihren eigenen Promotionen ebenso Erfolg haben.

Mein größter Dank gilt meiner Familie. Meine Eltern Mladenka und Bernd haben mir nicht nur alle Voraussetzungen gegeben, dieses Ziel zu erreichen, sondern mich mein gesamtes Leben unterstützt und an mich geglaubt. Ich danke meinem Bruder Andreas dafür, dass er mir regelmäßig den Rücken freigehalten hat, sodass ich mich auf mein Studium und meine Promotion konzentrieren konnte. Ich danke meiner Partnerin Ira für die fortwährende Unterstützung und Ablenkung, mit der sie sichergestellt hat, dass ich mich nicht in meiner Dissertation verliere. Außerdem danke ich ihrem Vater Juri, der mir in den letzten Jahren ein sehr enger Freund wurde, mir in vielfältigster Weise geholfen hat und den ich immer um Rat fragen konnte.

Frankfurt, September 2022 Thomas Schmitt

Contents

Abbreviations and Symbols **VII**

Abstract **XV**

1 Introduction **1**
1.1 Motivation 1
1.2 Contributions 4
1.3 Outline of this Thesis 6

2 Building Energy Management with Single-Objective MPC **9**
2.1 Introduction 10
2.2 Related Work 11
2.2.1 Model Predictive Control (MPC) 11
2.2.2 Microgrid Control 14
2.3 Modeling 16
2.3.1 State Space Descriptions 16
2.3.2 Objectives 24
2.3.3 Problem Formulations 31
2.4 Simulation Studies 36
2.4.1 Simulation Data 36
2.4.2 MPC Framework PARODIS 38
2.4.3 Comparison to State-of-the-Art Control 42
2.4.4 Hierarchical Control of Temperature Zones 45
2.4.5 Electric Vehicle Charging 50
2.5 Summary 55

3 Importance of Forecasting Accuracy **57**
3.1 Introduction 57
3.2 Related Work 58
3.3 Simulation Study 60
3.3.1 MPC Formulation 60
3.3.2 Data Sources and Handling 61

3.3.3 Results . . . 64
3.3.4 Conclusion . . . 69
3.4 Summary . . . 70

4 Dynamic Multi-Objective Optimization 71
4.1 Introduction . . . 71
4.2 Related Work . . . 74
4.2.1 Multi-Objective Optimization . . . 74
4.2.2 A Posteriori Decision Making Strategies . . . 81
4.2.3 Multiple Objectives in MPC . . . 84
4.3 Pareto Front Determination . . . 86
4.4 Automatized Metric-Based Decision Making . . . 89
4.4.1 Normalizations . . . 89
4.4.2 Metrics . . . 90
4.5 Automatized Preference-Based Decision Making . . . 92
4.5.1 Knee Region Determination . . . 92
4.5.2 Choosing a Solution . . . 94
4.5.3 Discussion of the Preference for Knee Points . . . 95
4.6 Summary . . . 97

5 Building Energy Management with Multi-Objective MPC 99
5.1 Introduction . . . 99
5.2 Related Work . . . 100
5.3 Simulation Studies . . . 102
5.3.1 Pareto Functionalities in PARODIS . . . 102
5.3.2 Fixed Metrics . . . 104
5.3.3 Preference-Based Knee Region Approach . . . 112
5.4 Summary . . . 122

6 Conclusions 123
6.1 Summary . . . 123
6.2 Future Directions . . . 125

A Appendix: Numerical Results from Simulation Studies 127
A.1 Electric Vehicle Charging, Section 2.4.5 . . . 127
A.2 Metric-Based Decision Making, Section 5.3.2 . . . 128
A.3 Preference-Based Decision Making, Section 5.3.3 . . . 129

List of Own Publications 131

Bibliography 133

Abbreviations and Symbols

Abbreviations

AEP	Angle to the extreme points
ATN	Angle to the neighbor points
AWDS	Adaptive weight determination scheme
BEM	Building energy management
BPS	Building performance software
CHIM	Convex hull of individual minima
CHP	Combined heat and power plant
CI	Carbon intensity
CUP	Closest to Utopia point
DER	Distributed energy resource
DM	Decision maker
EMPC	Economic Model Predictive Control
ESS	Energy storage system
EV	Electric vehicle
FPBI	Focus point boundary intersection
HL	Higher level
HVAC	Heating, ventilation, and air conditioning
LL	Lower level
LP	Linear programming
MILP	Mixed-integer linear programming
MINLP	Mixed-integer nonlinear programming
MOO	Multi-objective optimization
MPC	Model Predictive Control
NBI	Normal boundary intersection
NLP	Nonlinear programming
OCP	Optimal control problem
ODE	Ordinary differential (or difference) equation
PV	Photovoltaic
QP	Quadratic programming
RBC	Rule-based control
RES	Renewable energy source
TES	Thermal energy storage

Symbols

Notation

y	Scalar or vector
y_i	For a vector it is its i-th entry. For scalars and functions, the index is only descriptive.
y^i	For a vector, it denotes a specific point, e. g. from a set of points. Otherwise, the superscript is only descriptive.
$\boldsymbol{y}$	Sequence of a vector y throughout the prediction horizon
$y(n\|k)$	Predicted value for $y(k+n)$ at time step k
$\boldsymbol{I}_{n_1 \times n_2}$	Identity matrix with dimensions $n_1 \times n_2$
$\mathbf{0}_{n_1 \times n_2}$	Matrix consisting of only zeroes with dimensions $n_1 \times n_2$
$\mathbf{1}_{n_1 \times n_2}$	Matrix consisting of only ones with dimensions $n_1 \times n_2$
$\bigwedge_{i=1}^{q} y^i$	Cross product of vectors $y^1, \ldots, y^q$
$\vec{e}^i$	i-th unit vector, e. g. $\vec{e}^1 = \big(1,\ 0,\ \cdots,\ 0\big)$
$i \in [1, q]$	For an integer i (e. g. an index), the interval $[1,\ q]$ refers to the interval of integers, i. e. $i \in [1,\ q] \mathrel{\widehat{=}} i \in \{1, ..., q\}$

Latin Uppercase Letters

A_{PV}	Surface area of PV plant in m^2
A	System matrix of linear state space model
B	Input matrix of linear state space model
C_{bat}	Capacity of stationary battery in kWh
C_{EV}	Accumulated capacity of all EVs in kWh
$C_{\mathrm{EV,arr}}$	Accumulated arriving EV capacity in kWh
$C_{\mathrm{EV,dep}}$	Accumulated departing EV capacity in kWh
$C_{\mathrm{EV},i}$	Capacity of EV at charging station i in kWh
$C_{\mathrm{EV,arr},i}$	Capacity of arriving EV at charging station i in kWh
$C_{\mathrm{EV,dep},i}$	Capacity of departing EV at charging station i in kWh
C_{th}	Thermal capacity of the building in $^{\mathrm{kWh}}/_{\mathrm{K}}$
$C_{\mathrm{th},i}$	Thermal capacity of the building temperature zone i in $^{\mathrm{kWh}}/_{\mathrm{K}}$
$\mathcal{D}$	Distance plane in preference-based decision making approach

E	Energy stored in stationary battery in kWh
E_{EV}	Accumulated energy of all EVs in kWh
$E_{\mathrm{EV,arr}}$	Accumulated arriving EV energy in kWh
$E_{\mathrm{EV,dep}}$	Accumulated departing EV energy in kWh
$E_{\mathrm{EV},i}$	Energy of EV at charging station i in kWh
$E_{\mathrm{EV,arr},i}$	Energy of arriving EV at charging station i in kWh
$E_{\mathrm{EV,dep},i}(k)$	Energy of departing EV at charging station i in kWh
$E_{\mathrm{EV,des},i}$	Desired energy from EV at charging station i in kWh
H_{air}	Heat transfer coefficient to the outside air in $^{\mathrm{kW}}/_{\mathrm{K}}$
$H_{\mathrm{air},i}$	Heat transfer coefficient of the building temperature zone i to the outside air in $^{\mathrm{kW}}/_{\mathrm{K}}$
I_{sol}	Solar irradiance in $\frac{\mathrm{kW}}{\mathrm{m}^2}$
$J(\cdot)$	(Vector of) objective function(s)
$\tilde{J}$	Normed objective vector
$\tilde{J}^{\mathrm{b}}$	Base point for knee region
$J^{\mathrm{extreme},i}$	i-th extreme point on Pareto front
$\tilde{J}^{\mathrm{focus}}$	(Normed) focus point in FPBI
J^{nadir}	Nadir point
J^{utopia}	Utopia point
${}^{\mathrm{d}}\tilde{J}$	Objective vector normed with dynamic normalization scheme
${}^{\mathrm{f}}\tilde{J}$	Objective vector normed with fixed normalization scheme
ΔJ_i	Width of Pareto front for i-th objective
$\mathbb{J}$	Set of Pareto solutions
$\tilde{\mathbb{J}}$	Set of normed Pareto solutions
$\bar{\mathbb{J}}$	Set of normed Pareto solutions which are part of the knee region
N_{pred}	Length of the prediction horizon
$\mathcal{O}(k)$	Optimal control problem at time step k
$P_{\mathrm{bat,max}}$	Maximum charging power for stationary battery in kW
P_{charge}	Electrical charging power for stationary battery in kW

P_{chp}	Electrical power from CHP in kW
$P_{\text{chp,max}}$	Maximum electrical power from CHP in kW
P_{dem}	Electrical power demand from building in kW (must be met)
P_{EV}	Accumulated (dis-)charging power for all EVs in kW
$P_{\text{EV},i}$	(Dis-)charging of EV at charging station i in kW
$P_{\text{EV,i,max}}$	Maximum possible (dis-)charging power for EV i
$P_{\text{EV,max}}$	Maximum possible accumulated (dis-)charging power for all EVs
P_{grid}	Electrical power bought from or sold to grid in kW
$P_{\text{grid,max}}$	Maximum electrical power bought from or sold to grid in kW
$P_{\text{grid,peak}}(k)$	Maximum peak for P_{grid} occurred until time step k
P_{pos}	Slack variable for reformulation of industry cost function
P_{ren}	Electrical power from RESs in kW
$\mathcal{P}$	Preference plane
$\dot{Q}_{\text{chp}}$	Heating power from CHP in kW
$\dot{Q}_{\text{cool}}$	Cooling power from air conditioning system in kW
$\dot{Q}_{\text{cool},i}$	Cooling power allocated to temperature zone i in kW
$\dot{Q}_{\text{cool,max}}$	Maximum cooling power from air conditioning system in kW
$\dot{Q}_{\text{heat},i}$	Heating power allocated to temperature zone i in kW
$\dot{Q}_{\text{rad}}$	Heating power from gas heating in kW
$\dot{Q}_{\text{tot}}$	Total heating power in kW
S	Disturbance matrix of linear state space model
ToA_i	Time of arrival of EV at charging station i
$\text{ToD}_{\text{est},i}$	Estimated time of departure of EV at charging station i
ToD_i	Time of departure of EV at charging station i
T_{s}	Sampling time (step size) in h
$\text{T}_{\text{sojourn},i}$	Sojourn time of EV at charging station i
$\mathbb{U}$	Set to which inputs u are constrained, i. e. $u \in \mathbb{U}$
$V_{\text{f}}(\cdot)$	Terminal cost function
$\mathbb{X}$	Set to which states x are constrained, i. e. $x \in \mathbb{X}$

$\mathbb{X}_\mathrm{f}$	Set to which final states are constrained, i. e. $x(N_\mathrm{pred}\|k) \in \mathbb{X}_\mathrm{f}$

Latin Lowercase Letters

c_cur	Current constant CHP, $P_\mathrm{chp} = c_\mathrm{cur} \cdot \dot{Q}_\mathrm{chp}$
c_grid	Electricity costs from grid in $\frac{€}{\mathrm{kWh}}$
d	Disturbance vector
$d_\mathrm{cup}(\cdot)$	CUP metric
$d_{\mathrm{EV},i}\ (k)$	Departure indication function for charging station i
${}^\mathrm{F}d^i$	i-th direction vector in FPBI
${}^\mathrm{F}\hat{d}^i$	i-th auxiliary direction vector in FPBI
Δd^awds	Distance threshold in AWDS
e_avg	Average prediction error for P_ren in kW
$f(x(k),u(k))$	Dynamic function for nonlinear system
$g(\cdot)$	Inequality constraints function
$h(\cdot)$	Equality constraints function
$\ell(\cdot)$	Stage cost function
$m_\mathrm{EV,i}$	Binary variable indicating if an EV is available at charging station i
$\hat{n}$	Normal vector of CHIM in NBI
n^f	Search direction in FPBI
p	Preference vector for preference-based decision making approach
p_bat	Preference value battery costs
p_comf	Preference value comfort costs
p_mon	Preference value monetary costs
q	Number of objectives in MOO problem

${}^{\mathrm{F}}r$	Resolution for each direction in FPBI
r_{lim}	Design parameter in preference-based decision making approach controlling the influence of the DM's preferences
s_{err}	Error scale for PV prediction
s_{EV}	Slack variable for lower level in hierarchical control of EVs
s_{P1}, s_{P2}	Slack variables for reformulation of peak costs
Δs	Step size vector in FPBI
t_0	Time step at the beginning of a prediction horizon
u	Input vector
w	Weight vector
w_{bat}	Optimization weight for battery costs
w_{comf}	Optimization weight for comfort costs
w_{mon}	Optimization weight for monetary costs
w_{slack}	Punishment weight for slack variables
x	State vector
z	Decision variable vector

Greek Letters

$\alpha_{\mathrm{AEP}}(\cdot)$	AEP metric
$\alpha_{\mathrm{ATN}}(\cdot)$	ATN metric
β_{ij}	Heat transfer coefficient between temperature zones i and j
β^{NBI}	Vector for CHIM construction in NBI
β_{PV}	Constant for influence of operating temperature of PV plant
${}^{\mathcal{D}}\delta(\cdot)$	Distance to distance plane
ε_{c}	Energy efficiency ratio for the cooling machine

η_{PV}	Reference efficiency of PV plant
ϑ_{air}	Air temperature in °C
ϑ_{b}	Building temperature in °C
$\vartheta_{\mathrm{b},i}$	Temperature of building temperature zone i in °C
$\vartheta_{\mathrm{b,min}}$, $\vartheta_{\mathrm{b,max}}$	Lower and upper limit for building temperature in °C
ϑ_{set}	Desired set point temperature in °C
Φ	Matrix of direction vectors of CHIM in NBI

Abstract

Today's goals for the reduction of CO_2 emissions are significantly impacting both the civil and the industrial sector. The increasing share of renewable energy sources leads to more volatile and challenging conditions for power consumption. The building sector is responsible for approximately a third of both CO_2 emissions and energy consumption in Germany. At the same time, it offers the potential to adapt to the changing conditions by the intelligent use of energy storage systems. These can, e. g., be stationary batteries, electric vehicles at charging stations, heat tanks or the building itself. The control system for the power flow between these elements is called a building energy management (BEM) system. As the control strategy, Model Predictive Control (MPC) is an obvious choice. It allows optimal control while incorporating forecasts of, e. g., power demand, renewable energy production and air temperature.

However, in a complex control setting such as BEM, multiple contradicting objectives are to be minimized. For example, next to the reduction of monetary costs, the building's temperature is supposed to be kept at a comfortable level, electric vehicles have to be charged sufficiently, battery degradation should be kept low and CO_2 emissions have to be reduced. To directly optimize real-world objectives such as the examples given above, Economic Model Predictive Control (EMPC) can be utilized, in which the cost function for the optimal control problem (OCP) does not need to be quadratic, but can be of arbitrary form. However, if multiple objectives have to be respected, usually this is done in form of a weighted sum. Thereby, the weights are chosen either from experience or such that all objectives are of the same magnitude. While this is a reasonably simple approach, it neglects that, especially for BEM systems, the OCP varies significantly with the volatile outer conditions. Therefore, the trade-off which is chosen by the fixed weights varies over time, too.

The simultaneous optimization of contradicting objectives is called multi-objective optimization (MOO). Usually, the set of all 'optimal' solutions is approximated and a (human) decision maker (DM) afterwards selects

a solution which represents his preferences the most. This is appropriate in the case of one-time optimizations, which is usually the case in MOO. However, we want to use MOO for the permanent control of a BEM system.

Therefore, we propose an extended conceptualization of *dynamic MOO*, which is the systematic combination of MPC and MOO. At every time step, a multi-objective OCP is formulated and an approximation of the Pareto front is derived as its solution, i. e. the set of all optimal compromises. Then, a solution is automatically chosen. To this end, we present two different options. In the *metric-based automatized decision making* strategy, the Pareto front is first normalized. Then, a metric is calculated for every solution and the solution with the best value is chosen. We present two normalization schemes and three metrics a DM can choose from. In the *preference-based automatized decision making* strategy, preferences formulated by the DM a priori are utilized. First, a knee region is determined from the normalized Pareto front to exclude solutions which are too extreme. Then, the preferences are used to construct a hyperplane with which a solution from the knee region is finally selected.

The applicability of the proposed methods to the BEM problem is shown in long-term simulations. To this end, we show how the most important elements in a BEM system can be modeled while obtaining well-solvable convex optimization problems. Furthermore, we present a new method to determine an approximation of the Pareto front which is more apt for the case of dynamic MOO and its varying conditions.

Kurzfassung

Die heutigen Ziele zur Reduzierung von CO_2 beeinflussen bereits sowohl den privaten als auch den industriellen Energieverbraucher spürbar. Der steigende Anteil an erneuerbaren Energien in der Stromerzeugung führt zu volatileren und herausfordernden Bedingungen in der Stromnutzung. Der Gebäudesektor ist dabei verantwortlich für jeweils ca. ein Drittel des Stromverbrauchs und der Erzeugung von CO_2-Emissionen in Deutschland. Gleichzeitig verfügt er über das Potenzial, sich den sich ändernden Bedingungen durch die intelligente Nutzung von Energiespeichersystemen anzupassen. Dies können zum Beispiel stationäre Batterien, Elektroautos an Ladestationen, Wärmespeicher oder auch das Gebäude selbst sein. Zur Regelung der Leistungsflüsse zwischen diesen Elementen dient ein Gebäudeenergiemanagementsystem. Dabei ist die modellprädiktive Regelung (MPC) als Regelungsmethode eine naheliegende Wahl, da sie eine optimale Regelung unter der Berücksichtigung von Vorhersagen für zum Beispiel den Energieverbrauch, die Energieerzeugung durch erneuerbare Energien und der Lufttemperatur erlaubt.

In einem komplexen System wie dem Gebäudeenergiemanagement müssen jedoch mehrere, sich widersprechende Kriterien gleichzeitig optimiert werden. Dies sind zum Beispiel die Minimierung der monetären Kosten, die Regulierung der Gebäudetemperatur, das ausreichende Laden von Elektroautos, die Minimierung der Batteriealterung und die Reduzierung von CO_2-Emissionen. Mit einer ökonomischen MPC können solche Kriterien direkt optimiert werden, da die Gütefunktion für das Optimalsteuerungsproblem nicht der üblichen quadratischen Struktur entsprechen muss, sondern von beliebiger Form sein darf. Wenn wie im vorliegenden Fall mehrere Kriterien berücksichtigt werden müssen, geschieht dies üblicherweise in Form einer gewichteten Summe. Die Gewichte werden dabei entweder aus Erfahrung gewählt oder so, dass alle Kriterien in der gleichen Größenordnung liegen. Dieser Ansatz ist zwar vergleichsweise einfach umsetzbar, vernachlässigt jedoch, dass insbesondere bei Gebäudeenergiemanagementsystemen die äußeren Bedingungen volatil sind und

sich damit die Optimalsteuerungsprobleme über die Zeit signifikant ändern. Daher variiert auch der Kompromiss zwischen den Kriterien, der durch die festen Gewichte ausgewählt wird.

Die gleichzeitige Optimierung mehrerer, sich widersprechender Kriterien nennt man multikriterielle Optimierung. Für gewöhnlich wird dabei die Menge aller "optimaler" Lösungen approximiert und einem (menschlichen) Entscheider präsentiert, der daraus die Lösung auswählt, die seinen Präferenzen am besten entspricht. Dieser Vorgang ist gut geeignet für einmalige Optimierungen, wie sie in der multikriteriellen Optimierung üblich sind. Im vorliegenden Fall soll die multikriterielle Optimierung jedoch für die permanente Regelung eines Gebäudeenergiemanagementsystems verwendet werden.

Daher wird in dieser Arbeit ein erweitertes Konzept der *dynamischen multikriteriellen Optimierung* präsentiert, das MPC und multikriterielle Optimierung systematisch kombiniert. Dazu wird in jedem Zeitschritt ein multikriterielles Optimalsteuerungsproblem aufgestellt und eine Approximation der Pareto-Front, d. h. die Menge aller optimalen Kompromisse, als Lösung bestimmt. Von dieser wird im Anschluss automatisiert eine einzelne Lösung ausgewählt. Dazu werden zwei Möglichkeiten vorgestellt. Bei der *metrikbasierten Entscheidungsfindungsstrategie* wird die Pareto-Front zunächst normalisiert. Daraufhin wird jede Lösung hinsichtlich einer Metrik bewertet und die beste ausgewählt. Dazu stehen zwei Normalisierungsmethoden und drei Metriken zur Verfügung. In der *präferenzbasierten Entscheidungsfindungsstrategie* werden zuvor formulierte Präferenzen eines Entscheiders verwendet. Dazu wird zuerst aus der ebenfalls normalisierten Pareto-Front eine Region von Kniepunkten bestimmt, die zu extreme Lösungen ausschließt. Dann wird mit Hilfe der Präferenzen eine Hyperebene konstruiert, mit der die finale Lösung aus der zuerst bestimmten Region an Kniepunkten ausgewählt wird.

Die Eignung der vorgeschlagenen Methoden für die Regelung eines Gebäudeenergiemangementsystems wird durch Langzeitsimulationen gezeigt. Dazu wird erläutert, wie dessen wichtigste Elemente so modelliert werden können, dass gleichzeitig gut lösbare konvexe Optimierunsprobleme entstehen. Des weiteren wird eine neue Methode zur Bestimmung einer Approximation der Pareto-Front vorgestellt, die für den Fall der dynamischen multikriteriellen Optimierung und den damit einhergehenden volatilen Bedingungen besser geeignet ist.

1 Introduction

This introductory chapter starts with the motivation of this dissertation. Then, the scientific contributions are summarized. Lastly, the structure and outline of this thesis is presented.

1.1 Motivation

Politicians and governments all over the world declared the reduction of CO_2 emissions one of their highest priorities. The resulting energy policies have a huge impact on both the industrial and civil sector, and changes will be necessary on the production as well as the consumption side. The increasing share of renewable energy sources (RESs) leads to a more volatile energy production. In Germany, RESs have already been responsible for 42.1 % of the gross electricity consumption in 2019 and their share is supposed to reach 65 % by 2030 and 80 % by 2050. At the same time, the German government's official goal is to increase the total number of electric vehicles (EVs) to 7 to 10 million until 2030 [20].[1] However, a recent report from a national committee already proposes the need of 14 million EVs until 2030 to meet aggravated EU climate goals [101]. These changes go along with a necessary decentralization of the power grid. The building sector, which was responsible for 35 % of the energy consumption and 33 % of CO_2 emissions in 2015 in Germany and is supposed to be '*nearly climate neutral*' until 2050 [21], thereby has a significant role. While the conditions for energy usage become more challenging, as e. g. the increase in peak costs in Figure 1.1 shows, buildings also have the potential for more intelligent energy usage. For example, the increasing usage of EVs is not only a stress factor for the power grid, but charging stations connected

[1] In August 2021, there have been approximately 500,000 (purely) electric vehicles in Germany, according to the German *Bundesministerium für Wirtschaft und Energie*, `https://www.bmwi.de/Redaktion/DE/Pressemitteilungen/2021/08/20210802-erstmals-rollen-eine-million-elektrofahrzeuge-auf-deutschen%2Dstrassen.html`, accessed on 22.11.2021.

to buildings also represent an opportunity of load shifting through the EVs' large batteries. The thermal capacity of a building can be used as a passive storage without additional, monetary investments. Furthermore, especially larger buildings or compounds of buildings can be enhanced by further (active) storages such as heat tanks or stationary batteries, as well as producers such as combined heat and power plants (CHPs) or their own RESs, e. g. photovoltaic (PV) systems. As an alternative to industry electricity, companies (and in the future possibly also private consumers) could also participate in the electricity intraday market with its highly fluctuating but, on average, lower energy prices. Note that this combination of producers, storages and consumers in buildings fulfill all requirements for a microgrid, i. e. there is no significant difference from the control perspective. If the energy flows in a building are controlled, the responsible control system is called a building energy management (BEM) system. However, most of a BEM system's elements are subject to volatile conditions, which make an intelligent control necessary that appropriately reacts to the changing environment. This makes Model Predictive Control (MPC) a perfect candidate.

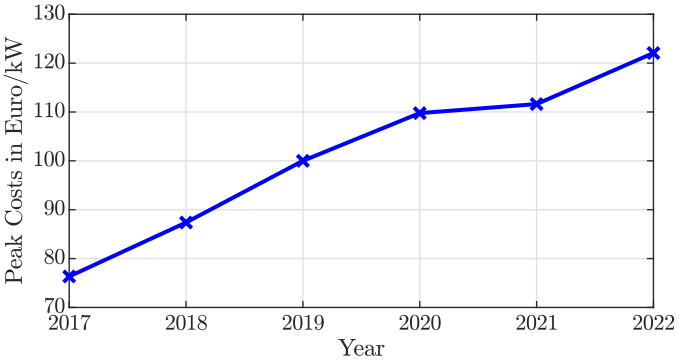

Figure 1.1: Exemplary progress of German peak costs. In Germany, industry electricity clients receive significantly lower prices per kWh electricity compared to private consumers, but have to pay peak costs (also called demand charges) in addition. At the end of the year, the highest power peak averaged over fixed 15 min intervals is punished with a high factor. For the exemplary medium-sized company building considered in this thesis, it increased from $76.34 \frac{€}{kW}$ in 2017 to $122.07 \frac{€}{kW}$ in 2022, i. e. by 59.90 % in 5 years.

The basic idea of MPC is very straightforward. Given a discrete dynamic system at time t_0, an optimal control problem over a prediction horizon

$[t_0, t_0 + N_{\text{pred}} - 1]$ is formulated at every time step. However, only the first time step of the optimal input trajectory is applied. Then, at $t = t_0 + 1$ the optimal control problem is repeated over $[t_0 + 1, t_0 + N_{\text{pred}}]$. Using economic MPC, an arbitrary cost function can be used in the optimization problem. This is more appropriate for BEM because the objectives to be optimized can be formulated better in terms of real-world elements than by quadratic expressions of the states and input variables. For example, the most obvious objective is the reduction of monetary costs, which is often (but not necessarily, e. g. in case of peak costs) a linear expression of the decision variables. A second relevant objective can be the building temperature, which can be beneficial as a passive storage as mentioned before, since heating, ventilation, and air conditioning (HVAC) systems are huge energy consumers. Further relevant objectives exist, such as CO_2 emissions and the degradation of battery systems, both stationary or from EVs. Note that this is a very important topic, since current hopes on the German energy transition base heavily on the use of (lithium-ion) batteries, while the understanding of their degradation is an active field of research and resources in their production have a significant environmental impact [4, 95].

While the exemplary objectives stated above are all relevant, they cannot directly be compared to each other, as they have different units, magnitudes and meanings. Thus, only an 'optimal' compromise between the objectives can be achieved. The field of simultaneous optimization of such contradicting objectives or criteria is called multi-objective optimization (MOO).[2] Thereby, a (human) decision maker (DM) is supported in deriving and choosing a so-called *Pareto optimal* solution. However, in the control context, the MOO problem has to be solved at every time step – instead of only once, which is the usual case in MOO. Furthermore, due to the varying conditions of a BEM system, a once formulated preference of a DM might not result in the same type of compromise at different times. Thus, the optimal control problem has to be addressed *dynamically*. While the literature on both MPC and MOO is rich, the combination of both has not been given sufficient attention. This dissertation is aiming at closing this gap.

[2] Note that if more than 3 objectives are considered, usually the term *many-objective* optimization is used. While most methods developed in this thesis are applicable to an arbitrary number of objectives, we apply them only to 2 or 3 objectives in simulation. Thus, we use the term multi-objective optimization throughout this thesis.

1.2 Contributions

The main contribution of this thesis is the systematic combination of MOO and MPC, which we refer to as *dynamic MOO*.[3] The basic principle is to formulate the optimal control problem (OCP) at every time step as a multi-objective optimization problem, determine the Pareto front, and then automatically choose a solution. The *methodological contributions* are the

- development of efficient linear models for BEM systems (or microgrids in general), e. g. by reformulation of nonlinear cost terms, resulting in convex optimization problems which can be solved reliably and fast enough for MOO purposes,
- presentation of a new method to sample the Pareto front which overcomes problems of state-of-the-art methods in the dynamic setting, and
- presentation of two general strategies for the automatized decision making process,
  1) by first normalizing the Pareto front approximation and then choosing the solution which optimizes a fixed metric. Hereby, a new so-called fixed normalization scheme is presented, which tackles the problem that nonlinear cost terms and varying conditions can lead to severe differences in the extremes of the Pareto front.
  2) As the core contribution of this thesis, a new approach to incorporate preferences of a DM by a geometric interpretation in the objective space is presented, which allows for easy formulation of preferences while at the same time ensuring that no unreasonable solutions are selected. It has further advantages, such as that the impact of the DM's preferences can be varied a-priori, but additionally depends on the landscape of possible solutions. Furthermore, so-called knee points, which are considered the most desirable solutions, are inherently preferred.

[3] Note that in literature, the term 'dynamic MOO' is usually used for MOOs which are slightly changing over time. This characteristic is then utilized in the optimization and determination of the Pareto front with evolutionary strategies. However, our usage differs in that the changes in the MOO problem derive from the use of MPC and we extend the concept by the additional decision making step.

A big challenge in dynamic MOO is that the chosen solution represents only the costs for one time step – and even not quite so, because the costs shown in the Pareto front are those for the entire prediction horizon, but only the first step of the horizon is applied, as usual for MPC. Moreover, the decision made now can affect the conditions and thus options in the future, which cannot be modeled in a straightforward way. However, only the accumulated long-term costs are relevant for the DM. Thus, long-term simulations have to be conducted to show empirically the efficacy of any dynamic MOO approach. For all simulations in this thesis, we use the model of a medium-sized office building with real-world measurement data. The *empirical contributions* for the dynamic MOO are the

- analysis of the two dynamic MOO strategies and their long-term effects, showing that
  1) the first strategy with its different normalization schemes and fixed metrics results in overall good costs and compromises, but it is difficult to know a priori which combination will favor which objectives;
  2) this problem is overcome by the second approach, which shows that not only the overall results are good, but the DM's preferences are properly represented in the long-term costs as well.

Independently of the consideration of multiple objectives, a lack in current literature of BEM or microgrid control is the analysis of how prediction errors affect the cost outcome. Thus, further empirical contributions specific to the energy management problem are the

- use of real-world solar irradiance forecasts from weather services to empirically analyze the relationship between forecast accuracy and cost savings,
- thereby showing that regular forecasts can successfully be used to shave electricity peaks in a MPC setting and
- that despite a one-day horizon, prediction accuracy for RES production is only relevant in the short-term for the example building considered here.

1.3 Outline of this Thesis

This thesis starts with single-objective BEM and subsequently builds on that to finish with the multi-objective control of the medium-sized company building which serves as our example. Thereby, instead of a general 'state of the art' chapter at the beginning, every chapter has its own literature review. Furthermore, every chapter ends with simulation studies (except for the purely methodological Chapter 4) and a short summary.

Chapter 2 presents a single-objective MPC approach to the building energy management problem. It starts with the problem description and elaborates on the key challenges. We continue with a review of current single-objective MPC approaches and then build the foundation for our own approach, i. e., we present models with different degrees of detail and complexity and show how the objectives to be minimized can be reformulated as well solvable convex optimization problems. Multiple simulation studies show the applicability of our approach, its superiority over non-predictive control schemes and the possibility of hierarchization to reduce computational burdens.

In Chapter 3, we analyze the influence of forecasting errors. We use real-world weather forecasts of solar irradiance to calculate photovoltaic power output predictions. By adjusting the prediction error, we show in simulation that current weather forecasts can successfully be used to reduce peak costs. However, significant additional savings are possible if the prediction accuracy is increased within the first couple of hours.

In Chapter 4, we first introduce the basics of MOO and give an overview of how multiple objectives have been treated in MPC so far. Then, we build the methodological foundations for our main contribution, the dynamic MOO. We present different ways to construct an approximation of the Pareto front with deterministic scalarization methods, among them the focus point boundary intersection (FPBI) method, a new approach more suitable for the dynamic setting with varying conditions. Then, we present two different methods to automatize the compromise selection from the Pareto front. First, we propose different normalization schemes and metrics. Second, we present a new approach with which preferences from a decision maker can be incorporated while ensuring the restriction to reasonable areas of the Pareto front.

In Chapter 5, we apply both of these approaches to the building energy management problem, i. e. solving it with dynamic MOO. Multiple simula-

tion studies show their applicability and the different effects on the types of compromises which result in the long term.

We conclude in Chapter 6 with a short summary and remarks on possible future directions for both dynamic MOO in general and the control of building energy management systems.

2 Building Energy Management with Single-Objective MPC

In this chapter, we will define and solve the building energy management (BEM) problem with single-objective economic MPC. After a short introduction with the focus on existing challenges, we will review the current literature of MPC approaches. Then, we explain how a BEM system can be modeled adequately for the use of MPC. We present multiple simulation studies and finish with a summary.

This chapter is based on and has partly been published in the following publications:

[S1] T. Schmitt, J. Engel, T. Rodemann, and J. Adamy. Application of Pareto optimization in an economic model predictive controlled microgrid. In *2020 28th Mediterranean Conference on Control and Automation (MED)*, pages 868–874. IEEE, 2020.

[S3] T. Schmitt, T. Rodemann, and J. Adamy. Multi-objective model predictive control for microgrids. *at - Automatisierungstechnik*, 68(8):687 – 702, 2020.

[S4] T. Schmitt, J. Engel, M. Hoffmann, and T. Rodemann. PARODIS: One MPC framework to control them all. Almost. In *2021 IEEE Conference on Control Technology and Applications (CCTA)*, 2021.

[S9] J. Engel, T. Schmitt, T. Rodemann, and J. Adamy. Hierarchical economic model predictive control approach for a building energy management system with scenario-driven EV charging. *IEEE Transactions on Smart Grid*, 13(4):3082–3093, 2022.

Note that [S9] builds on the results of the Master's thesis [39].

2.1 Introduction

In the control context, instead of a *(building) energy management system*, the term *microgrid* is often used. Both phrases refer to an entity with energy producers, consumers and storages. The control task is to find suitable (if possible optimal) input trajectories for all actuators, i. e. satisfying demands and constraints while, usually, minimizing various costs. The microgrid under consideration can vary from a single residential home [29] to a large university campus consisting of multiple individual buildings and plants [116]. If all components are owned or controlled by a single shareholder, a centralized approach is usually employed, i. e. a single optimization (or optimal control) problem is formulated for the entire system. If multiple shareholders (or agents) with different interests share some part of the energy system, often decentralized approaches are necessary. Note that throughout this thesis, only the case of a single microgrid is considered. Therein, we sometimes model parts of the microgrid separately in more detail as a system of its own and control them in a hierarchical setup, which can also be referred to as a distributed system. However, this is not considered as a decentralized approach since there are no competing interests or limited information exchanges. Furthermore, we limit our control aspect to the secondary control level of a microgrid [108], i. e. the dispatch and unit commitment problem of producers and consumers, but not the primary control level, such as inverter output and frequency control. In this case, the energy management problem is also called *optimal dispatch control problem*.

The main challenges in microgrid control are

- modeling the microgrid appropriately, i. e. reproducing the physical behavior of all relevant parts with sufficient accuracy,
- formulating constraints and cost functions such that the resulting optimization problem is solvable (well enough), and
- finding a reasonable compromise between the objectives.

For the modeling of a microgrid, mainly two basic approaches exist. In the first, ordinary differential (or difference) equations (ODEs) are determined for all storage systems. Actuators and constraints are incorporated into these ODEs. Depending on the modeling complexity, this results in either linear or non-linear systems, often including binary variables to cover start-up/shut-down decisions. The second approach is to use higher modeling

languages or software such as Simulink, Modelica, EnergyPlus or other building performance software (BPS) tools. In this way, complex dependencies and rules can be modeled with little effort. However, this comes at the cost of limited insight into the model itself and an optimization problem that is in general harder to solve. A review of various BPS tools can be found in [100].

While MPC is a popular approach to generating control actions for a microgrid due to the possibility of respecting constraints on states and inputs and forecasts of demands and disturbances, several other methods exist. Not all of them are equally applicable to the two modeling approaches. Despite some heuristic approaches and artificial intelligence methods, an optimization problem in some form is formulated in most cases. Then, the two main options are deterministic or meta-heuristic optimization methods. Deterministic optimization methods include linear, quadratic, mixed integer and nonlinear programming methods. They might fail in case of harsh nonlinearities modeled in complex BPS models. In this case, meta-heuristic optimization methods including evolutionary strategies, genetic algorithms (GA), Particle Swarm Optimization and others are preferable. These are also the usual combinations: ODE modeling + deterministic optimizers or BPS-based modeling + meta-heuristic optimizers, which can also be described as simulation-based optimization. The MPC framework can be used in both cases.

2.2 Related Work

Both MPC and Microgrid control have experienced large attention in the research community in the last decade(s). Thus, we restrict ourselves to an introduction to the basics of MPC and a short survey of the different approaches to both modeling and the (optimal) dispatch control problem of centralized microgrids.

2.2.1 Model Predictive Control (MPC)

Notation In the following and throughout the rest of this thesis, sequences of scalars or vectors are typeset in bold, e. g. $\boldsymbol{u}(k) = [u(k), u(k+1), \dots, u(k+N_\mathrm{p}-1)]$. Furthermore, as is common in the context of control theory, x denotes the state vector and u the input vector.

In the context of MPC, a predicted value for $r(k+n)$ at time step k is denoted by $r(n|k)$.

The basic concept of MPC is simple. Considering a discrete dynamic system of the form

$$x(k+1) = f(x(k), u(k)), \tag{2.1}$$

the idea is to formulate an optimal control problem (OCP) over a prediction horizon N_{pred} at every time step k. Namely, the next N_{pred} steps of the input vector u are optimized. However, only the first optimized step $u(0|k)$ is applied to the system - then, the actually resulting state $x(k+1)$ is measured and the process is repeated. In reality, the real state $x(k+1)$ may deviate from the predicted state $x(1|k)$ due to various reasons such as modeling errors and unknown disturbances.

In regular (tracking) MPC, the objective function of the OCP usually has a quadratic form. If a set point of $x_{\text{set}} = \big(0, \ \dots \ , \ 0\big)$ is chosen, it would be

$$J^{\text{QR}}(x(k), u(k)) = \sum_{k=0}^{N_{\text{p}}-1} x(k)^{\intercal} Q x(k) + u(k)^{\intercal} R u(k) + V_{\text{f}}^{\text{QR}}(x(N_{\text{p}})), \tag{2.2}$$

where Q is positive semidefinite and R is positive definite. V_{f} is called the *terminal cost function*. It is optional and might be a quadratic expression, too. Stability can be ensured in different ways, e. g. by constraints on the terminal state $x(N_{\text{pred}})$ or by appropriate terminal costs. Since stability analysis is not part of this dissertation, the reader is referred to the standard literature for details, e. g. [28, 115].

An important extension of MPC is *economic* MPC (EMPC). The main difference is that, instead of only quadratic, the cost function can be of arbitrary form, resulting in

$$J(x(k), u(k)) = \sum_{k=0}^{N_{\text{p}}-1} \ell(x(k), u(k)) + V_{\text{f}}(x(N_{\text{p}})), \tag{2.3}$$

where $\ell(x(k), u(k))$ are the *stage costs*. The name economic MPC has its historical origin in the new opportunity to directly optimize economic costs, instead of following a trajectory from a real-time optimizer, and has first been introduced in [44] in 2010. Since then, EMPC has seen many developments, both on stability analysis [5, 6, 52, 114] and results on its

performance and feasibility [98, 99] as well as on further extensions, e. g. to robust or distributed MPC [11–13, 37, 97]. However, as discussed in [43], especially for (significant) disturbances acting on the system - which might even be beneficial, as is partially the case in this thesis - many problems regarding the stability and performance analysis remain open. Furthermore, for the dynamic models used in this thesis, constraints on the inputs are loose enough such that the OCP remains feasible and constraints on the states can be kept. Thus, no stability analyses are conducted and the reader is referred to the aforementioned literature for additional information.

The OCP formulated at each time step is defined by the objective function and its constraints, which include the system dynamics (2.1). Additionally, box constraints $x(k) \in \mathbb{X}$, $u(k) \in \mathbb{U}$ usually apply. However, any constraints of the form $g(x(k), u(k)) \leq 0$ and $h(x(k), u(k)) = 0$ are valid. The standard OCP at time step k can then be expressed as

$$\begin{aligned}
\mathcal{O}_{\mathrm{Eco}}(k)\colon \quad & \min_{\boldsymbol{u}} \sum_{n=0}^{N_\mathrm{p}-1} l(x(n|k), u(n|k)) + V_\mathrm{f}(N_\mathrm{pred}|k) && && \text{(2.4a)}\\
\text{s. t. } & x(n+1|k) = f(x(n|k), u(n|k)) && \forall\ n = 0, \dots, N_\mathrm{pred} - 1 && \text{(2.4b)}\\
& x(0|k) = x_0, && && \text{(2.4c)}\\
& x(n|k) \in \mathbb{X}, \quad u(n|k) \in \mathbb{U}, && \forall\ n = 0, \dots, N_\mathrm{pred} - 1 && \text{(2.4d)}\\
& g(x(n|k), u(n|k)) \leq 0, && \forall\ n = 0, \dots, N_\mathrm{pred} - 1 && \text{(2.4e)}\\
& h(x(n|k), u(n|k)) = 0, && \forall\ n = 0, \dots, N_\mathrm{pred} - 1 && \text{(2.4f)}\\
& x(N_\mathrm{pred}|k) \in \mathbb{X}_\mathrm{f}. && && \text{(2.4g)}
\end{aligned}$$

Note that, for the rest of the thesis, we omit the explicit predictive notation $r(n|k)$ for readability and only write $r(k+n)$ or $r(k)$ if there is no need to distinguish between them. Furthermore, $\mathbb{X}_\mathrm{f} = \mathbb{X}$ is assumed if not otherwise stated, such that a separate constraint (2.4g) is not necessary, but included instead by stating $k = 1, \dots, N_\mathrm{pred}$ (instead of $0, \dots, N_\mathrm{pred} - 1$). Namely, while $x(0|k)$ should always satisfy all constraints, the current state cannot be manipulated. Thus, state constraints for the time step k itself are unnecessary in the OCP, but may lead to implementation problems due to numerical boundaries. Lastly, we forego statements on the value of the initial state such as (2.4c) when formulating different control schemes.

In conclusion, the main advantage of MPC is its capability for optimal control with constraints on both states and inputs. Additionally, in EMPC, economic objectives can directly be optimized, which allows us to also

consider transient costs instead of only determining an optimal set point. A huge advantage for the purpose of this thesis is the possibility to include predictions of uncontrollable influences, too.

2.2.2 Microgrid Control

The aforementioned properties make EMPC a natural candidate for the control of microgrids. While many other approaches have been used, we limit the literature review in this section to (E)MPC approaches. Some approaches based on other methods, e. g. computational intelligence, are presented in Section 5.2 in the context of multi-objective microgrid control.

Different technical definitions of a microgrid exist, but most share the following prerequisites: A microgrid consists of producers (also called distributed energy resources (DERs)), consumers and storages (also called energy storage systems (ESSs)) and might be connected to the host power system, e. g. the public power grid [108]. If not, it is said to be in *islanded mode*.

The single entities of these producers, consumers and storages vary. Most commonly, the temperature of a building or single rooms and the corresponding HVAC systems are modeled and controlled due to the large energy consumption for both heating and cooling [26, 27, 29, 61, 82–84, 103, 105, 110, 119, 122, 124, 133, 142, 146, 153]. In this way, the thermal capacity can be utilized as a storage or buffer, which is also referred to as a *passive* thermal energy storage (TES). Furthermore, water tanks can be used as *active* TES for both heating and cooling [29, 65, 110, 119, 122, 132, 133].

Secondly, stationary batteries are frequently used for the storage of electrical energy [26, 45, 46, 57, 65, 67, 107, 124, 130, 133, 134]. Their state of charge can be expressed either implicitly as the result of the power balance, or by explicit charging and discharging powers, which is necessary if efficiencies shall be respected [45, 46, 65, 67, 107, 124, 130]. Losses from self discharging are only rarely considered, while they are easy to model [65, 124].

As additional producers, combined heat and power plants (CHPs) are interesting due to their high efficiency and the coupling of thermal and electrical power, but modeled less frequently [65, 133]. Fuel cells and electrolyzers are used to store excessive renewable energy as hydrogen [26, 45, 134].

The control of EVs is more specific and not a standard component in

microgrid control. However, the literature on EV control is rich, too. EVs can be modeled either individually [64, 65, 103, 129, 130], as fleets [68] or both. In the latter case, they are usually considered in a hierarchical setup [73]. Furthermore, many approaches exist which do not utilize the receding horizon control scheme [51,139] or are focused only on EV charging control without the context of a microgrid.

The limitation in modeling lies in the complexity of the resulting OCP, which depends on the system dynamics, the constraints and the objectives. Mostly, they are chosen such that they result in a linear programming (LP) or quadratic programming (QP) problem [26, 29, 45, 46, 57, 65, 82, 117, 124, 132–134, 153], which are convex and thus easy to solve [23]. Nonlinearities may occur in the system dynamics [61] or in the objective function [67], but often stem only from additional constraints [27, 107]. If the OCP is a nonlinear programming (NLP) problem, it generally cannot be guaranteed that the global optimum is found. Sometimes a piece-wise linear approximation of the nonlinearities is possible, resulting in a mixed-integer linear programming (MILP) problem [9, 133]. Furthermore, mixed-integer formulations are frequently necessary due to binary on/off variables [45, 93, 124, 132, 133].

If a larger number of temperature zones, EVs or similar entities have to be controlled, the computational cost of the resulting OCP can become unmanagable due to the rapidly increasing complexity. Then, multiple agents or (sub-)systems are used. Their setup can be either hierarchical [29, 67, 132] or distributed [27, 93, 122], depending on the communication structure. Every agent may then have their own OCP [27, 67, 68, 73, 93, 122, 132]. Some lower level agents might also use non-optimal control schemes which use reference points from the higher level agents [110, 119]. In this case, even BPS models may be used in a co-simulation setting [29, 72].

The most common objective to be minimized are monetary costs, often indirectly expressed by the total energy consumption. If the building's temperature is modeled, it is usually optimized either by a reference point [26, 29, 93, 103, 122, 132, 133] or constrained to be within comfortable limits [82, 84, 105, 124, 153]. Sometimes, other comfort indices are used [29]. Less common is the consideration of battery degradation costs [45, 57, 67], which is most likely due to both the non-trivial task of modeling it in general [3] and the resulting increase of the OCP's complexity.

Depending on the objectives, either regular (tracking) [26,61,93,105,117,122, 134, 153] or economic MPC [29, 45, 46, 57, 64, 65, 67, 82, 107, 110, 119, 130, 132, 133] is used. Frequently, forecasts for e. g. air temperature, humidity, solar

irradiance, power demand or occupancy are incorporated, either perfect or with deviations [26, 29, 45, 64, 67, 68, 72, 73, 83, 84, 105, 107, 129, 130, 133, 142, 146, 147]. To account for their uncertainties, robust [61, 65, 134, 142, 147] or stochastic [46, 65, 73, 83, 105, 107, 129, 133, 146] MPC approaches can be used. They cannot always be clearly distinguished, especially if they are based on scenarios [65, 83, 107, 133, 134, 146] instead of probability distributions [46, 73, 105, 129].

It is noteworthy that the majority of studies are only simulation-based. A few approaches have been tested under laboratory conditions [117, 134] and even fewer in real-world applications [153].

Note that only a (small) part of the existing publications has been covered here to illustrate the most important options and properties, since hundreds of publications exist. For a more comprehensive overview, the reader is referred to the various existing reviews which focus on different aspects each, see e. g. [1, 30, 38, 42, 69, 89, 104, 135, 150, 151].

2.3 Modeling

The appropriate modeling of a microgrid is one of the main challenges in its control. Following G.E.P. Box's credo: '*all models are wrong but some are useful*' [22], in this section we first show how the basic entities of a (corporate) building with various power sources can be modeled in a hierarchical setting of linear state space systems. Then, we define objectives which can be used as optimization goals and use reformulation techniques to obtain a well solvable (convex) optimization problem within our MPC framework.

2.3.1 State Space Descriptions

Throughout this thesis, the medium-sized office building which is shared by the Honda Research Institute Europe and Honda Research & Development Europe in Offenbach, Germany is used as an application example. The selection of power sources and storages presented in the following have been chosen accordingly. However, note that the model descriptions can be easily adapted to most buildings. In the following, we present multiple state space models of different complexity, which can (but do not have to) be used in a hierarchical setting, as exemplary illustrated in Figure 2.1.

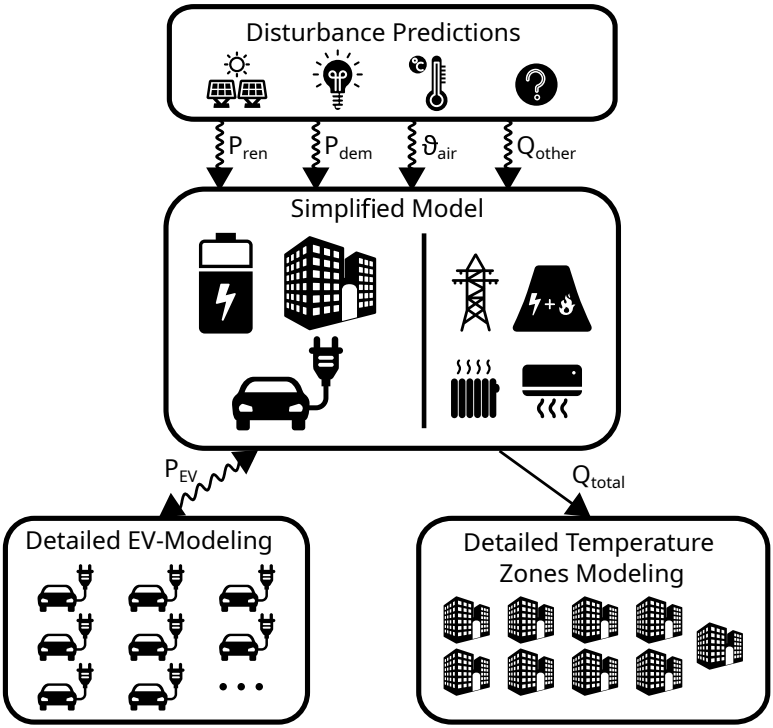

Figure 2.1: Exemplary hierarchical modeling of a corporate building with one higher level and two lower level systems. The lower level systems represent a single entity of the building in more detail (here: the EV charging stations and the temperature zones).

Higher Level: Building Model with Single Temperature Zone

In the simplest case, we consider a building with a single temperature zone and a stationary battery. Note that, in contrast to the higher level system in Figure 2.1, we first leave out any EVs, since this simpler model is used throughout most of the simulation studies in this thesis.

The building's temperature ϑ_b can be modeled by an ODE such as

$$\dot{\vartheta}_\mathrm{b}(t) = \frac{1}{C_\mathrm{th}} \left(H_\mathrm{air} \big(\vartheta_\mathrm{air}(t) - \vartheta_\mathrm{b}(t) \big) + \sum_i \dot{Q}_i(t) \right), \tag{2.5}$$

where $\sum_i \dot{Q}_i$ stands for all thermal powers acting on the building [110]. Here, we consider the heating powers $\dot{Q}_\mathrm{chp}$ from a CHP and $\dot{Q}_\mathrm{rad}$ from a gas heating, cooling power $\dot{Q}_\mathrm{cool}$ from an air conditioning system, and heat losses $\dot{Q}_\mathrm{other}$ to the ground. C_th denotes the building's thermal capacity and H_air the heat transfer coefficient to the outside air temperature ϑ_air.

Another ODE for the stationary battery is necessary. If (self-discharging) losses are neglected, the change of its energy level $E(t)$ is simply given by

$$\dot{E}(t) = \sum_j P_j(t), \tag{2.6}$$

where $\sum_j P_j(t)$ stands for all electrical powers fed into or drawn from the battery. Here, we consider the produced electrical power P_chp from the CHP, the power P_grid bought from or sold to the grid, the (uncontrollable) renewable energy P_ren from a PV system and the (uncontrollable) power demand P_dem, e. g. consumption from offices, which must be met at all times. Note that the CHP can only produce electrical power P_chp and thermal power $\dot{Q}_\mathrm{chp}$ at the same time (see Table 2.1).

Using $E(t)$ and $\vartheta_\mathrm{b}(t)$ as states, a linear state space model of the microgrid is derived,

$$\begin{bmatrix} \dot{E}(t) \\ \dot{\vartheta}_\mathrm{b}(t) \end{bmatrix} = \begin{bmatrix} 0 & 0 \\ 0 & -\frac{H_\mathrm{air}}{C_\mathrm{th}} \end{bmatrix} \cdot \begin{bmatrix} s_\mathrm{c}(t) \\ \vartheta_\mathrm{b}(t) \end{bmatrix} \cdots$$
$$+ \begin{bmatrix} 1 & 1 & -\frac{1}{\eta_\mathrm{rad}} & \frac{1}{\varepsilon_\mathrm{c}} \\ 0 & \frac{1}{c_\mathrm{cur} \cdot C_\mathrm{th}} & \frac{1}{C_\mathrm{th}} & \frac{1}{C_\mathrm{th}} \end{bmatrix} \cdot \begin{bmatrix} P_\mathrm{grid}(t) \\ P_\mathrm{chp}(t) \\ \dot{Q}_\mathrm{rad}(t) \\ \dot{Q}_\mathrm{cool}(t) \end{bmatrix} \cdots$$

$$+\begin{bmatrix}1 & 1 & 0 & 0\\ 0 & 0 & \frac{H_{\mathrm{air}}}{C_{\mathrm{th}}} & \frac{1}{C_{\mathrm{th}}}\end{bmatrix}\cdot\begin{bmatrix}P_{\mathrm{ren}}(t)\\ P_{\mathrm{dem}}(t)\\ \vartheta_{\mathrm{air}}(t)\\ \dot{Q}_{\mathrm{other}}(t)\end{bmatrix}. \tag{2.7}$$

Note that, for the gas heating, an efficiency η_{rad} and for the air condition and energy efficiency ratio ε_{c} are considered.

For the rest of this thesis, we refer to the following discretized version of system (2.7) as the model HL-1. Namely, a discrete linear state space model in the form of

$$x_{\mathrm{HL1}}(k+1) = A_{\mathrm{HL1}}x_{\mathrm{HL1}}(k) + B_{\mathrm{HL1}}u_{\mathrm{HL1}}(k) + S_{\mathrm{HL1}}d_{\mathrm{HL1}}(k) \tag{2.8a}$$

is derived, i. e.

$$\begin{aligned}\begin{bmatrix}E(k+1)\\ \vartheta_{\mathrm{b}}(k+1)\end{bmatrix} &= \begin{bmatrix}1 & 0\\ 0 & -\mathrm{e}^{\frac{-H_{\mathrm{air}}}{C_{\mathrm{th}}}}\end{bmatrix}\cdot\begin{bmatrix}E(k)\\ \vartheta_{\mathrm{b}}(k)\end{bmatrix}\cdots\\ &+\begin{bmatrix}T_{\mathrm{s}} & T_{\mathrm{s}} & 0 & \frac{T_{\mathrm{s}}}{\varepsilon_{\mathrm{c}}}\\ 0 & \frac{\mu}{c_{\mathrm{cur}}} & \mu & \mu\end{bmatrix}\cdot\begin{bmatrix}P_{\mathrm{grid}}(k)\\ P_{\mathrm{chp}}(k)\\ \dot{Q}_{\mathrm{rad}}(k)\\ \dot{Q}_{\mathrm{cool}}(k)\end{bmatrix}\cdots\\ &+\begin{bmatrix}T_{\mathrm{s}} & T_{\mathrm{s}} & 0 & 0\\ 0 & 0 & H_{\mathrm{air}}\cdot\mu & \mu\end{bmatrix}\cdot\begin{bmatrix}P_{\mathrm{ren}}(k)\\ P_{\mathrm{dem}}(k)\\ \vartheta_{\mathrm{air}}(k)\\ \dot{Q}_{\mathrm{other}}(k)\end{bmatrix},\end{aligned} \tag{2.8b}$$

where $\mu = \frac{1-\mathrm{e}^{-\frac{H_{\mathrm{air}}}{C_{\mathrm{th}}}T_{\mathrm{s}}}}{H_{\mathrm{air}}}$ with T_{s} being the sampling rate. Constraints $x \in \mathbb{X} \subseteq \mathbb{R}^n$ on the states, $u \in \mathbb{U} \subset \mathbb{R}^m$ on the inputs, $d \in \mathbb{D} \subset \mathbb{R}^q$ on the disturbances and on the rate of change of the states, $(x(k+1) - x(k)) \in \Delta\mathbb{X} \subseteq \mathbb{R}^n$, apply. $\mathbb{U}$ and $\mathbb{D}$ are compact. Note that all uncontrollable influences have been modeled as disturbances d_{HL1}. The input constraints are chosen generously such that all disturbances can be compensated, e. g. $P_{\mathrm{grid}} \in [-1000\,\mathrm{kW}, 1000\,\mathrm{kW}]$ whereas $P_{\mathrm{dem}} \in [-650\,\mathrm{kW}, 0]$. Thus, feasibility can be ensured for any $x_0 \in \mathbb{X}$. Table 2.1 gives an overview of the model parameters.

Table 2.1: Building model parameters for model HL-1 from (2.8).

Parameter	Description	Value
T_s	Sampling time (step size) in h	0.5
C_th	Thermal capacity of the building in $^{\mathrm{kWh}}/_{\mathrm{K}}$	1792.06
H_air	Heat transfer coefficient to outside air in $^{\mathrm{kW}}/_{\mathrm{K}}$	341.94
ε_c	Energy efficiency ratio for the cooling machine	2.5
c_cur	Current constant CHP, $P_\mathrm{chp} = c_\mathrm{cur} \cdot \dot{Q}_\mathrm{chp}$	0.667

Higher Level: Building Model with Single Temperature Zone and EV Charging Station

In the following, we will augment the HL-1 model (2.8) by a single amalgamated charging station for EVs. Namely, we accumulate 30 single charging stations by summing up the capacities, energy levels and possible charge rates of available EVs. Later, we present a lower level model consisting of the EVs charging stations only, with which the following model can be used in a hierarchical setup. Both higher and lower level model parts of the EV charging stations have been developed in the process of a Master's thesis [39].

The HL model including the EV charging station, called HL-2, is expressed as an extended version of (2.8) by

$$\underbrace{\begin{bmatrix} x_{\mathrm{HL1}}(k+1) \\ E_\mathrm{EV}(k+1) \\ C_\mathrm{EV}(k+1) \end{bmatrix}}_{x_{\mathrm{HL2}}(k+1)} = \underbrace{\begin{bmatrix} A_\mathrm{HL1} & \mathbf{0}_{2\times 2} \\ \mathbf{0}_{2\times 2} & \boldsymbol{I}_{2\times 2} \end{bmatrix}}_{A_\mathrm{HL2}} \underbrace{\begin{bmatrix} x_{\mathrm{HL1}}(k) \\ E_\mathrm{EV}(k) \\ C_\mathrm{EV}(k) \end{bmatrix}}_{x_{\mathrm{HL2}}(k)} \cdots$$
$$+ \underbrace{\begin{bmatrix} B_\mathrm{HL1} & \begin{bmatrix} -T_s \\ 0 \end{bmatrix} \\ \mathbf{0}_{1\times 4} & T_s \\ \mathbf{0}_{1\times 4} & 0 \end{bmatrix}}_{B_\mathrm{HL2}} \underbrace{\begin{bmatrix} u_{\mathrm{HL1}}(k) \\ P_\mathrm{EV}(k) \end{bmatrix}}_{u_{\mathrm{HL2}}(k)} \cdots$$

$$+ \underbrace{\begin{bmatrix} S_{\mathrm{HL1}} & \mathbf{0}_{2\times1} & \mathbf{0}_{2\times1} & \mathbf{0}_{2\times1} & \mathbf{0}_{2\times1} \\ \mathbf{0}_{1\times4} & 1 & -1 & 0 & 0 \\ \mathbf{0}_{1\times4} & 0 & 0 & 1 & -1 \end{bmatrix}}_{S_{\mathrm{HL2}}} \underbrace{\begin{bmatrix} d(k) \\ E_{\mathrm{EV,arr}}(k) \\ E_{\mathrm{EV,dep}}(k) \\ C_{\mathrm{EV,arr}}(k) \\ C_{\mathrm{EV,dep}}(k) \end{bmatrix}}_{d_{\mathrm{HL2}}(k)}, \quad (2.9)$$

where x_{HL1}, u_{HL1}, d_{HL1}, A_{HL1}, B_{HL1} and S_{HL1} are as in (2.8), E_{EV} and C_{EV} are the accumulated energies and capacities of all EVs currently connected to the charging stations (in kWh), $E_{\mathrm{EV,arr}}(k)$ and $C_{\mathrm{EV,arr}}(k)$ are the accumulated energies and capacities of all new EVs arriving at time step k, $E_{\mathrm{EV,dep}}(k)$ and $C_{\mathrm{EV,dep}}(k)$ are the same of all departing EVs at time step k and P_{EV} is the total charging (or discharging) power accumulated over all EVs. $\boldsymbol{I}_{n_1\times n_2}$ denotes the identity matrix of dimensions $n_1 \times n_2$ and $\mathbf{0}_{n_1\times n_2}$ a matrix consisting of only zeroes with dimensions $n_1 \times n_2$.

Lower Level: Detailed EV charging stations model

With the HL-2 model, we calculate only the total (dis-)charging power P_{EV} for all EVs. To distribute P_{EV} between the single charging stations, we use a lower level model where every charging station is modeled individually. In the following, we present a linear time-invariant model which is used for the simulation studies in this thesis. For a linear time-variant model which is more suitable for stochastic MPC approaches, the reader is referred to [39]. We assume that 30 charging stations are available. However, the model description can easily be adapted to any number of charging stations.

The time-invariant model LL-EV is defined similarly to the the higher level model HL-2, i. e. the arriving and departing of EVs are realized through disturbances. It is given by

$$x_{\mathrm{LLEV}}(k+1) = \underbrace{\boldsymbol{I}_{60\times60}}_{A_{\mathrm{LLEV}}} \underbrace{\begin{bmatrix} E_{\mathrm{EV},1}(k) \\ \vdots \\ E_{\mathrm{EV},30}(k) \\ C_{\mathrm{EV},1}(k) \\ \vdots \\ C_{\mathrm{EV},30}(k) \end{bmatrix}}_{x_{\mathrm{LLEV}}(k)} + \underbrace{T_{\mathrm{s}} \begin{bmatrix} \boldsymbol{I}_{30\times30} \\ \mathbf{0}_{30\times30} \end{bmatrix}}_{B_{\mathrm{LLEV}}} \underbrace{\begin{bmatrix} P_{\mathrm{EV},1}(k) \\ \vdots \\ P_{\mathrm{EV},30}(k) \end{bmatrix}}_{u_{\mathrm{LLEV}}(k)} \cdots$$

$$+ \underbrace{\begin{bmatrix} \boldsymbol{I}^{+-}_{30\times 60} & \boldsymbol{0}_{30\times 60} \\ \boldsymbol{0}_{30\times 60} & \boldsymbol{I}^{+-}_{30\times 60} \end{bmatrix}}_{S_{\mathrm{LLEV}}} \underbrace{\begin{bmatrix} E_{\mathrm{EV,arr},1}(k) \\ E_{\mathrm{EV,dep},1}(k) \\ \vdots \\ E_{\mathrm{EV,arr},30}(k) \\ E_{\mathrm{EV,dep},30}(k) \\ C_{\mathrm{EV,arr},1}(k) \\ C_{\mathrm{EV,dep},1}(k) \\ \vdots \\ C_{\mathrm{EV,arr},30}(k) \\ C_{\mathrm{EV,dep},30}(k) \end{bmatrix}}_{d_{\mathrm{LLEV}}(k)}, \tag{2.10a}$$

$$\boldsymbol{I}^{+-}_{30\times 60} = \begin{bmatrix} 1 & -1 & 0 & 0 & \cdots & 0 & 0 \\ 0 & 0 & 1 & -1 & \cdots & 0 & 0 \\ \vdots & \vdots & & \ddots & \ddots & & \\ \vdots & \vdots & & & \ddots & \ddots & \\ 0 & 0 & \cdots & & & 1 & -1 \end{bmatrix}. \tag{2.10b}$$

$E_{\mathrm{EV,arr},i}(k)$ and $C_{\mathrm{EV,arr},i}(k)$ are the energy and capacity of an EV arriving at the charging station i at time step k (in kWh), $E_{\mathrm{EV,dep},i}(k)$ and $C_{\mathrm{EV,dep},i}(k)$ are the same for an EV departing from charging station i at time step k, and $P_{\mathrm{EV},i}$ is the (dis-)charging power from charging station i.

Lower Level: Multi Temperature Zone Model

The assumption of a single temperature zone is highly simplified. In reality, every room would constitute a temperature zone at its own (and even within a room, the temperature would not be homogeneous). Thus, we present a model with multiple temperature zones. Since we will use it in a hierarchical setting as illustrated in Figure 2.1, we neglect the electrical energy system's part.

If multiple temperature zones are respected, the temperature $\vartheta_{\mathrm{b},i}$ of zone i in the continuous-time case can be described by

$$\dot{\vartheta}_{\mathrm{b},i}(t) = -\frac{H_{\mathrm{air},i}}{C_{\mathrm{th},i}}(\vartheta_{\mathrm{b},i}(t) - \vartheta_{\mathrm{air}}(t)) - \sum_{j\neq i} \frac{\beta_{ij}}{C_{\mathrm{th},i}}(\vartheta_{\mathrm{b},i}(t) - \vartheta_{\mathrm{b},j}(t)) \ldots$$
$$+ \frac{1}{C_{\mathrm{th},i}}\Big(\dot{Q}_{\mathrm{heat},i}(t) + \dot{Q}_{\mathrm{cool},i}(t) + \dot{Q}_{\mathrm{other},i}(t)\Big), \tag{2.11}$$

where $C_{\mathrm{th},i}$ is the thermal capacity of zone i, $H_{\mathrm{air},i}$ is the heat transfer coefficient between zone i and the outside air, β_{ij} is the heat transfer coefficient between zones i and j, $\dot{Q}_{\mathrm{heat},i}$ and $\dot{Q}_{\mathrm{cool},i}$ are the respective heating and cooling powers allocated to zone i, and $\dot{Q}_{\mathrm{other},i}$ are the heat losses from zone i to the ground. Note that we distinguish between heating and cooling powers to forego the necessity of binary variables in the constraints when used in the hierarchical setup with the single-zone building models.

Assuming 9 temperature zones, the continuous-time state-space description for model LL-TEMP is given by

$$\dot{x}_{\mathrm{LLT}}(t) = A_{\mathrm{LLT}}^{\mathrm{Cont.}} x_{\mathrm{LLT}}(t) + B_{\mathrm{LLT}}^{\mathrm{Cont.}} u_{\mathrm{LLT}}(t) + S_{\mathrm{LLT}}^{\mathrm{Cont.}} d_{\mathrm{LLT}}(t), \tag{2.12a}$$

with

$$x_{\mathrm{LLT}}(t) = \begin{bmatrix} \vartheta_{\mathrm{b},1}(t) & \cdots & \vartheta_{\mathrm{b},9}(t) \end{bmatrix}^\intercal, \tag{2.12b}$$

$$u_{\mathrm{LLT}}(t) = \begin{bmatrix} \dot{Q}_{\mathrm{heat},1}(t) & \cdots & \dot{Q}_{\mathrm{heat},9}(t) & \dot{Q}_{\mathrm{cool},1}(t) & \cdots & \dot{Q}_{\mathrm{cool},9}(t) \end{bmatrix}^\intercal, \tag{2.12c}$$

$$d_{\mathrm{LLT}}(t) = \begin{bmatrix} \vartheta_{\mathrm{air}}(t) & \dot{Q}_{\mathrm{other},1} & \cdots & \dot{Q}_{\mathrm{other},9} \end{bmatrix}^\intercal, \tag{2.12d}$$

$$A_{\mathrm{LLT}}^{\mathrm{Cont.}} = \begin{bmatrix} \frac{-H_{\mathrm{air},1} - \sum_{j\neq 1} \beta_{1j}}{C_{\mathrm{th},1}} & \frac{\beta_{12}}{C_{\mathrm{th},1}} & \cdots & \frac{\beta_{19}}{C_{\mathrm{th},1}} \\ \frac{\beta_{21}}{C_{\mathrm{th},2}} & \frac{-H_{\mathrm{air},2} - \sum_{j\neq 2} \beta_{2j}}{C_{\mathrm{th},2}} & \cdots & \frac{\beta_{29}}{C_{\mathrm{th},2}} \\ \vdots & \vdots & \ddots & \vdots \\ \frac{\beta_{91}}{C_{\mathrm{th},9}} & \frac{\beta_{92}}{C_{\mathrm{th},9}} & \cdots & \frac{-H_{\mathrm{air},9} - \sum_{j\neq 9} \beta_{9j}}{C_{\mathrm{th},9}} \end{bmatrix}, \tag{2.12e}$$

$$B_{\mathrm{LLT}}^{\mathrm{Cont.}} = \begin{bmatrix} \frac{1}{C_{\mathrm{th},1}} & 0 & \cdots & 0 & \frac{1}{C_{\mathrm{th},1}} & 0 & \cdots & 0 \\ 0 & \frac{1}{C_{\mathrm{th},2}} & \cdots & 0 & 0 & \frac{1}{C_{\mathrm{th},2}} & \cdots & 0 \\ \vdots & & \ddots & \vdots & \vdots & & \ddots & \vdots \\ 0 & \cdots & 0 & \frac{1}{C_{\mathrm{th},9}} & 0 & \cdots & 0 & \frac{1}{C_{\mathrm{th},9}} \end{bmatrix}, \tag{2.12f}$$

$$S_{\mathrm{LLT}}^{\mathrm{Cont.}} = \begin{bmatrix} \frac{H_{\mathrm{air},1}}{C_{\mathrm{th},1}} & \frac{1}{C_{\mathrm{th},1}} & 0 & \cdots & 0 \\ \vdots & 0 & \frac{1}{C_{\mathrm{th},2}} & \cdots & 0 \\ \vdots & \vdots & \ddots & \vdots & \\ \frac{H_{\mathrm{air},9}}{C_{\mathrm{th},9}} & 0s & \cdots & 0 & \frac{1}{C_{\mathrm{th},9}} \end{bmatrix}. \tag{2.12g}$$

By discretization with the sampling time T_{s}, we obtain the discrete state space model

$$x_{\mathrm{LLT}}(k+1) = A_{\mathrm{LLT}} x_{\mathrm{LLT}}(k) + B_{\mathrm{LLT}} u_{\mathrm{LLT}}(k) + S_{\mathrm{LLT}} d_{\mathrm{LLT}}(k), \tag{2.13}$$

whose analytical form we omit for brevity. The numerical values of the building parameters are given in Table 2.2 and have been provided by an external consulting specialist.[1]

Table 2.2: Building parameters for model LL-TEMP, i. e. thermal capacities $C_{\mathrm{th},i}$, heat transfer coefficients $H_{\mathrm{air},i}$ and β_{ij}. Note that $\beta_{ij} = \beta_{ji}$. Otherwise, all β_{ij} not listed below are zero, e. g. $\beta_{12} = 0$.

	in $^{\mathrm{kWh}}/_{\mathrm{K}}$		in $^{\mathrm{kW}}/_{\mathrm{K}}$		in $^{\mathrm{kW}}/_{\mathrm{K}}$
$C_{\mathrm{th},1}$	230.88	$H_{\mathrm{air},1}$	3.69	β_{29}	48.40
$C_{\mathrm{th},2}$	476.29	$H_{\mathrm{air},2}$	9.82	β_{34}	345.60
$C_{\mathrm{th},3}$	214.27	$H_{\mathrm{air},3}$	3.65	β_{56}	1100.48
$C_{\mathrm{th},4}$	103.68	$H_{\mathrm{air},4}$	2.79	β_{58}	23.40
$C_{\mathrm{th},5}$	330.14	$H_{\mathrm{air},5}$	4.79	β_{68}	8.00
$C_{\mathrm{th},6}$	330.14	$H_{\mathrm{air},6}$	6.19		
$C_{\mathrm{th},7}$	99.456	$H_{\mathrm{air},7}$	3.19		
$C_{\mathrm{th},8}$	2.40	$H_{\mathrm{air},8}$	0.03		
$C_{\mathrm{th},9}$	4.80	$H_{\mathrm{air},9}$	0.04		

2.3.2 Objectives

In the following subsection, we formulate possible optimization criteria as cost functions within the MPC context. Note that possible reformulations are explored in Section 2.3.3. Furthermore, if not otherwise stated, the single cost functions are formulated for a single time step and would be summed over the entire prediction horizon, i. e. at time step k, the total cost would be

$$J_i(k) = \sum_{n=0}^{N_{\mathrm{p}}-1} \ell_i(n|k). \tag{2.14}$$

First, we summarize objectives for the higher level (HL) systems. Then, we do so for the different lower level (LL) systems.

HL: Monetary Costs: Industry and Intraday Pricing

The most obvious and common objective is to minimize the occuring monetary costs. In the microgrid setting considered here, these arise from

[1] EA Systems Dresden GmbH, `https://www.ea-energie.de/`, accessed on 09/14/21

gas costs from the use of the CHP and the gas heating and electricity costs from buying/selling energy from/to the grid.

The gas costs are given by

$$\ell_{\mathrm{mon,chp}}(k) = 0.12\,\frac{€}{\mathrm{kWh}} \cdot T_\mathrm{s} \cdot P_\mathrm{chp}(k) \tag{2.15}$$

and

$$\ell_{\mathrm{mon,heat}}(k) = 0.0464\,\frac{€}{\mathrm{kWh}} \cdot T_\mathrm{s} \cdot \dot{Q}_\mathrm{rad}(k). \tag{2.16}$$

For the electricity costs, we distinguish between two cases.

Industry Pricing First, in German industry pricing, the energy costs $\ell^{\mathrm{industry}}_{\mathrm{mon,grid}}$ for buying/selling electricity from/to the power grid are fixed. On top of that, high peak costs $\ell_{\mathrm{mon,peak}}$ apply. Namely, at the end of a calendar year, the highest peak averaged over fixed 15 min time slots is punished with for example $c_{\mathrm{grid,peak}} = 100.01\,€/\mathrm{kW}$.

The regular energy costs in the industry scenario can be described by

$$\ell^{\mathrm{industry}}_{\mathrm{mon,grid}}(k) = \left(c_{\mathrm{grid,buy}} \cdot P^{+}_{\mathrm{grid}}(k) + c_{\mathrm{grid,sell}} \cdot P^{-}_{\mathrm{grid}}(k)\right) \cdot T_\mathrm{s}, \tag{2.17}$$

where $P^{+}_{\mathrm{grid}}(k) = P_{\mathrm{grid}}(k)$ if $P_{\mathrm{grid}}(k) > 0$, i. e. if energy is bought from the grid, and $P^{+}_{\mathrm{grid}}(k) = 0$ if $P_{\mathrm{grid}}(k) < 0$. $P^{-}_{\mathrm{grid}}(k)$ is defined accordingly for selling energy to the grid. We assume $c_{\mathrm{grid,buy}} = 0.13\,€/\mathrm{kWh}$ for buying and $c_{\mathrm{grid,sell}} = 0.07\,€/\mathrm{kWh}$ for selling. To describe $\ell^{\mathrm{industry}}_{\mathrm{mon,grid}}$ in dependence of our input and decision variable P_{grid}, (2.17) is formulated as

$$\begin{aligned}\ell^{\mathrm{industry}}_{\mathrm{mon,grid}}(k) = \big(&c_{\mathrm{grid,buy}} \cdot \max(0, P_{\mathrm{grid}}(k)) \ldots \\ &- c_{\mathrm{grid,sell}} \cdot \max(0, -P_{\mathrm{grid}}(k))\big) \cdot T_\mathrm{s}.\end{aligned} \tag{2.18}$$

The peak costs in the industry pricing scenario are given by

$$\ell_{\mathrm{mon,peak}}(k) = c_{\mathrm{grid,peak}} \cdot \max(0, P_{\mathrm{grid}}(k) - P_{\mathrm{grid,peak}}(k)). \tag{2.19}$$

Since our prediction horizon N_p is significantly smaller than one year, we punish every new peak according to the difference to the maximum peak $P_{\mathrm{grid,peak}}(k)$ which has occurred until time step k. Furthermore, $P_{\mathrm{grid,peak}}$ may change within N_p, e. g. if the predicted $P_{\mathrm{grid}}(2|k) > P_{\mathrm{grid,peak}}(k)$, then $P_{\mathrm{grid,peak}}(3|k) = P_{\mathrm{grid}}(2|k)$ and for $t \geq k+3$, new peak costs only occur

for $P_{\mathrm{grid}}(t) > P_{\mathrm{grid,peak}}(2|k)$. A solution to this problem is presented in Section 2.3.3 together with the general reformulation of max-terms.

Combined with the gas costs, the monetary costs in the industry scenario are given by

$$\ell_{\mathrm{mon}}^{\mathrm{industry}}(k) = \ell_{\mathrm{mon,grid}}^{\mathrm{industry}}(k) + \ell_{\mathrm{mon,peak}}(k) + \ell_{\mathrm{mon,chp}}(k) + \ell_{\mathrm{mon,heat}}(k). \quad (2.20)$$

Note that, due to the discontinuities in (2.18) and (2.19), including (2.20) in the MPC objective function without any reformulation would result in a nonlinear programming problem, which is in general hard to solve.

Intraday Market In the second scenario, we assume participation in the electricity intraday market. Thus, the electricity (grid) costs depend on the current market price,

$$\ell_{\mathrm{mon,grid}}^{\mathrm{market}}(k) = c_{\mathrm{grid}}^{\mathrm{market}}(k) \cdot T_{\mathrm{s}} \cdot P_{\mathrm{grid}}(k). \quad (2.21)$$

Together with the gas costs (2.15) and (2.16), the monetary costs in the intraday scenario are given by

$$\ell_{\mathrm{mon}}^{\mathrm{market}}(k) = \ell_{\mathrm{mon,grid}}^{\mathrm{market}}(k) + \ell_{\mathrm{mon,chp}}(k) + \ell_{\mathrm{mon,heat}}(k). \quad (2.22)$$

Note that in this case, no reformulation is necessary as including (2.22) in the MPC objective function results in a linear program.

HL: (Temperature) Comfort Costs

Since we model the building's temperature as a state, we have to incentivize its control. Instead of only defining constraints which have to be kept, we additionally define a desired set point $\vartheta_{\mathrm{set}} = 21°\mathrm{C}$, from which we punish deviations quadratically,

$$\ell_{\mathrm{comf}}(k) = \left(\vartheta_{\mathrm{b}}(k) - \vartheta_{\mathrm{set}}\right)^2 \cdot T_{\mathrm{s}}. \quad (2.23)$$

Note that the sampling time T_{s} is only relevant if it varies throughout the prediction horizon, i. e. if it is actually time-variant $T_{\mathrm{s}}(k)$. Otherwise, it is only a scalar factor which could be compensated with an appropriate weight.

HL: Ecological Costs

With increasing monetarily punishment of CO_2 emissions, they could be included in the monetary costs. However, especially to meet self-imposed limits, it might be necessary to respect them in the form of an objective on their own. This is possible by considering the carbon intensity (CI) for each actuator, i. e. how much CO_2 is emitted per kWh energy. The following cost terms have been derived in a student cooperation [56]. The CI factors for the CHP and the gas heating are derived from the general life-cycle emissions of a gas plant. Namely, a gas plant with an average efficiency of 0.6 [111] has a median CI of 490 $\frac{\mathrm{g\,CO_2}}{\mathrm{kWh}}$ [123]. Thus, for the combustion of natural gas, we assume a general $\mathrm{CI_{gas}} = 490 \cdot 0.6 \, \frac{\mathrm{g\,CO_2}}{\mathrm{kWh_{gas}}} = 294 \, \frac{\mathrm{g\,CO_2}}{\mathrm{kWh_{gas}}}$. For the gas heating, we assume an efficiency of $\eta_{\mathrm{rad}} = 0.97$, which results in

$$\mathrm{CI_{heat}} = \frac{\mathrm{CI_{gas}}}{\eta_{\mathrm{rad}}} = 303.09 \, \frac{\mathrm{g\,CO_2}}{\mathrm{kWh}}. \tag{2.24}$$

The CHP produces electrical and thermal energy at the same time (see Table 2.1). Thus, the CI for *electrical* energy produced by the CHP is comparatively high with

$$\mathrm{CI_{CHP}} = \frac{\mathrm{CI_{gas}}}{\eta_{\mathrm{CHP}} \cdot \frac{1}{1+\frac{1}{c_{\mathrm{cur}}}}} = 823.74 \, \frac{\mathrm{g\,CO_2}}{\mathrm{kWh}}. \tag{2.25}$$

where $\eta_{\mathrm{CHP}} = 0.892$ is the overall efficiency of the CHP. For electricity from the power grid, we use the estimated CI by the German Umweltbundesamt for the eletricity mix in 2019 [63],

$$\mathrm{CI_{grid}} = 401 \, \frac{\mathrm{g\,CO_2}}{\mathrm{kWh}}. \tag{2.26}$$

Together, the ecological costs are given by

$$\ell_{\mathrm{eco}}(k) = \Big(\mathrm{CI_{grid}} P_{\mathrm{grid}}(k) + \mathrm{CI_{CHP}} P_{\mathrm{chp}}(k) + \mathrm{CI_{heat}} \dot{Q}_{\mathrm{rad}}(k) \Big) \cdot T_{\mathrm{s}}. \tag{2.27}$$

HL: Battery Degradation Costs

The results in this section have been derived in the process of a Master's thesis [39]. Modeling battery degradation accurately is a complex research field by itself. The relation between degradation and charging can be highly nonlinear and depends on the battery technology [3,140]. However, it is too

important to neglect entirely and can be approximated. Thus, we propose a comparatively simple cost function, i. e. we punish

- the total energy throughput of the battery,
- the average state of charge and
- the (absolute) charge rate.

Additionally, the depth of discharge and the operating temperature are relevant. However, the operating temperature cannot be controlled directly and would be very complex to model. Therefore, it is neglected. The depth of discharge is respected by constraining the battery's lower limit.

Stationary Battery For the stationary battery, the charging power is not an input (or decision) variable itself, but implicitly given by $P_{\text{charge}}(k) = E(k+1) - E(k)$. For example, for the HL-1 model, this is equivalent to

$$P_{\text{charge}}(k) = P_{\text{grid}}(k) + P_{\text{chp}}(k) + \frac{\dot{Q}_{\text{cool}}(k)}{\varepsilon_{\text{c}}} + P_{\text{ren}}(k) + P_{\text{dem}}(k). \quad (2.28)$$

The cost term for the energy throughput is

$$\ell^{\text{stat}}_{\text{bat,E}}(k) = \frac{|P_{\text{charge}}(k)|}{C_{\text{bat}}} \cdot T_{\text{s}}(k). \quad (2.29)$$

The charge rate is punished proportionally to the maximum possible value $P_{\text{charge,max}}$,

$$\ell^{\text{stat}}_{\text{bat,CR}}(k) = \frac{|P_{\text{charge}}(k)|}{P_{\text{charge,max}}} \cdot T_{\text{s}}(k). \quad (2.30)$$

Since the average state of charge has to be calculated over the entire prediction horizon, we state here its total cost form,

$$J^{\text{stat}}_{\text{bat,SoC}}(k) = \frac{1}{N_{\text{p}}+1} \sum_{n=0}^{N_{\text{p}}} \frac{E(n|k)}{C_{\text{bat}}(n|k)} \cdot T_{\text{s}}(n|k). \quad (2.31)$$

The total degradation costs for the stationary battery are then given by

$$J^{\text{stat}}_{\text{bat}}(k) = w^{\text{stat}}_{\text{bat,E}} J^{\text{stat}}_{\text{bat,E}}(k) + w^{\text{stat}}_{\text{bat,CR}} J^{\text{stat}}_{\text{bat,CR}}(k) + w^{\text{stat}}_{\text{bat,SoC}} J^{\text{stat}}_{\text{bat,SoC}}(k), \quad (2.32)$$

where $\left(w^{\text{stat}}_{\text{bat,E}},\ w^{\text{stat}}_{\text{bat,CR}},\ w^{\text{stat}}_{\text{bat,SoC}}\right) = \left(10,\ 0.1,\ 1\right)$ are weights derived from simulations and represent the cost terms' relative importance from experience.

HL EV Battery For the accumulated EV battery, the degradation costs are calculated similarly to the stationary battery. However, we have to introduce an additional variable M_{EV} which indicates whether any EV is available or not,

$$M_{\mathrm{EV}}(k) = \begin{cases} 1 & C_{\mathrm{EV}}(k) > 0 \\ 0 & \text{otherwise.} \end{cases} \tag{2.33}$$

Then, the single parts can be expressed by

$$\ell^{\mathrm{EV}}_{\mathrm{bat,E}}(k) = M_{\mathrm{EV}}(k) \cdot \frac{|P_{\mathrm{EV}}(k)|}{C_{\mathrm{EV}}} \cdot T_{\mathrm{s}}(k), \tag{2.34}$$

$$\ell^{\mathrm{EV}}_{\mathrm{bat,CR}}(k) = M_{\mathrm{EV}}(k) \cdot \frac{|P_{\mathrm{EV}}(k)|}{P_{\mathrm{EV,max}}} \cdot T_{\mathrm{s}}(k), \tag{2.35}$$

$$J^{\mathrm{EV}}_{\mathrm{bat,SoC}}(k) = \frac{1}{N_{\mathrm{p}}+1} \sum_{n=0}^{N_{\mathrm{p}}} M_{\mathrm{EV}}(k) \cdot \frac{E_{\mathrm{EV}}(n|k)}{C_{\mathrm{EV}}(n|k)} \cdot T_{\mathrm{s}}(n|k), \tag{2.36}$$

and the total cost is given by

$$J^{\mathrm{EV}}_{\mathrm{bat}}(k) = w^{\mathrm{EV}}_{\mathrm{bat,E}} J^{\mathrm{EV}}_{\mathrm{bat,E}}(k) + w^{\mathrm{EV}}_{\mathrm{bat,CR}} J^{\mathrm{EV}}_{\mathrm{bat,CR}}(k) + w^{\mathrm{EV}}_{\mathrm{bat,SoC}} J^{\mathrm{EV}}_{\mathrm{bat,SoC}}(k), \tag{2.37}$$

where $\left(w^{\mathrm{EV}}_{\mathrm{bat,E}},\, w^{\mathrm{EV}}_{\mathrm{bat,CR}},\, w^{\mathrm{EV}}_{\mathrm{bat,SoC}}\right) = \left(10,\, 0.1,\, 1\right)$ are chosen as for the stationary battery.

LL: EV Battery Degradation Costs

For the LL EV model LL-EV, the battery degradation cost for each individual EV is defined similarly to the HL. Namely, we first introduce an additional variable $m_{\mathrm{EV,i}}$, which indicates whether an EV is available at the charging station i or not,

$$m_{\mathrm{EV,i}}(k) = \begin{cases} 1 & C_{\mathrm{EV},i}(k) > 0 \\ 0 & \text{otherwise.} \end{cases} \tag{2.38}$$

Then, the single parts can be expressed by

$$\ell^{\mathrm{EV,i}}_{\mathrm{bat,E}}(k) = m_{\mathrm{EV,i}}(k) \cdot \frac{|P_{\mathrm{EV},i}(k)|}{C_{\mathrm{EV},i}} \cdot T_{\mathrm{s}}(k), \tag{2.39}$$

$$\ell^{\mathrm{EV,i}}_{\mathrm{bat,CR}}(k) = m_{\mathrm{EV,i}}(k) \cdot \frac{|P_{\mathrm{EV},i}(k)|}{P_{\mathrm{EV,i,max}}} \cdot T_{\mathrm{s}}(k), \tag{2.40}$$

$$J_{\text{bat,SoC}}^{\text{EV,i}}(k) = \frac{1}{N_\text{p}+1} \sum_{n=0}^{N_\text{p}} m_{\text{EV,i}}(n|k) \cdot \frac{E_{\text{EV},i}(n|k)}{C_{\text{EV},i}(n|k)} \cdot T_\text{s}(n|k), \quad (2.41)$$

and the total cost is given by

$$J_{\text{bat}}^{\text{EV,i}}(k) = w_{\text{bat,E}}^{\text{EV,i}} J_{\text{bat,E}}^{\text{EV,i}}(k) + w_{\text{bat,CR}}^{\text{EV,i}} J_{\text{bat,CR}}^{\text{EV,i}}(k) + w_{\text{bat,SoC}}^{\text{EV,i}} J_{\text{bat,SoC}}^{\text{EV,i}}(k), \quad (2.42)$$

where $\left[w_{\text{bat,E}}^{\text{EV,i}},\ w_{\text{bat,CR}}^{\text{EV,i}},\ w_{\text{bat,SoC}}^{\text{EV,i}}\right] = [10,\ 0.1,\ 1]$ are chosen as for the higher level.

LL: EV Charging Satisfaction

On the LL, we also use a cost function for the charging satisfaction of each individual EV. Since the arriving and departing of EVs is very hard to predict, we model probability distributions from which we sample multiple possible scenarios. Assuming that N_scen scenarios are available, the charge satisfaction is defined as

$$l_{\text{Soc}}^{\text{EV,i}}(k) = d_{\text{EV},i}(k)(\min[E_{\text{EV},i}(k) - E_{\text{EV,des},i},\ 0])^2 \quad (2.43)$$

where $E_{\text{EV,des},i}$ is usually set to 90 % of the EV's total capacity. $d_{\text{EV},i}(k)$ is the departure indication function, i. e.

$$d_{\text{EV},i}(k) = \frac{N_{\text{dep},i}(k)}{N_\text{scen}} \quad (2.44)$$

and $N_{\text{dep},i}(k)$ is the number of scenarios in which the EV i departs at time step k.

Note that with $\min(y, z) = -\max(-y, -z)$, the min-term in (2.43) can be transformed into a linear programming problem the same way as the max-terms of the monetary costs in the industry scenario, which will be explained in Section 2.3.3.

LL: (Temperature) Comfort Costs

For the LL temperature zones model LL-TEMP, we adapt a similar cost function as (2.23) for the HL. However, we sum up all single zones' temperature deviations weighted by their thermal capacities $C_{\text{th},i}$,

$$\ell_{\text{comf,LL}}(k) = \sum_{i=1}^{9} \frac{C_{\text{th},i}}{C_\text{th}} (\vartheta_{\text{b,i}}(k) - \vartheta_\text{set})^2 \cdot T_\text{s}. \quad (2.45)$$

Without the weighting, it would always be beneficial to heat (or cool) the smaller temperature zones first.

2.3.3 Problem Formulations

In this section, we will first summarize general constraints valid for most of the simulations conducted in this thesis. Then, we will explain how the monetary costs can be reformulated such that a nonlinear programming problem is avoided. Lastly, as an example, we formulate the optimization problem with multiple cost functions for the HL-1 model, which is used in most of the simulation studies in this thesis. Necessary extensions for special cases such as hierarchical control schemes are skipped here and will be instead introduced in the corresponding simulation studies to improve readability.

General Constraints

In the following, we summarize the general constraints which apply to all models if they include the corresponding entity. We formulate the state constraints in dependence of constant parameters, whose values are listed in Table 2.3. Note that for EV control, the capacities and maximum charging values depend on the number of vehicles and their assumed individual values. Thus, details are given in the corresponding simulation study, together with slack variables and special constraints for the hierarchical setups.

State Constraints Both the building's total temperature as well as each zone's temperature are subject to box constraints,

$$\vartheta_{\mathrm{b,min}} \leq \vartheta_{\mathrm{b}}(k) \leq \vartheta_{\mathrm{b,max}}, \tag{2.46}$$

$$\vartheta_{\mathrm{b,min}} \leq \vartheta_{\mathrm{b,i}}(k) \leq \vartheta_{\mathrm{b,max}} \quad \text{for } i = 1 \dots 9. \tag{2.47}$$

The stationary battery has constraints both on its total energy level E and the maximum charging/discharging power P_{charge}, which is not a decision variable itself. It can be expressed as the change of E between two time steps,

$$0.15 \cdot C_{\mathrm{bat}} \leq E(k) \leq 0.85 \cdot C_{\mathrm{bat}}, \tag{2.48a}$$

$$-P_{\mathrm{bat,max}} \leq P_{\mathrm{charge}}(k) = \frac{E(k+1) - E(k)}{T_{\mathrm{s}}(k)} \leq P_{\mathrm{bat,max}}. \tag{2.48b}$$

Table 2.3: General parameter values for constraints on states (top) and inputs (bottom).

Parameter	Description	Value
C_{bat}	Battery capacity	98 kWh
$P_{\text{bat,max}}$	Maximum battery charging and discharging power	32.9 kW
$\vartheta_{\text{b,min}}$	Minimum building temperature	19 °C
$\vartheta_{\text{b,max}}$	Maximum building temperature	23 °C
$P_{\text{grid,max}}$	Maximum electrical power from grid	1000 kW
$P_{\text{chp,max}}$	Maximum electrical power output from CHP	199 kW
$\dot{Q}_{\text{rad,max}}$	Maximum (thermal) heating power from electrical radiator	600 kW
$\dot{Q}_{\text{cool,max}}$	Maximum cooling power from cooling machine	−440 kW

Note that all state constraints apply for $k = 1 \dots N_{\text{pred}}$, i. e. not for the current but for the time step after the end of the actual prediction horizon.

Input Constraints All inputs are subject to box constraints,

$$-P_{\text{grid,max}} \leq P_{\text{grid}}(k) \leq P_{\text{grid,max}}, \tag{2.49a}$$
$$0 \leq P_{\text{chp}}(k) \leq P_{\text{chp,max}}, \tag{2.49b}$$
$$0 \leq \dot{Q}_{\text{rad}}(k) \leq \dot{Q}_{\text{rad,max}}, \tag{2.49c}$$
$$\dot{Q}_{\text{cool,max}} \leq \dot{Q}_{\text{cool}}(k) \leq 0. \tag{2.49d}$$

All constraints on the inputs apply for $k = 0 \dots N_{\text{pred}} - 1$.

Reformulation of Monetary Costs with Industry Pricing

If industry pricing is assumed, including the monetary costs as stated in (2.18), (2.19), (2.20) in the optimization problem would lead to a nonlinear programming problem due to the max-terms. However, using an epigraph reformulation [23, 80], it is possible to reformulate them to a relaxed version which, when included in the optimization problem, still leads to the

same optimum, but is only a linear programming problem. Similar linear programming tricks can e. g. be found in [19]. (Note that, if for example the comfort costs are included, too, the resulting optimization problem becomes a quadratic programming problem.)

Grid Costs The main idea is to replace each max-term by an additional decision variable. For (2.18), we introduce

$$P_{\text{pos}}(n|k) \stackrel{!}{=} \max(0, P_{\text{grid}}(n|k)), \tag{2.50}$$

which is achieved by respecting two additional constraints,

$$P_{\text{pos}}(n|k) \geq 0, \tag{2.51a}$$
$$P_{\text{pos}}(n|k) \geq P_{\text{grid}}(n|k). \tag{2.51b}$$

Note that the two sides of (2.50) are not equivalent, but by replacing the right hand side of (2.50) in (2.18) with P_{pos} $(n|k)$, the new problem formulation is a relaxed version of the old one. Figure 2.2 illustrates this behaviour.

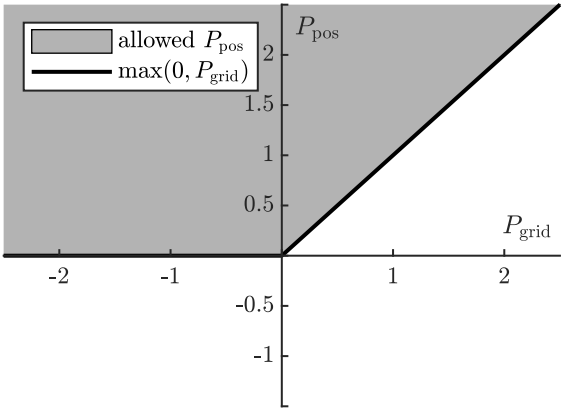

Figure 2.2: Comparison of $\max(0, P_{\text{grid}}(k))$ and its relaxed replacement P_{pos}.

Consequently, if (2.50) holds, the second max-term in (2.18) can be expressed as

$$-\max(0, -P_{\text{grid}}(n|k)) \stackrel{\triangle}{=} P_{\text{grid}}(n|k) - P_{\text{pos}}(n|k). \tag{2.52}$$

Together, the grid costs can then be expressed as

$$\ell_{\mathrm{mon,grid}}^{\mathrm{industry}}(n|k) = \big(c_{\mathrm{grid,buy}} \cdot P_{\mathrm{pos}}(n|k) \ldots + c_{\mathrm{grid,sell}} \cdot (P_{\mathrm{grid}}(n|k) - P_{\mathrm{pos}}(n|k))\big) \cdot T_{\mathrm{s}}. \tag{2.53}$$

Considering (2.53) as part of the cost function, it becomes clear that P_{pos} will be minimized to fulfill (2.50) as long as $c_{\mathrm{grid,buy}} > c_{\mathrm{grid,sell}}$, which is true. Note that with this reformulation, N_{p} additional decision variables and $2N_{\mathrm{p}}$ additional constraints are incorporated into the optimization problem.

Peak Costs The same trick can be used to replace the max-term(s) in (2.19). Namely, it is computationally advantageous to calculate $\ell_{\mathrm{mon,peak}}$ not for every prediction step n individually, but over the whole prediction horizon $n = 0, \ldots, N_{\mathrm{p}}-1$, since $P_{\mathrm{grid,peak}}(n+1|k)$ depends on $P_{\mathrm{grid,peak}}(n|k)$ and only the maximum value of P_{grid} matters. Thus, the peak costs in each optimization step are given by

$$J_{\mathrm{mon}}^{\mathrm{peak}}(k) = c_{\mathrm{grid,peak}} \cdot \max\left(0, \max_{k=0,\ldots,N_{\mathrm{p}}-1}\Big(P_{\mathrm{grid}}(n|k)\Big) - P_{\mathrm{grid,peak}}(k)\right). \tag{2.54}$$

Considering (2.54), the linear programming trick has to be applied twice. Namely, first the inner max-term is replaced by an additional decision variable v,

$$s_{\mathrm{P1}}(k) \stackrel{!}{=} \max_{n=0,\ldots,N_{\mathrm{p}}-1}\big(P_{\mathrm{grid}}(n|k)\big), \tag{2.55}$$

which is s. t. N_{p} constraints

$$s_{\mathrm{P1}}(k) \geq P_{\mathrm{grid}}(n|k) \quad \forall n = 0, \ldots, N_{\mathrm{p}} - 1. \tag{2.56}$$

Note that, in contrast to P_{pos} in (2.51a), only one decision variable and N_{p} constraints are added to the optimization problem for the reformulation of this max-term. Again, (2.55) will be fulfilled in the optimization due to the minimization of the costs.

Using (2.55) in (2.54), the peak costs can be described as

$$J_{\mathrm{mon}}^{\mathrm{peak}}(k) \mathrel{\widehat{=}} c_{\mathrm{grid,peak}} \cdot \max\big(0, s_{\mathrm{P1}}(k) - P_{\mathrm{grid,peak}}(k)\big). \tag{2.57}$$

Again, the max-term in (2.57) is replaced by

$$s_{\mathrm{P2}}(k) \stackrel{!}{=} \max\big(0, s_{\mathrm{P1}}(k) - P_{\mathrm{grid,peak}}(k)\big), \tag{2.58}$$

and constrained to

$$s_{\mathrm{P2}}(k) \geq 0, \tag{2.59a}$$
$$s_{\mathrm{P2}}(k) \geq s_{\mathrm{P1}}(k) - P_{\mathrm{grid,peak}}(k), \tag{2.59b}$$

i. e. for replacement (2.58), only one additional decision variable with only two constraints is needed for the entire prediction horizon. Furthermore, (2.58) will again be fulfilled when minimizing the peak costs, which can now be expressed as

$$\tilde{J}_{\mathrm{mon}}^{\mathrm{peak}}(k) = c_{\mathrm{grid,peak}} \cdot s_{\mathrm{P2}}(k). \tag{2.60}$$

In total, we can formulate the monetary costs for the industry scenario as

$$\tilde{J}_{\mathrm{mon}}^{\mathrm{indus}}(k) = \tilde{J}_{\mathrm{mon}}^{\mathrm{peak}}(k) + \sum_{n=0}^{N_{\mathrm{p}}-1} \tilde{\ell}_{\mathrm{mon,grid}}^{\mathrm{industry}}(n|k) + \ell_{\mathrm{mon,chp}}(n|k) + \ell_{\mathrm{mon,heat}}(n|k), \tag{2.61}$$

whose inclusion in optimization results in a linear programming problem.

In summary, to use the monetary costs with industry pricing as an objective, (2.61) has to be included in the cost function and (2.51), (2.56) and (2.59) have to be included as constraints. This makes a total of $N_{\mathrm{p}} + 2$ additional decision variables and $3N_{\mathrm{p}} + 2$ additional constraints, which is the price for transforming the nonlinear into a linear programming problem.

Optimal Control Problem for the HL-1 Model

In this section, we will formulate the optimal control problem (OCP) when we apply MPC to the HL-1 model with monetary costs (industry pricing) and comfort costs as objectives. We will optimize them as a weighted sum, which is the most common approach. Note that we will build on that for all multi-objective optimization approaches presented in this thesis in Chapters 4 and 5.

With $\tilde{J}_{\mathrm{mon}}^{\mathrm{indus}}$ from (2.61) and J_{comf} calculated as usual from (2.23), the optimal control problem at time step k can be formulated as

$$\mathcal{O}_{\mathrm{HL-1}}^{\mathrm{Mon.(Ind),Comf.}}(k): \min_{\boldsymbol{u}, \boldsymbol{P}_{\mathrm{pos}}, s_{\mathrm{P1}}, s_{\mathrm{P2}}} w_{\mathrm{mon}} \cdot \tilde{J}_{\mathrm{mon}}^{\mathrm{indus}}(k) + w_{\mathrm{comf}} \cdot J_{\mathrm{comf}}(k), \tag{2.62}$$
$$\text{s. t. } (2.8\mathrm{b}),$$
$$(2.46), (2.48), (2.49),$$
$$(2.51), (2.56), (2.59).$$

Note that, due to the quadratic comfort costs, (2.62) is a quadratic programming problem and thus convex, which is very well solvable with today's optimization methods.

2.4 Simulation Studies

In this section, we present multiple simulation studies based on the different building models and objectives presented before. Thereby, we use only single-objective optimization methods, i. e. the different objectives are combined in a weighted sum only. In Section 2.4.1, we first describe the simulation data which is used for all studies. In Section 2.4.2, we shortly introduce the MPC framework PARODIS which has been developed for the purpose of this thesis. In Section 2.4.3, we present the first simulations comparing our MPC approach to state-of-the-art PID and heuristic controls, which are mostly used in current buildings. In Section 2.4.4, we use a hierarchical setting of the models HL-1 and LL-TEMP to demonstrate how the MPC approach can be used for more complex models while keeping computational burdens low. Finally, in Section 2.4.5, we show how a large number of EV charging stations can be controlled using MPC, again making use of a hierarchical model setup.

2.4.1 Simulation Data

For the simulations in this chapter, mostly measurement data from the Honda Research building in Offenbach, Germany from January 2018 - June 2019 have been used. Data is necessary for all disturbances acting on the system. In case of the standard model HL-1, these are the produced power from the RES P_{ren}, the building's power demand P_{dem}, the outdoor air temperature ϑ_{air} and other thermal power disturbances $\dot{Q}_{\mathrm{other}}$.

Since the building's PV system was upgraded within the time-period of this PhD project and no direct measurement data were available, we use measurements of the solar irradiance I_{sol} and estimate P_{ren} from it. Their relationship can generally be described by

$$\tilde{P}_{\mathrm{ren}} = \eta_{\mathrm{PV}} \cdot A_{\mathrm{PV}} \cdot I_{\mathrm{sol}} \cdot (1 - \beta_{\mathrm{PV}}(T_{\mathrm{cell}} - 25\,^{\circ}\mathrm{C})), \tag{2.63}$$

with η_{PV} being the reference efficiency, A_{PV} the surface area, T_{cell} the operating temperature of the cell and a constant $\beta_{\mathrm{PV}} \approx 0.04$ [125]. For the

purpose of this thesis, we neglect the temperature influence, resulting in the linear approximation

$$P_{\text{ren}}(k) = \eta_{\text{PV}} \cdot A_{\text{PV}} \cdot I_{\text{sol}}(k) \tag{2.64}$$

with $\eta_{\text{PV}} = 18.76\,\%$. For most simulation studies, A_{PV} is assumed such that P_{ren} has a maximum peak of 150 kW. Figure 2.3 shows exemplary trajectories for P_{ren}.

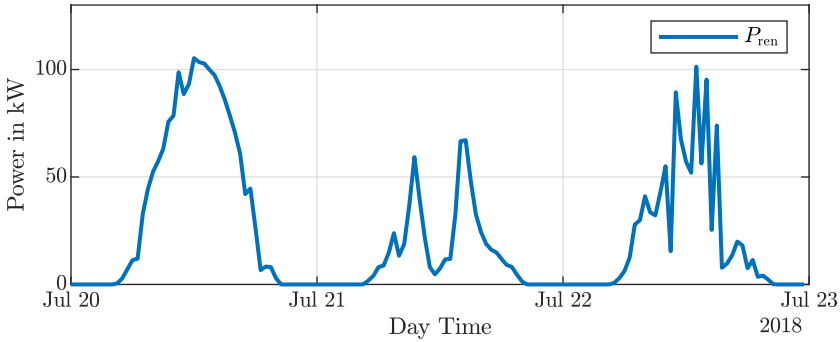

Figure 2.3: Assumed power production P_{ren} of the PV plant from 20th to 23rd of July in 2018.

The building's power demand P_{dem} has been measured directly. However, the power consumption of the cooling machines has been subtracted, since we model their energy consumption explicitly. Overall, P_{dem} regularly exceeds -500 kW. Figure 2.4 shows exemplary measurements of P_{dem}. The outdoor air temperature ϑ_{air} has been measured by a weather station on the building's roof. It varies between $-9.03\,^{\circ}\text{C}$ to $36.8\,^{\circ}\text{C}$. As additional thermal disturbances $\dot{Q}_{\text{other}}$, constant losses to the ground of -12.89 kW are assumed, if not otherwise stated.

In addition to the measurement data, we use historical energy prices from the intraday market if not industry, but intraday pricing is assumed for the monetary costs. Data from the German Bundesnetzagentur is used. In 2018, the mean electricity costs on the intraday market have been $0.0471\ \frac{€}{\text{kWh}}$ with extremes of $-0.03\ \frac{€}{\text{kWh}}$ and $0.161\ \frac{€}{\text{kWh}}$. Note that negative prices are possible if general production from RESs is high in comparison to the demand.

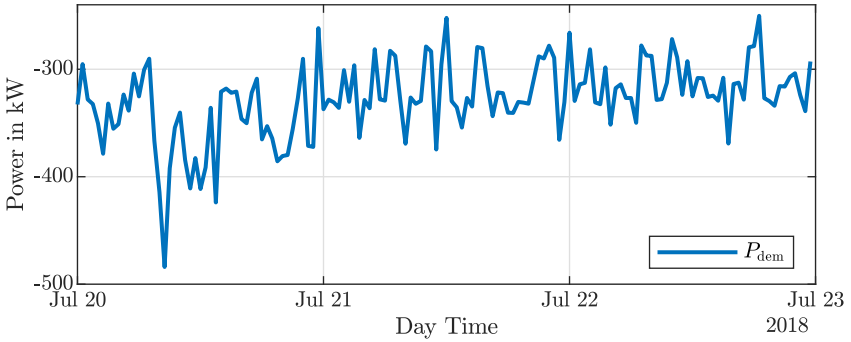

Figure 2.4: The building's power demand P_{dem} from 20th to 23rd of July in 2018.

2.4.2 MPC Framework PARODIS

For implementation and simulation of the models and control schemes developed in this thesis, we implemented a new MATLAB MPC framework, called PARODIS – **Par**eto **o**ptimal MPC framework for **di**stributed **s**ystems [S4]. It is open-source, available on GitHub[2] and has also been published at the IEEE Conference on Control Technology and Applications (CCTA 2021) [S4], from where parts of the description here have been taken. It provides generality to a great extent while maintaining flexibility and easy usage. It is different from other MPC frameworks in that it i) supports distributed (hierarchical) systems, ii) provides convenient interfaces to use large-scale datasets for predicted and actual disturbances, iii) respects scenarios for uncertain disturbances and parameters in a customizable fashion and iv) as its main innovation, provides integrated support for multiple objectives by automated generation of the Pareto front and selection of solutions. Its capabilities for multi-objective optimization (point (iv)) will be explored in more detail in Section 5.3.1. Here, we shortly describe its features and conception for single-objective MPC.

Functionality PARODIS allows fully parameterized (and thus time-variant) descriptions of discrete state space systems in the form

$$x(k+1) = f(x(k), u(k), d(k), k), \tag{2.65}$$

[2] `https://github.com/teamparodis/parodis`, accessed on 09/14/21.

where x, u and d are the state, input and disturbance vectors, respectively. Multiple systems, in PARODIS called *agents*, can be defined and controlled in a distributed (or hierarchical) fashion. Model predictive controllers are defined for every agent by default, whereby the cost functions can be defined arbitrarily, i. e. as in economic MPC. However, controllers could easily be exchanged. There are two specialties of PARODIS. First, it distinguishes not only between predicted and real disturbances d, but it also supports the consideration of *multiple scenarios* in the prediction of disturbances and parameters, thus advocating it for the use of scenario-based stochastic MPC. As sources, either function handles or `csv`-files can be defined, thus allowing for easy import of large data sets for long-term simulations. Furthermore, the incorporation of scenarios in the optimization problem is customizable. Second, it ships with algorithms for multi-objective optimization, i. e. both methods for determining the Pareto front for multiple objectives and methods for automatic selection of a solution, which is repeated at every time step. We elaborate on them in Section 5.3.1. PARODIS utilizes YALMIP [81] and its symbolic variables to formulate the optimization problem, which makes the large selection of solvers supported by YALMIP accessible.[3]

Concept PARODIS is object-oriented. All necessary information is wrapped in an instance of the `Simulation`-class, which may contain multiple instances of the `Agent`- and `TimeSeries`-classes (figures), as illustrated in Figure 2.5.

A simplified flow chart diagram is shown in Figure 2.6. In distributed or hierarchical MPC approaches, agents usually interact with each other and (possibly) *negotiate* what actions they should take in the current time step. In PARODIS, this interaction is called the *negotiation* and is separate from the agents' actual step. There are two options for this negotiation: The first one is for the agents to execute their *negotiation step* in a fixed order. Here, their OCP is solved as usual and a user-defined callback is called afterwards. Using this callback, agents can exchange information freely. The second option is a user-defined interaction using `simulation.negotiationHandle`: This is a user-defined function, where any arbitrary algorithm can be implemented. In this function, all agents, controllers and simulation data can be accessed. After the negotiation, the

[3] See `https://yalmip.github.io/allsolvers/`, accessed on 09/14/21, for an overview.

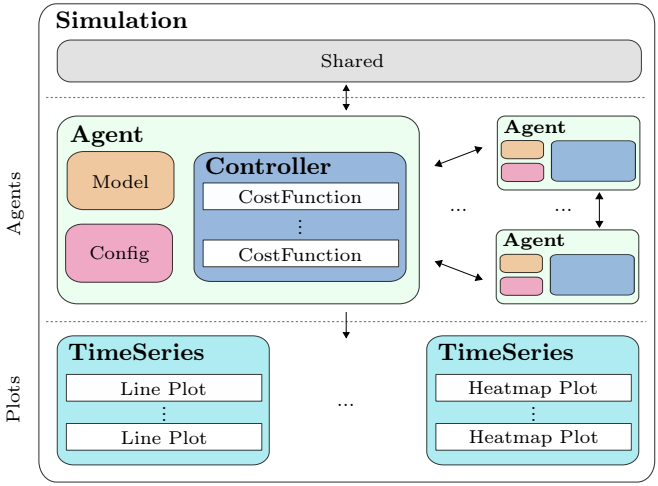

Figure 2.5: Structure of a simulation setup in PARODIS. Boxes with a bold title represent an instance of the respective class. An agent fully defines a system and consists of a model, a `Controller` instance and some optional configuration. Every `TimeSeries` instance creates one figure with an arbitrary number of subplots and may contain elements of any agent. In the simulation's *shared* struct, agents can store information of any kind. It is cleared after every iteration.

actual simulation step is executed. Note that multiple optional callback-functions exist and enable the user to adjust the standard simulation flow, e. g. `agent.callbackMeasureState()` to update an agent's state before optimization.

PARODIS supports different agent sampling times, as long as the first steps of the agents' horizons are multiples of each other. Thus, an execution order is determined at the beginning. Figure 2.7 illustrates this. Within the iteration of a simulation step, every agent's `doStep()`-function is called following this execution order. Thereby, all disturbances and parameters are set. Then, the optimal trajectory is determined, plots are updated and the first input is applied.

The `Controller`-class is responsible for the formulation and solving of the OCP. At the time of writing, three different controller classes are available, the `SymbolicController`, the `ExplicitController` and the `ParetoController`. The `ParetoController` supports all multi-objective

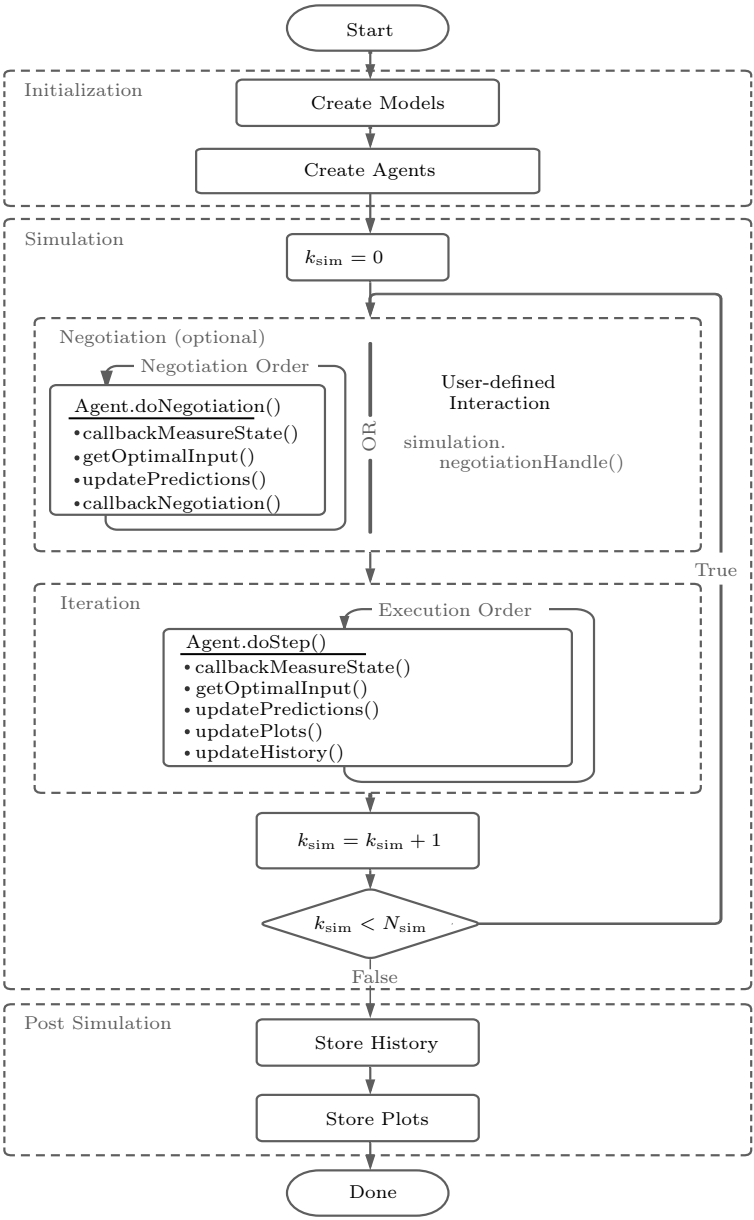

Figure 2.6: Flowchart diagram for PARODIS.

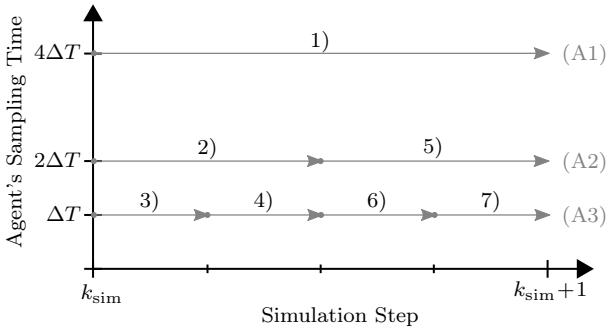

Figure 2.7: Exemplary iteration for a simulation with 3 agents and sampling times $4\Delta T$ (A1), $2\Delta T$ (A2), and ΔT (A3). Slower agents step first. Thus, the execution order would be `[A1, A2, A3, A3, A2, A3, A3]`.

optimization features and is thus omitted here. The `SymbolicController` and `ExplicitController` only differ in their internal operating principle and are thus better suited for different purposes. The `SymbolicController` makes use of YALMIP's `optimizer` feature by pre-compiling a fully parameterized optimization problem, which makes it very efficient for smaller problems. The `ExplicitController` re-builds the OCP at every time step explicitly, which makes it more suitable for larger problems. For instructions on the usage of PARODIS, the reader is referred to [S4] and the wiki of the GitHub repository.

2.4.3 Comparison to State-of-the-Art Control

Today, most buildings' HVAC systems and energy storages such as batteries are still regulated either by simple PID controllers or heuristic rules [1]. Thus, we first want to compare the (E)MPC strategy to such a state-of-the-art approach, which we refer to as the *baseline* solution in the following. The standard HL-1 model is used and monetary costs with industry pricing and comfort costs are considered as objectives. Note that parts of this simulation study have been published in [S1].

Baseline Control Approach We develop a deterministic controller combining *if-then-else* rules and a discrete P controller. Its aim is to maintain the building's temperature ϑ_{b} at the desired set point of 21°C

as close as possible, thereby trying to avoid new peaks by utilizing the stationary battery. Its limitations are that only currently measurable information may be used, i. e. $P_{\mathrm{dem}}(k), P_{\mathrm{ren}}(k), \vartheta_{\mathrm{air}}(k)$ are assumed to be known, while the heating losses to the ground $\dot{Q}_{\mathrm{other}}(k)$ are unknown. Furthermore, no predictive behavior is possible.

For this purpose, we first reformulate and discretize (2.5) to express ϑ_{b} in dependence of the overall heating power $\dot{Q}_{\mathrm{tot}} = \dot{Q}_{\mathrm{chp}} + \dot{Q}_{\mathrm{rad}} + \dot{Q}_{\mathrm{cool}}$,

$$\vartheta_{\mathrm{b}}(k+1) = -\,\mathrm{e}^{\frac{-H_{\mathrm{air}}}{C_{\mathrm{th}}}} \cdot \vartheta_{\mathrm{b}}(k) + \frac{1-\mathrm{e}^{-\frac{H_{\mathrm{air}}}{C_{\mathrm{th}}}T_{\mathrm{s}}}}{H_{\mathrm{air}}} \cdot \dot{Q}_{\mathrm{tot}}(k). \tag{2.66}$$

We choose a simple proportional controller to determine the input $\dot{Q}_{\mathrm{tot}}$ by

$$\dot{Q}_{\mathrm{tot}}(k) = k_{\mathrm{P}} \cdot (\vartheta_{\mathrm{b}}(k) - \vartheta_{\mathrm{set}}), \tag{2.67}$$

where k_{P} is chosen such that the only eigenvalue of (2.66) is at the origin, i. e. we use dead-beat control. Note that this is the best we can do with a P controller to keep ϑ_{b} at the desired temperature.

$\dot{Q}_{\mathrm{tot}}$ is split into $\dot{Q}_{\mathrm{chp}}$, $\dot{Q}_{\mathrm{rad}}$ and $\dot{Q}_{\mathrm{cool}}$ as follows. If $\dot{Q}_{\mathrm{tot}} \geq 0$, the CHP is used as much as possible, since it cheaply produces both heating and electrical power. Only if $\dot{Q}_{\mathrm{chp}}$ is running at its maximum, the gas radiator $\dot{Q}_{\mathrm{rad}}$ is used. If $\dot{Q}_{\mathrm{tot}} < 0$, the building must be cooled, thus $\dot{Q}_{\mathrm{cool}} = \dot{Q}_{\mathrm{tot}}$.

Furthermore, it must be determined whether the stationary battery should be charged, discharged or neither, i. e. P_{charge} has to be defined. Since the battery shall be used for peak-shaving, the following strategy is applied. The battery is only discharged if a new peak is arising. If so, it is discharged only as much as necessary to avoid a new peak. Otherwise, it is charged as much as possible without culminating in a new peak. All energy and (dis-)charging constraints (2.48) are respected, too.

With $\dot{Q}_{\mathrm{chp}}$, $\dot{Q}_{\mathrm{rad}}$, $\dot{Q}_{\mathrm{cool}}$ and P_{charge} determined, the corresponding P_{grid} is given by

$$\begin{aligned} P_{\mathrm{grid}}(k) = -\Big(& P_{\mathrm{dem}}(k) + P_{\mathrm{ren}}(k) + c_{\mathrm{cur}} \cdot \dot{Q}_{\mathrm{chp}}(k) \dots \\ & + \frac{\dot{Q}_{\mathrm{cool}}(k)}{\varepsilon_{\mathrm{c}}} + P_{\mathrm{charge}}(k) \Big). \end{aligned} \tag{2.68}$$

MPC Strategies The OCP for the MPC approaches is the same as (2.62). We use three different settings for the weights. In the first, we put

the focus only on the comfort costs, i. e. $\left(w^{\mathrm{A}}_{\mathrm{mon}},\, w^{\mathrm{A}}_{\mathrm{comf}}\right) = \left(10^{-5},\, 1\right)$. In the second, we use equal weights $\left(w^{\mathrm{B}}_{\mathrm{mon}},\, w^{\mathrm{B}}_{\mathrm{comf}}\right) = \left(0.5,\, 0.5\right)$, which is the same as if no weighting was used. In the third, we use adjusted weights derived a posteriori from a multi-objective optimization study (explained later in Section 5.3.2), $\left(w^{\mathrm{C}}_{\mathrm{mon}},\, w^{\mathrm{C}}_{\mathrm{comf}}\right) = \left(0.2647,\, 0.7353\right)$. We set the prediction horizon to 24 h with 48 steps of 30 min each, which results in a total of 291 decision variables and 915 constraints (due to the reformulation of the monetary costs as described before). As for all simulation studies in this thesis, GUROBI [55] is used as a solver. Using the `SymbolicController`, solving a single optimization problem takes ≈ 0.05 s on an Intel Xeon CPU E5-1607 v4 with 3.10 GHz.

Results The results for a 1-year simulation with data from 2018 as described in Section 2.4.1 are presented in Figure 2.8. The baseline solution performs well in terms of average temperature deviation with 0.11 °C, since dead-beat-control is applied as long as the constraints are not active. Thus, the temperature deviates from the given set point of 21°C mainly due to the uncompensated disturbances $\dot{Q}_{\mathrm{other}}$. However, it performs worst in terms of monetary costs. Since the air conditioning is used regardless of possible new peak costs, the maximum peak rises to 650.25 kW, resulting in unnecessarily high peak and total monetary costs of $\approx$ 362,000 €. However, the MPC approach with focus put only on the comfort clearly outperforms the baseline controller. It manages to keep the temperature nearly perfectly at the desired set point with an average temperature deviation of only 0.0039°C while resulting in still lower overall costs of 358,638 €.

In comparison, the MPC approach with equal weights $w^{\mathrm{A}}_{\mathrm{mon}} = w^{\mathrm{A}}_{\mathrm{comf}} = 0.5$ leads to a significant cost reduction of 36,764 €. The maximum peak is reduced to 384.46 kW, which turned out to be unavoidable due to the maximum demand $P_{\mathrm{dem}} = -630.55$ kW in January. However, since no weighting is applied, the average temperature deviation is uncomfortably high at 0.51 °C. Using the adjusted weight set C instead leads to a good and desirable trade-off between both objectives, i. e. savings of 32,806 € with an average temperature deviation of 0.2430 °C.

Conclusion The results show how (E)MPC can successfully utilize the building's storages (thermal capacity, stationary battery) to avoid unnecessarily high peaks while controlling the temperature. However, appropriate weighting is essential to obtain a suitable compromise.

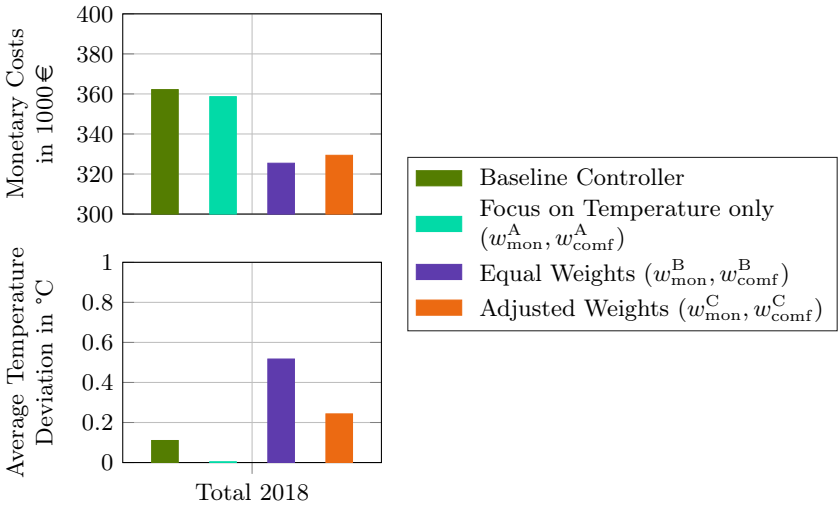

Figure 2.8: Simulation results for 2018. An initial peak of 250 kW has been used, for which the peak costs are not included. For better comprehension, the average temperature deviations are displayed instead of the actual optimization costs J_{comf}.

2.4.4 Hierarchical Control of Temperature Zones

The models presented in Section 2.3.1, especially the higher level models, are a strong simplification of a real building. The simplification is necessary to keep model equations at a complexity low enough to keep the optimization problem, which results from the application of MPC, tractable. However, we propose a hierarchical setup to take advantage of the optimal control strategies on all essential entities on the higher level model, while more detailed lower level models of single entities can distribute allocated total powers. In this simulation study, we use a hierarchical setup of the building's temperature zones, illustrated in Figure 2.9.

Control Strategy For the higher level system, we again use model HL-1. However, in contrast to Section 2.4.3, there are two differences. First, we assume no heating disturbances (losses to the ground), i. e. $\dot{Q}_{\text{other}} = 0$. This is only for simplicity. (Otherwise, we would have to distribute them between the single temperature zones on the lower level.) Second, we additionally

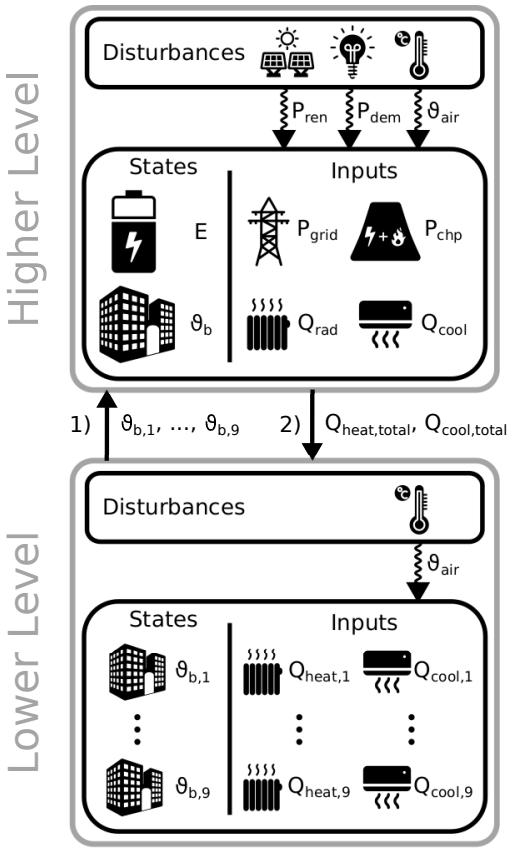

Figure 2.9: Higher and lower level models for the hierarchical control of the building's temperature zones. The higher level first measures all zone temperatures $\vartheta_{\mathrm{b},1}, \ldots, \vartheta_{\mathrm{b},9}$ from the lower level and updates the averaged building temperature ϑ_{b}. Then, it solves its OCP and communicates the total heating and cooling powers, $\dot{Q}_{\mathrm{heat,total}}$ and $\dot{Q}_{\mathrm{cool,total}}$, to the lower level, which distributes them between the 9 temperature zones.

respect the battery costs (2.32), but only to prevent unnecessary charging and discharging. Thus, while we use the adjusted weights $\left(w^{\mathrm{B}}_{\mathrm{mon}},\, w^{\mathrm{B}}_{\mathrm{comf}}\right) = \left(0.2647,\, 0.7353\right)$ for the monetary and comfort costs, we choose the weight on the battery degradation comparatively low at $w^{\mathrm{B}}_{\mathrm{bat}} = 0.01$.

For the lower level system, we use model LL-TEMP with $\dot{Q}_{\mathrm{other},i} = 0\ \forall\, i = 1 \dots 9$. The only objective is (2.45). However, since the lower level is supposed to distribute the powers provided from the higher level, we have to add the constraints

$$\sum_{i=1}^{9} \dot{Q}_{\mathrm{heat},i} = \dot{Q}_{\mathrm{rad}} + \frac{P_{\mathrm{chp}}}{c_{\mathrm{cur}}}, \tag{2.69a}$$

$$\sum_{i=1}^{9} \dot{Q}_{\mathrm{cool},i} = \dot{Q}_{\mathrm{cool}}, \tag{2.69b}$$

$$0 \leq \dot{Q}_{\mathrm{heat},i} \leq \dot{Q}_{\mathrm{rad}} + \frac{P_{\mathrm{chp}}}{c_{\mathrm{cur}}} \quad \forall\, i = 1 \dots 9, \tag{2.69c}$$

$$\dot{Q}_{\mathrm{cool}} \leq \dot{Q}_{\mathrm{cool},i} \leq 0 \quad \forall\, i = 1 \dots 9. \tag{2.69d}$$

Note that if large differences between higher and lower level models would exist, the lower level's optimization problem could be kept feasible by adding slack variables in (2.69a) and (2.69b), as we will do in Section 2.4.5 for the EV models.

Overall, the resulting OCP on the lower level is

$$\begin{aligned} \mathcal{O}_{\mathrm{LL-TEMP}}\colon \min_{\boldsymbol{u}_{\mathrm{LLT}}}\ & J_{\mathrm{comf,LL}}(k), \\ \text{s.t. } & (2.13), (2.47), (2.69). \end{aligned} \tag{2.70}$$

Results Figure 2.10 shows the trajectories of the higher level. Figure 2.11 shows the corresponding temperatures and thermal powers of the single zones as heat maps.

In summary, the results show that the hierarchical approach can successfully be used to control multiple single temperature zones by the allocated total heating and cooling powers. In this way, multiple objectives and entities can be respected at the higher level and the computational burden can be kept low enough to use more advanced optimization methods like the ones we will introduce in Chapter 4.

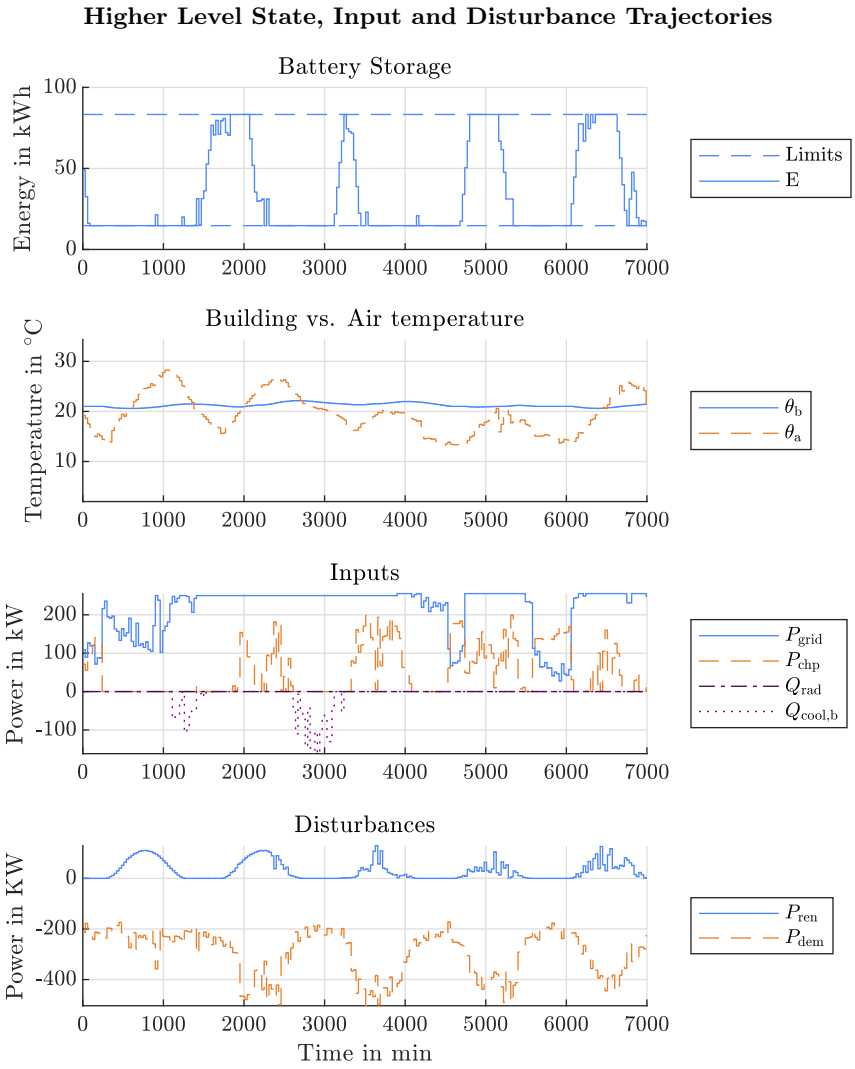

Figure 2.10: Trajectories of the higher level system for the 5 day simulation with data from June 2018. The battery is kept at its minimum and only charged and discharged to avoid new peaks of P_{grid}. The building temperature fluctuates slightly around the desired 21 °C.

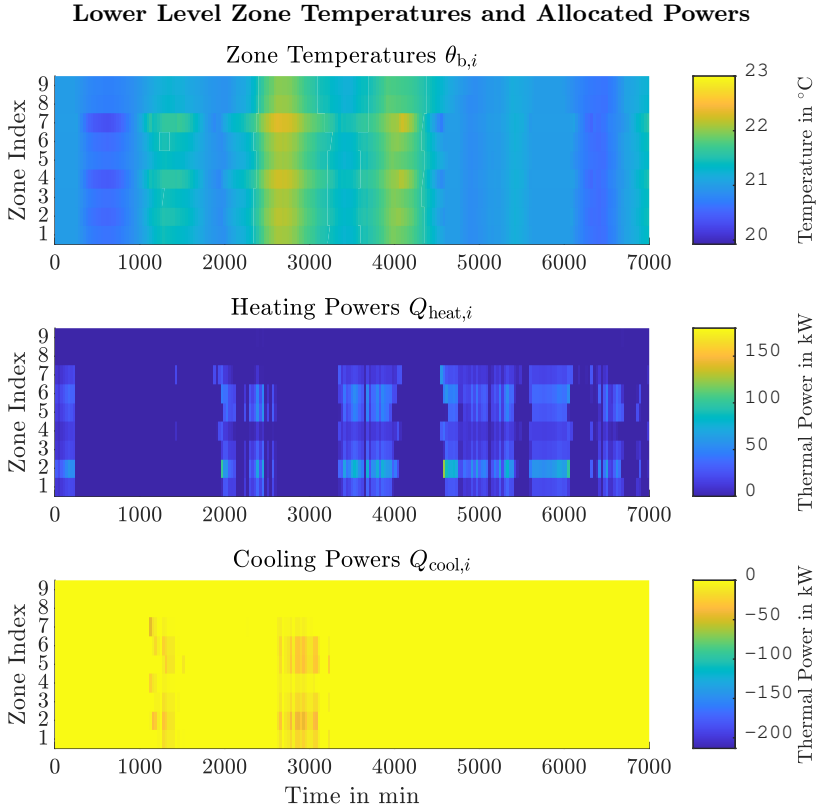

Figure 2.11: Heat maps of the lower level system, i. e. the zone temperatures $\vartheta_{b,i}$ as well as the single heating and cooling powers, $\dot{Q}_{heat,i}$ and $\dot{Q}_{cool,i}$. The absolute powers for zones 8 and 9 are very low due to their small thermal capacities in comparison to zone 1-7.

2.4.5 Electric Vehicle Charging

As the last simulation study with single-objective MPC only, we use a hierarchical setup to control 30 EV charging stations connected to the building. Namely, we use model HL-2 on the higher and model LL-EV on the lower level as illustrated in Figure 2.12. Note that the results presented in this section partly have been derived in the process of a Master's thesis [39], which also led to the publication [S9].

Simulation Data For the building's power demand, PV production and air temperature, data from 2018 is used as described in Section 2.4.1. Since no data for EVs from the real building site is available, data from the NASA Jet Propulsion laboratory and Adaptive Charging Network of the California Institute of Technology [75] is used to derive probability distributions. Namely, a Gaussian mixture model is fitted to the available data, from which artificial charging sessions can then be drawn.

In general, a session at a charging station i is characterized by the EV's time of arrival ToA_i, its time of departure $\mathrm{ToD}_i = \mathrm{ToA}_i + \mathrm{T}_{\mathrm{sojourn},i}$, its initial energy $E_{\mathrm{EV,init},i}$, its total capacity $C_{\mathrm{EV},i}$ and the desired total energy $E_{\mathrm{EV,des},i}$. As predictions, N_{scen} scenarios are drawn from the probability distributions and averaged. Note that for the time of departure, we use estimations $\mathrm{ToD}_{\mathrm{est},i} \sim \mathcal{N}(\mathrm{ToD}_i, (0.5\,\mathrm{h})^2)$, i. e. we assume that the EV user estimates his departure with a standard deviation of 0.5 h. We assume $C_{\mathrm{EV},i} = 50\,\mathrm{kWh}$ and $P_{\mathrm{EV,i,max}} = 10\,\mathrm{kW}$ for all EVs. On average, the required energy is 12 kWh and 1.35 sessions occur per charging station.

MPC Control Strategies Similar to the hierarchical setting for the temperature zones, the higher level model determines the aggregated charging power P_{EV} for all vehicles, which is then distributed on the lower level. However, here we optimize the higher level two times, which is due to a form of *negotiation* between the two levels. Namely, the lower level may deviate from the allocated charging power P_{EV} and use the adjusted power P'_{EV} instead. If so, the optimization on the higher level is repeated with $P_{\mathrm{EV}} = P'_{\mathrm{EV}}$, as explained below.

For the higher level, we respect the cost functions for the monetary costs, comfort costs, degradation of the stationary battery and, in addition to before, the degradation of the aggregated EV battery $J_{\mathrm{bat}}^{\mathrm{EV}}$ from (2.42).

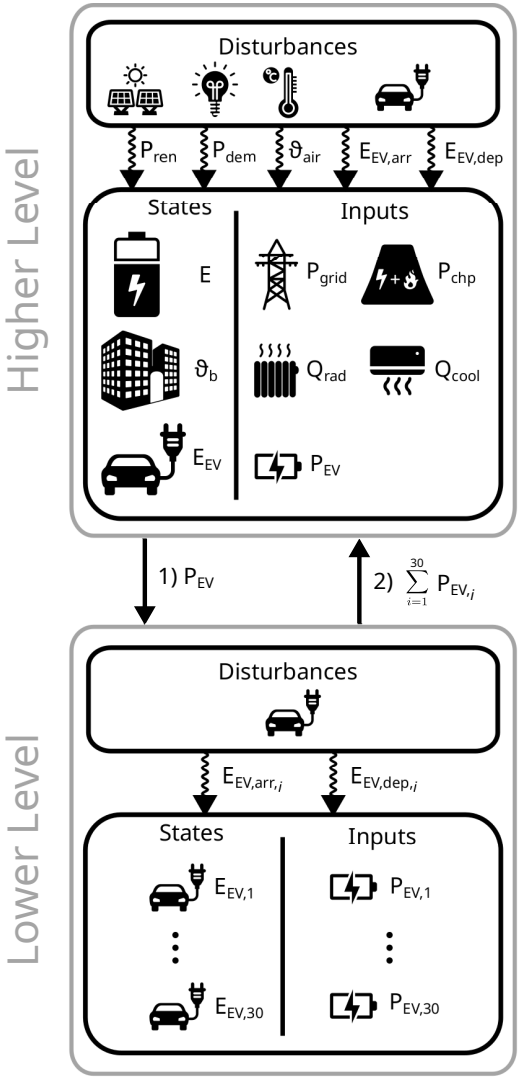

Figure 2.12: Higher and lower level models for the control of 30 EV charging stations. The higher level provides the lower level an aggregated total EV charging power P_{EV}, which is then distributed between the individual EVs. Afterwards, the lower level updates the higher level with the actually realized charging powers $P_{\mathrm{EV},i}$, which might deviate from the plan due to various single constraints on the lower level.

The EV charging is not incentivized in the objective function, but ensured by a time-varying lower constraint on E_{EV},

$$E_{\mathrm{EV,min}}(k) \leq E_{\mathrm{EV}}(k) \leq C_{\mathrm{EV}}(k) \quad \forall\, k = 1 \dots N_{\mathrm{pred}}. \tag{2.71}$$

The lower bound $E_{\mathrm{EV,min}}(k)$ is constructed as a piecewise linear tube rising from the initial level to 60 % of the maximum capacity, while avoiding unnecessary steep rises in dependence of the sojourn time $\mathrm{T}_{\mathrm{sojourn},i}$. Note that in addition to (2.71), the actual charge satisfaction with energy levels $\approx 90\,\%$ is achieved due to the assumption that cars leave with said 90 % at their ToD_i. Thus, on average, the aggregator charges all cars higher than the required 60 %. This way, flexibility in the charging process is maintained.

The constraints on the charge rates are time-varying, too, and depend on the number of EVs available, i. e.

$$-P_{\mathrm{EV,max}}(k) \leq P_{\mathrm{EV}}(k) \leq P_{\mathrm{EV,max}}(k) \quad \forall\, k = 0 \dots N_{\mathrm{pred}} - 1. \tag{2.72}$$

In total, the first OCP for the higher level is given by

$$\begin{aligned} \mathcal{O}^{\mathrm{1st}}_{\mathrm{HL}-2}(k)\colon \quad & \min_{\boldsymbol{u}_{\mathrm{HL2}}, \boldsymbol{P}_{\mathrm{pos}}, s_{\mathrm{P1}}, s_{\mathrm{P2}}} \; w_{\mathrm{mon}} \cdot \tilde{J}^{\mathrm{indus}}_{\mathrm{mon}}(k) + w_{\mathrm{comf}} \cdot J_{\mathrm{comf}}(k) \dots \\ & \qquad + w^{\mathrm{stat}}_{\mathrm{bat}} \cdot J^{\mathrm{stat}}_{\mathrm{bat}}(k) + w^{\mathrm{EV}}_{\mathrm{bat}} \cdot J^{\mathrm{EV}}_{\mathrm{bat}}(k), \qquad (2.73) \\ \text{s. t. } & (2.9), \\ & (2.46), (2.48), (2.49), \\ & (2.71), (2.72). \end{aligned}$$

For this simulation study, the weights have been set to $\big(w_{\mathrm{mon}},\, w_{\mathrm{comf}},\, w^{\mathrm{stat}}_{\mathrm{bat}},\, w^{\mathrm{EV}}_{\mathrm{bat}}\big) = \big(1,\, 3,\, 0.2,\, 0.2\big)$. If the lower level deviates from the allocated P_{EV}, the second round OCP is the same as the first one, but with an additional constraint, i. e.

$$\begin{aligned} \mathcal{O}^{\mathrm{2nd}}_{\mathrm{HL}-2}(k)\colon \; & \mathcal{O}^{\mathrm{1st}}_{\mathrm{HL}-2}(k) \qquad (2.74) \\ & \text{s. t. } P_{\mathrm{EV}}(k) = P'_{\mathrm{EV}}(k) \quad \forall\, k = 0 \dots N_{\mathrm{pred}} - 1. \end{aligned}$$

For the lower level, we use model LL-EV. Its sole task is to distribute the allocated power P_{EV} between the single EVs using MPC, mirroring the goals of the higher level. Thereby, constraints on the EVs' energy levels and charging powers similar to the higher level apply,

$$E_{\mathrm{EV,min},i}(k) \leq E_{\mathrm{EV},i}(k) \leq C_{\mathrm{EV},i}(k) \qquad \forall\, k = 1 \dots N_{\mathrm{pred}}, \tag{2.75}$$

$$-P_{\mathrm{EV,max},i}(k) \leq P_{\mathrm{EV},i}(k) \leq P_{\mathrm{EV,max},i}(k) \quad \forall\, k = 0 \dots N_{\mathrm{pred}} - 1. \tag{2.76}$$

Additionally, we have to constrain the sum of all charging powers $P_{\mathrm{EV},i}$ to the allocated power P_{EV}. However, the constraints (2.75) and (2.76) might make this impossible. Thus, we add a slack variable $s_{\mathrm{EV}}(k)$ which allows deviations, i. e.

$$P_{\mathrm{EV}}(k) = \sum_{i=1}^{30} P_{\mathrm{EV},i}(k) + s_{\mathrm{EV}}(k) \quad \forall\, k = 0 \dots N_{\mathrm{pred}} - 1. \tag{2.77}$$

The slack variable is included in the objective function with a high weighting factor $w_{\mathrm{slack}} = 2000$. This value is high enough to ensure that s_{EV} is only used if the problem is infeasible otherwise, but low enough to avoid numerical issues. Using the charge satisfaction costs from (2.43), the OCP of the lower level is then given by

$$\begin{aligned} \mathcal{O}_{\mathrm{LL-EV}}(k)\colon \min_{\boldsymbol{u}_{\mathrm{LLEV}}} & \sum_{i=1}^{30} J_{\mathrm{Soc}}^{\mathrm{EV,i}}(k) + J_{\mathrm{bat}}^{\mathrm{EV,i}}(k) + \sum_{n=0}^{N_{\mathrm{p}}-1} w_{\mathrm{slack}} \cdot s_{\mathrm{EV}}(k), \\ \text{s. t. } & (2.10), \\ & (2.75), (2.76), (2.77). \end{aligned} \tag{2.78}$$

Baseline Control Approach To assess the benefits of our MPC approach, we compare it to the use of rule-based controllers for the higher and/or lower level. On the higher level, the rule-based controller is mostly the same as in Section 2.4.3. Namely, the total thermal power $\dot{Q}_{\mathrm{tot}}$ is determined by the dead-beat control (2.67) and then split into $\dot{Q}_{\mathrm{chp}}$, $\dot{Q}_{\mathrm{rad}}$ and $\dot{Q}_{\mathrm{cool}}$. The only difference is that, in addition, the EV charging power P_{EV} is simply determined as the maximum possible power for all EVs. Thus, P_{grid} is given by

$$\begin{aligned} P_{\mathrm{grid}}(k) = -\Big(& P_{\mathrm{dem}}(k) + P_{\mathrm{ren}}(k) + c_{\mathrm{cur}} \cdot \dot{Q}_{\mathrm{chp}}(k) \dots \\ & + \frac{\dot{Q}_{\mathrm{cool}}(k)}{\varepsilon_{\mathrm{c}}} + P_{\mathrm{charge}}(k) + P_{\mathrm{EV}}(k) \Big). \end{aligned} \tag{2.79}$$

On the lower level, the rules depend on the higher level control. If we use the rule-based controller on the higher level, all cars are simply charged as much as possible without violating any constraints. If MPC is used on the higher level, the available charging power $P_{\mathrm{EV}}(k)$ is split between all cars proportionally to how much energy they need until they are fully charged. Similarly, if $P_{\mathrm{EV}}(k) < 0$, then the cars with the highest energy requirements are discharged the least.

Results We compare three different combinations, i. e. the proposed MPC approaches on both levels (denoted as MPC / MPC), only MPC on the higher level and rule-based control on the lower level (MPC / RBC) and rule-based control on both levels (RBC / RBC). Figure 2.13 shows the results for the 1-year simulations. Note that the average charge satisfaction is determined as in (2.43) with $E_{\mathrm{EV,des},i} = 0.9 \cdot C_{\mathrm{EV},i}$ for all EVs. For better interpretability, the battery degradation is calculated a posteriori with the rainflow cycle-counting algorithm [140], for which we assume a constant battery temperature of 25°C.

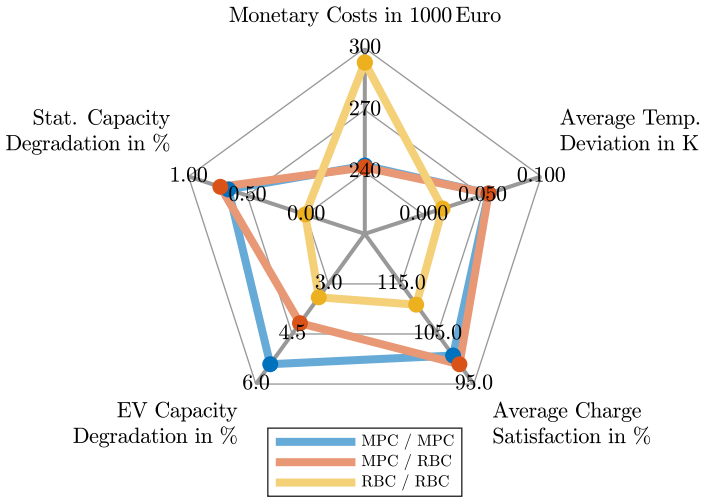

Figure 2.13: Results of 1-year simulations with different control strategies, denoted in the form of (higher level / lower level). An initial peak of 250 kW has been used, for which the peak costs are not included. Note that the axis for the average charge satisfaction has been inverted for better interpretability, i. e. values closer to the center are better. The numerical value can also be found in the appendix in Table A.1.

The results show that our MPC approach on the higher level successfully utilizes both the stationary and EV batteries to avoid unnecessary peak costs, resulting in significantly lower overall monetary costs, 243,037 € for (MPC / MPC) instead of 293,040 € for (RBC / RBC). If rule-based control is used on the lower level in combination with MPC (MPC / RBC), the monetary costs are even slightly lower at 242,228 €. However, this is because the MPC on the lower level occasionally demands more charging

power than the higher level MPC provides in the first step. This is necessary to satisfy the energy constraints for EVs which arrive with a very low state of charge. Thus, the average charge satisfaction is higher for (MPC / MPC) than for (MPC / RBC), i. e. 100.79 % vs. 97.47 %. The combination of rule-based control on both levels has the highest average charge satisfaction at 110.80 % because it generally charges as much as possible. Note that charge satisfactions greater than 100 % appear if the desired state of charge of 90 % is exceeded.

The results also show that if rule-based control is used at the higher level (RBC / RBC), the stationary battery is barely used and the EV batteries are never discharged, which results in the lowest degradation values for both. Furthermore, for (MPC / MPC) the degradation for the EV batteries is higher than for (MPC / RBC) because they are generally charged more and the stationary battery is used less instead.

Conclusion The simulation results show that the use of MPC is highly beneficial in terms of monetary costs in comparison to simple rule-based control while still achieving good results for the remaining objectives. Peaks can successfully be shaved and the EV batteries can be utilized as buffers while ensuring charge satisfaction. Even if a simple rule-based distribution is used on the lower level, the higher level MPC shows strong benefits, thus advocating the use of hierarchical model structures if computational expenses are too high otherwise.

2.5 Summary

In this section, an overview of the energy management problem for buildings and microgrids has been given first. MPC has been introduced as the most promising control strategy. Then, several linear state space models with different complexities have been derived to model the most essential parts of the energy management system of a real-world building. Mainly, electricity and the building's temperature are coupled by heating, ventilation, and air conditioning (HVAC) units and a combined heat and power plant (CHP). The resulting ODEs depend on controllable actuators such as a the CHP and HVAC units, the connection to the power grid etc., as well as uncontrollable influences such as the power production of a PV plant, the building's regular energy demand and the air temperature. Additionally, models to

incorporate electric vehicle charging stations into the energy management system have been proposed. We showed how for example nonlinear peak costs can be reformulated to obtain well solvable complex optimization problems. Simulation studies showed that the state space models can be successfully utilized, optionally in a hierarchical setup, to control the building's energy flows. Thereby, only single-objective economic MPC has been used by minimizing weighted sums of all considered objectives, already showing advantages over regular control schemes.

3 Importance of Forecasting Accuracy

In this chapter, we address the mostly neglected influence of the predictions used for the MPC of a microgrid. To this end, we first summarize the current state of research. Then, we use the main model HL-1 from Chapter 2 and conduct an extensive simulation study with real-world weather forecasts of the solar irradiance, which are used for predictions of the PV power production. Thereby, we empirically analyze the relationship between prediction errors and cost increases.

Note that parts of this chapter have already been presented in

[S5] T. Schmitt, T. Rodemann, and J. Adamy. The cost of photovoltaic forecasting errors in microgrid control with peak pricing. *Energies*, 14(9), 2021.

3.1 Introduction

Throughout Chapter 2, we assumed perfect predictions of all disturbances in the microgrid (except for the electric vehicles (EVs), for which a scenario-based MPC approach has been used). In the literature, either perfect predictions are utilized, too, or erroneous values from mathematical models are used. Then, robust or stochastic MPC approaches are frequently used to handle the prediction errors, as summarized in Section 2.2.2. However, the urgency for handling uncertainties depends on their impact, which again might depend heavily on the respective application. Specifically, the most common objective, monetary cost, varies with different pricing structures. With the high peak costs encountered in German industry pricing, for example, forecasting errors can have serious consequences. Thus, a systematic analysis of how (realistic) forecasting errors affect the control outcome is necessary.

One important source of uncertainties in modern microgrids is the use of PV plants as RESs. While their power production can be predicted from widely available weather forecasts [2, 74], simulation studies with real-world predictions are comparatively rare. Mostly, strategies to handle uncertainties are presented and the effect of the forecasting errors themselves is only investigated in the evaluation of the new strategy.

Thus, this chapter intends to address the gap in research on the effect of realistic uncertainties in microgrid control if unhandled, especially for the challenging case of peak costs and tries to answer the following questions:

- Are state of the art weather predictions already sufficient to reduce demand peaks?
- What is the correlation between prediction accuracy and resulting cost?
- What is the time horizon in which the prediction accuracy is relevant?

To this end, we first review the current state of research.

3.2 Related Work

An interesting example of an application using historical weather forecasts as predictions for the PV production is [106]. The uncertainties are accounted for by a stochastic MPC approach with chance constraints. The stochastic MPC outperforms a deterministic MPC, but the relationship between the forecasting error and the resulting (additional) energy use remains unclear. The effect of PV and wind power production forecasts on their integration in the German power grid is considered in [76]. Namely, the resulting control reserve power, the regime switches per week (i.e. how often a storage has to change between charging and discharging) and the storage energy losses are evaluated. However, the authors come to the conclusion that today's forecasts are sufficient and further improvement has no significant effects. In [120], an affine arithmetic method for microgrid control is introduced and compared, among others, to MPC methods. Three different levels of artificial forecasting errors are considered, for which the error increases linearly within the time horizon (but with three different slopes). The numerical results show that for regular MPC, costs increase significantly with the error level. In [149], a residential home with plannable loads and PV and wind energy sources is controlled. Five different levels

of uniformly distributed forecasting errors from 6 % to 30 % are respected, resulting in increasing costs. In [70], a microgrid with intraday pricing is considered. Simulation results suggest a perfectly linear relationship between a forecasting error varied between 19 % and 21 % and the costs. However, this cost increase seems negligible in comparison to additional costs from forecasting errors on electricity prices. In [88], a microgrid is controlled in a rolling horizon fashion with forecasts for both PV production and load demand. The authors scale the prediction error and show that the resulting operation costs increase stronger than linear with the normalized root mean square error of the forecasts. Costs arise from fuel consumption and the number of start-ups of generators. In [148], a microgrid with forecasts for electricity prices, load demand, PV and wind power generation is controlled using MPC. The forecasting error for PV generation is varied from 8 to 24 %. However, the results suggest no significant effect. In [58], an AC/DC microgrid model with a wind turbine and a PV plant is controlled in real-time. Reference points for power generation and use under uncertain forecasts are derived by a robust optimization of a mixed integer linear programming problem [16]. Forecast uncertainties are respected by possible variations of ±2 % of the power generation. Simulation results show an increase of total costs over the 200 s simulation period of 12.45 % for the worst-case scenario. In [147], a microgrid with multiple distributed generators and storages is controlled. Using dual decomposition, the optimization problem can be solved by a distributed algorithm. Uncertainties in wind forecasts are respected in a robust fashion by minimizing the worst-case transaction cost. However, no analysis of the cost impact in dependence of the uncertainty is conducted. In [85], a closed loop robust MPC approach is developed for the control of a building with uncertain heat gains. The effect of different uncertainty levels on thermal discomfort and energy consumption is evaluated for the proposed approach and the use of open loop robust MPC and only regular MPC. The robust MPC approaches are effective in reducing thermal comforts, however leading to an expense of energy consumption. In [84], this closed loop robust MPC approach is used for temperature control of a single room. In a comparison with regular MPC and a rule-based controller, it shows superior results only for an intermediate level of uncertainty (30 - 67 %). For the case of less uncertainty, the regular MPC is advantageous and for a higher uncertainty the rule-based controller is. In [142], different MPC variants are compared for the temperature control of a building. While the simulated thermal sensation of the inhabitants deteriorates with an increasing level of uncertainty for all control schemes, the energy consumption shows no clear

trend and varies by less than 1 %. In [83], a stochastic MPC approach is used to control the heating, ventilation and air conditioning (HVAC) unit and zone temperature of a building. For the uncertain loads (outside air temperature and occupancy), probability distributions are derived from historical data. Then, the expected energy consumption is minimized while satisfying chance constraints. The stochastic MPC approach is compared to a standard MPC, which uses expected values of the loads. The results suggest superiority of the stochastic MPC, if the uncertainty level is not too high, i. e. if the forecasting errors are scaled by a factor ≤ 5. In [46], stochastic MPC with explicit chance constraints is used for demand response in a residential energy management system. Uncertainties in PV power production and ambient temperature are modeled as normally distributed. A doubling of the standard deviation of the PV forecasting error leads to an increase in the required grid power of $\approx 43\,\%$.

While most results show a significant increase in cost for increasing errors, its form remains unclear [46, 58, 83–85, 106, 120, 149]. Or, if the relationship is investigated, peak costs are not included in the electricity pricing scheme [70, 88]. Real forecasting data is used in [88, 106, 147], while most works only use artificial errors [46, 58, 70, 76, 84, 85, 120, 142, 148, 149]. Furthermore, there is no investigation of the necessary time horizon length for predictions, i. e. on which time scale the prediction accuracy is relevant.

3.3 Simulation Study

To answer the questions raised in Section 3.1, we empirically analyze the effect of prediction errors on the monetary costs of our main microgrid model HL-1 with industry peak costs. We use real-world forecasts for the solar irradiance, translate them into predictions for P_{ren} and vary the prediction error artificially.

3.3.1 MPC Formulation

The OCP differs from the standard problem described in Section 2.3.3 in two ways, i. e. we use a different prediction horizon and a simplified version of the battery degradation as the third objective.

The prediction horizon still has an overall length of 24 h, but is split into 56 steps. However, since forecasting accuracy decreases with time, we sample

the first 8 h window more densely than the middle and last interval,

$$T_\mathrm{s}(k) = \begin{cases} 0.25\,\mathrm{h} & \text{if } k \in [0,\, 31], \\ 0.5\,\mathrm{h} & \text{if } k \in [32,\, 47], \\ 1\,\mathrm{h} & \text{if } k \in [48,\, 55]. \end{cases} \tag{3.1}$$

For the battery degradation, we neglect the influences of the charge rate and the average state of charge and punish only the energy throughput as in (2.29), i. e.

$$J_\mathrm{bat}^\mathrm{simp}(k) = \sum_{n=0}^{N_\mathrm{p}-1} \frac{|P_\mathrm{charge}(n|k)|}{C_\mathrm{bat}} \cdot T_\mathrm{s}(n|k). \tag{3.2}$$

The overall objective function is then given by

$$J_\mathrm{HL-1}^\mathrm{Pred.error}(k) = w_\mathrm{mon} \cdot \tilde{J}_\mathrm{mon}^\mathrm{indus}(k) + w_\mathrm{comf} \cdot J_\mathrm{comf}(k) + w_\mathrm{bat} \cdot J_\mathrm{bat}^\mathrm{simp}(k), \tag{3.3}$$

with $[w_\mathrm{mon},\, w_\mathrm{comf},\, w_\mathrm{bat}] = [0.2,\, 0.7,\, 0.1]$. Note that w_bat is chosen large enough to prevent the arbitrary charging and discharging of the battery, but small enough to keep the battery use for peak shaving rewarding. The resulting OCP is then given by

$$\begin{aligned} \mathcal{O}_\mathrm{HL-1}^\mathrm{Pred.error}(k)\colon \quad & \min_{\boldsymbol{u}, \boldsymbol{P}_\mathrm{pos}, s_\mathrm{P1}, s_\mathrm{P2}} \quad J_\mathrm{HL-1}^\mathrm{Pred.error}(k), \\ \text{s. t. } & (2.8\mathrm{b}), \\ & (2.46), (2.48), (2.49), \\ & (2.51), (2.56), (2.59). \end{aligned} \tag{3.4}$$

3.3.2 Data Sources and Handling

For the real disturbances, we use the same data as described in Section 2.4.1, only for a different time period, i. e. for 30 days starting from the 15$^\mathrm{th}$ of April, 2020. However, weather forecasts of the solar irradiance I_sol from a commercial weather service are used, from which predictions for P_ren are derived as in (2.64), i. e. we assume a linear relationship. Furthermore, we assume a larger PV plant, such that the effective power demand $P_\mathrm{ren} + P_\mathrm{dem}$ has negative peaks on most days, see Figure 3.1. This results in a range from a maximum effective demand of 349.94 kW to a maximum overproduction of 617.61 kW. We assume perfect knowledge of the building demand P_dem and outside air temperature ϑ_air and $\dot{Q}_\mathrm{other} = 0$. Weather forecast updates are available every ≈ 65 min. Figure 3.2 shows the true trajectory of I_sol for two days together with forecasts from different points in time.

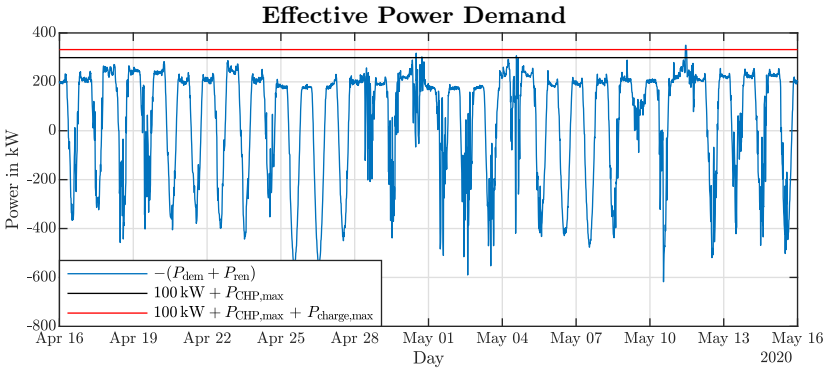

Figure 3.1: Effective power demand, i. e. building consumption and PV production summed, for the simulated time horizon. The black line shows the limit above which the CHP is insufficient to keep a peak of 100 kW. The red line shows the limit if the battery is discharged at its maximum, i. e. the theoretic demand limit for which the initial peak of 100 kW could be held. On May 11$^{\text{th}}$, a minimum peak of $P_{\text{grid}} \geq 118\,\text{kW}$ is unavoidable, even if the CHP and the battery are operated at their maximum.

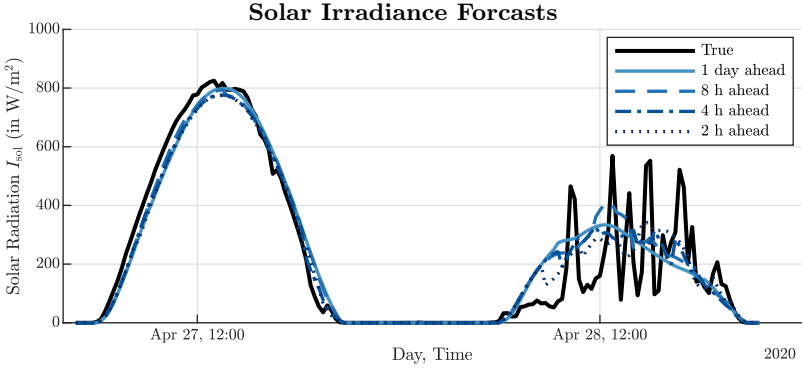

Figure 3.2: Exemplary forecasts (blue lines) and measurement (black line) of solar irradiance for two days in April 2020. For a sunny day (Apr 27), the forecasts do not change significantly over time and are reasonably accurate apart from a small delay. For a cloudy day (Apr 28), the day-ahead forecasts smoothen the variations in I_{sol}. The closer a forecast is, the more it resembles the ups and downs. However, even with only 2 h ahead, the prediction error is still significant.

Artificial Errors

To systematically analyze the effect of different prediction errors, we introduce artificial errors by scaling the actual prediction errors linearly. Let $P_{\text{ren}}(k)$ be the real value at time step k and $P_{\text{ren}}(n|k)$ the value of $P_{\text{ren}}(n+k)$ predicted at time step k (with $n \in [0,\, N_{\text{pred}}-1]$). Then, the new prediction with an error scale of s_{err} is

$$P_{\text{ren}}^{s_{\text{err}}}(n|k) = \min\Bigg(\max\Big(P_{\text{ren}}(n+k) + s_{\text{err}} \cdot \underbrace{\big(P_{\text{ren}}(n+k) - P_{\text{ren}}(n|k)\big)}_{\text{regular prediction error } e_{\text{ren}}(k)},\; P_{\text{ren}}^{\max}\Big),\; 0\Bigg). \quad (3.5)$$

Note that we limit predictions to physical limitations, i. e. $0 \leq P_{\text{ren}}^{s_{\text{err}}} \leq P_{\text{ren}}^{\max}$. Thus, we use the resulting mean absolute error within the prediction horizon for the subsequent analyses. It is calculated as

$$e_{\text{avg}}(s_{\text{err}}) = \frac{1}{N_{\text{sim}} \cdot N_{\text{pred}}} \sum_{k=1}^{N_{\text{sim}}} \sum_{n=0}^{N_{\text{pred}}-1} |P_{\text{ren}}^{s_{\text{err}}}(n|k) - P_{\text{ren}}(n+k)|, \quad (3.6)$$

where N_{sim} is the total number of simulation steps.

Treatment of Disturbances at the Current Time Step

A non-trivial challenge is the handling of prediction errors at the current time step. If no robust MPC approach is used, differences in predicted values $d(0|k)$ for disturbances and real values $d(k)$ lead to $x(k+1) \neq x(1|k)$, potentially violating state constraints. Figure 3.3 illustrates how predictions for the solar irradiance $I_{\text{sol}}(0|k)$ at the current time step and its true values $I_{\text{sol}}(k)$ can deviate. Thus, the error $e_{\text{ren}}(k) = P_{\text{ren}}(k) - P_{\text{ren}}(0|k)$ has to be handled, for which we propose two options.

First, in the *optimistic* scenario, we assume perfect measurements, i. e. $P_{\text{ren}}(0|k) = P_{\text{ren}}(k)$. This neglects that a measurement at time k is most likely to change within the time step (i. e. during the following 15 min) and thus does not represent the necessary average. In this case, no further handling of e_{ren} is necessary and all constraints will be fulfilled.

Second, in the *pessimistic* scenario, we assume no additional measurement at time k, which means that we use a value which has been predicted up to 65 min ago. We use heuristic rules to account for $e_{\text{ren}}(k)$. If $e_{\text{ren}}(k) > 0$ (i. e. higher PV production than expected), the surplus is balanced by decreasing

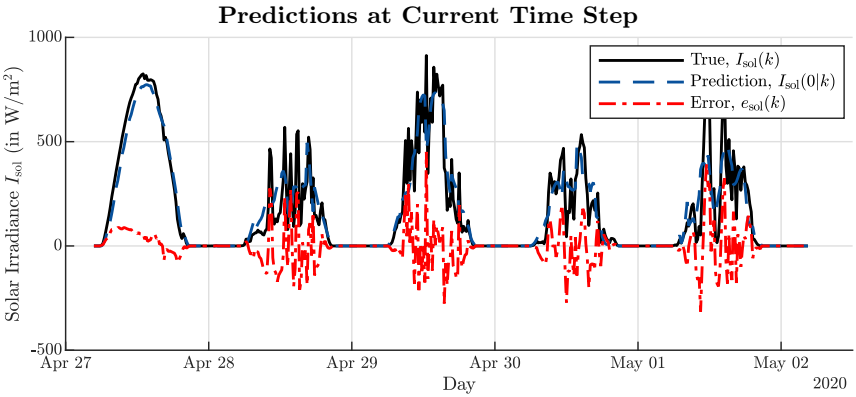

Figure 3.3: Exemplary comparison of true solar irradiance (black line) and most recent predictions available at the beginning of a time step (blue line) for 5 days. Besides forecasts being up to 65 min old, significant differences may occur due to the local distance between the site and the next weather station used for forecasting.

$P_{\text{grid}}(k)$. If $e_{\text{ren}}(k) < 0$ (i. e. lower PV production than expected), we discharge the stationary battery if this is necessary to prevent a new peak in P_{grid} (while respecting all constraints). Otherwise, again $P_{\text{grid}}(k)$ is used to compensate $e_{\text{ren}}(k)$.

3.3.3 Results

As before, the simulations have been conducted in PARODIS [S4]. With GUROBI as the solver, a single simulation of 30 days takes ≈ 150 s on an Intel i7-8550U notebook CPU.

Potential Savings

The general potential savings, i. e. the difference in cost between simulation with no and with perfect predictions, are shown for both scenarios (optimistic and pessimistic) in Figure 3.4. Assuming perfect predictions, the minimum monetary costs for the 30-day period are 21,980 € (including, however, the entire peak cost for the initially assumed peak of 100kW). If no predictions for P_{ren} are used (i. e. $P_{\text{ren}}(n|k) = 0 \; \forall n \in [0, N_{\text{pred}} - 1]$),

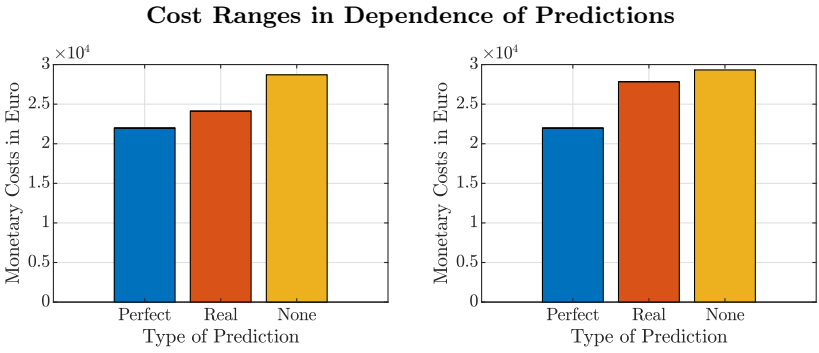

(a) Optimistic Scenario (b) Pessimistic Scenario

Figure 3.4: Monetary costs for simulations with perfect, real or no predictions for the (a) optimistic and (b) pessimistic scenario. The initial peak was set to 100 kW (for which peak costs are included). The pessimistic scenario shows overall higher costs if prediction errors are present.

they raise to 28,704 € and 29,324 € for the optimistic and pessimistic scenario, respectively. For the optimistic scenario, this results in potential savings of 6,724 € and we already reach 4,577 € with our current prediction quality. However, for the pessimistic scenario, we only reach savings of 1,491 € of the potential 7,344 €. This leads to the question of how good the predictions would need to be to achieve a certain amount of the potential savings.

Correlation between Prediction Accuracy and Costs

To systematically analyze the correlation between prediction accuracy and resulting costs, we run multiple simulations with different initial peaks $P_{\text{grid,peak}}(0) \in [100,\ 200]\,\text{kW}$ and vary $s_{\text{err}} \in [0,\ 8]$, leading to $e_{\text{avg}} \in [0,\ 269.6]\,\text{kW}$ as described by (3.6). Figure 3.5 shows the results for the optimistic scenario. With no prediction errors, the costs rise only with the initial peak costs (if $\geq 118\,\text{kW}$, which is unavoidable, see Figure 3.1). For low initial peaks (100 kW or 120 kW), the costs increase linearly until $e_{\text{avg}} =\approx 143.1\,\text{kW}$, from where they start to saturate. For high initial peaks, e_{avg} has no influence on the costs, since $P_{\text{grid,peak}}(0) + P_{\text{chp,max}} \geq -(P_{\text{dem}}(k) + P_{\text{ren}}(k))\ \forall k$, and thus it is not necessary to use the battery for peak shaving.

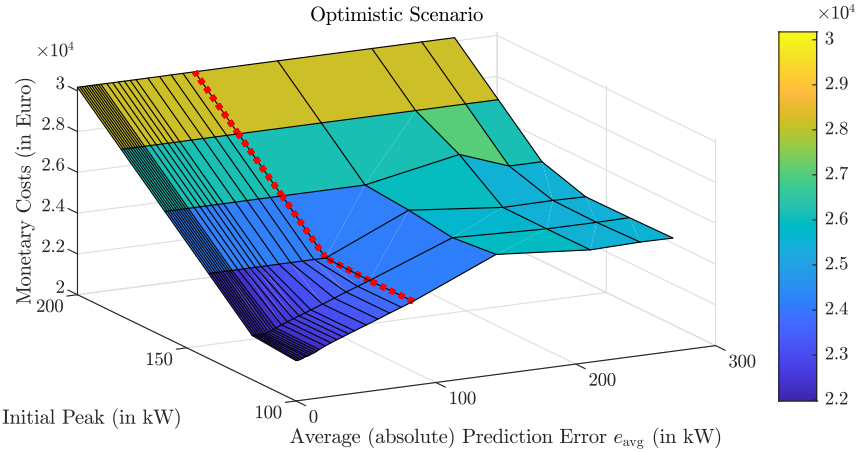

Figure 3.5: Monetary costs for different prediction errors and initial peaks in the optimistic scenario. Peak costs for the initial peaks are included. The red dotted line shows the error level with real predictions ($e_{\text{avg}}(s_{\text{err}}=1) = 83.76\,\text{kW}$).

Figure 3.6 shows the results for the pessimistic scenario. Here, the correlation is much less consistent and could be described by piece-wise linear functions for the different initial peaks. For lower initial peaks, the costs increase drastically for $e_{\text{avg}} > 0$. The higher the initial peak, the lower the slope becomes. However, in contrast to the optimistic scenario, costs do increase even for the highest initial peak of 200 kW. From $e_{\text{avg}} \approx 25\,\text{kW}$, the costs plateau (with one negative bump) and increase again with $e_{\text{avg}}(s_{\text{err}} > 1)$.

The negative bump, i. e. the decrease in costs with an increased average error, can be explained by an artifact of the underlying data and would change e. g. for other simulation time spans. To illustrate this, consider two simulations with $s_{\text{err}} = 0.5$ and $s_{\text{err}} = 1$. Usually, $s_{\text{err}} = 1$ will lead to higher peaks, e. g. at time step k_1. However, for a new demand peak at $k_2 > k_1$, the controller 1 with $s_{\text{err}} = 0.5$ would thus try to shave the peak by discharging the battery, whereas controller 2 with $s_{\text{err}} = 1$ would not. If then at $k_2 + 1$ an even higher peak occurs (previously unseen), controller 2 is in a better position and controller 1 might result in an overall higher peak. To conclude, luckily chosen higher prediction errors might lead to lower costs, but the general trend of increasing costs with higher errors is clear. Furthermore, the closer the error gets to 0, the more beneficial it

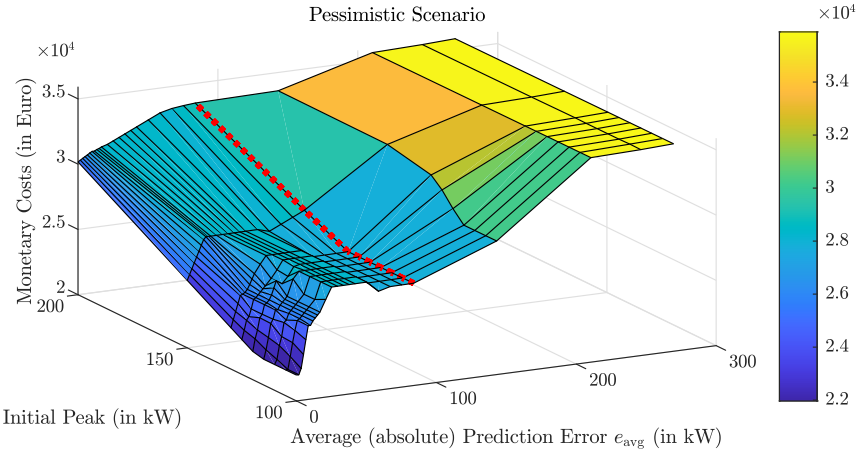

Figure 3.6: Monetary costs for different prediction errors and initial peaks in the pessimistic scenario. Peak costs for the initial peaks are included. The red dotted line shows the error level with real predictions ($e_{\text{avg}}(s_{\text{err}}=1) = 83.76\text{kW}$).

seems, due to the high impact of peak costs, as Figure 3.7 shows.

Influence of Prediction Accuracy within the Time Horizon

For the simulations shown in Figures 3.5 and 3.6, the prediction error has been scaled equally over the prediction horizon as described in (3.5). To analyze whether its influence is equal over the horizon as well, we run a simulation with perfect predictions for the first n_{perf} steps. Figure 3.8 shows the resulting additional costs compared to a simulation with overall perfect predictions. Note that $n_{\text{perf}} = 1$ for the optimistic and $n_{\text{perf}} = 0$ for the pessimistic scenario refer to the regular simulations (with real predictions). Furthermore, the pessimistic scenario with $n_{\text{perf}} = 1$ is the same as the regular optimistic scenario. In both scenarios, all additional costs are already avoided with $n_{\text{perf}} = 5$, i. e. with perfect predictions for the first 75 min. Note that this is significantly shorter than a complete charging and discharging cycle of the stationary battery, which would take 250 min.

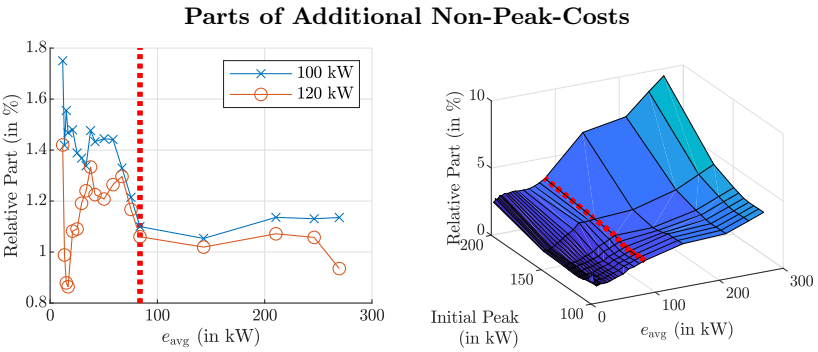

(a) Optimistic Scenario (b) Pessimistic Scenario

Figure 3.7: Parts of additional monetary costs which are not caused by higher peaks for the (a) optimistic and (b) pessimistic scenario. Again, the red lines indicate the real average prediction error.
For the optimistic scenario (a), only simulations with initial peaks of 100 kW or 120 kW are shown, since with higher initial peaks, generally, no new peaks occur. For lower initial peaks, they dominate, i. e. the non-peak costs are negligible ($\leq 2\,\%$).
For the pessimistic scenario (b), the part of additional non-peak costs increases with both higher e_{avg} and initial peaks of P_{grid}. However, in the most relevant part with initials peaks $\leq 120\,\text{kW}$, they are still low ($\leq 5\,\%$).

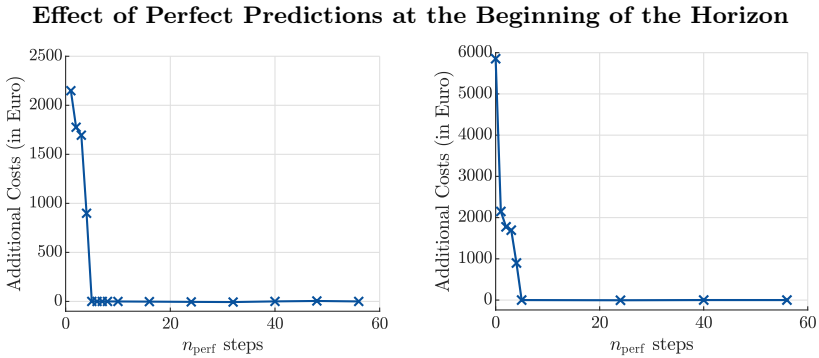

(a) Optimistic Scenario (b) Pessimistic Scenario

Figure 3.8: Additional costs in comparison to perfect simulation when the first n_{perf} steps of the prediction horizon are perfectly predicted. For both the optimistic (a) and pessimistic (b) scenario, additional costs are avoided for $n_{\text{perf}} \geq 5$.

3.3.4 Conclusion

For both scenarios, there is a significant correlation between monetary costs and the prediction error, only its form varies. For the optimistic scenario, it is mostly linear, for the pessimistic it is peace-wise linear - in reality, it would be somewhere in between. Furthermore, the major part of the cost increase is due to additional peak costs (90 to 99 %). In both cases, current weather forecasts can already be utilized successfully to reduce costs, but further improvements would be rewarding, especially at the beginning of the prediction horizon. For the presented setting, prediction accuracy of only the first 75 min is relevant. Note that most likely, this depends on the dynamics of the microgrid model. For example, this time span might increase if minimum up and down times for combustion engines or other producers apply. Nevertheless, the employment of technologies for short-term predictions such as sky cameras to monitor local cloud movements seem promising. With these methods, real-world applications would shift towards our optimistic scenario, since the average value for the first 15 min could be predicted more reliably. Furthermore, the results suggest that a MPC approach designed to account for prediction errors, either stochastic or robust, may be promising. However, a systematic comparison of the control with and without a stochastic/robust method would be necessary to test their effectiveness for different prediction errors.

3.4 Summary

In this chapter, we analyze the effect of prediction errors on the monetary costs in microgrid control if no special MPC scheme dedicated to account for uncertainties (i. e. stochastic or robust) is used. To this end, we use real-world weather forecasts from a 30 day period in April/May 2020 for the solar irradiance and translate them into predictions of the PV power output. Then, we artificially scale the prediction error to empirically sample the correlation between the average prediction error and cost increase. We use the main building model HL-1 from Chapter 2. To handle the prediction error at the current time step, we introduce two options. First, we assume perfect knowledge (measurement) of the current power output, which on average would need to be the same over the next 15 min (referred to as the optimistic scenario). Second, we assume no additional measurement, but the use of previously made forecasts (up to 65 min old) and compensate for errors in the power production by heuristic rules (referred to as the pessimistic scenario).

As our main contributions, we show that, for a realistic microgrid setting of a medium-sized company building with real-world data,

- using real-world solar irradiance forecasts from weather services as predictions for PV power generation can reduce peak costs,
- the cost reduction scales with the prediction error, specifically
  - if PV generation is known at the current time step, the costs increase linearly with the prediction error,
  - if only predictions are used for the current time step, the correlation resembles a piece-wise linear function, with a significantly higher slope for lower errors, and
- our results suggest that the prediction accuracy for PV generation is only relevant within a short period at the beginning of the prediction horizon.

4 Dynamic Multi-Objective Optimization

This chapter constitutes the methodological main part of this thesis. Namely, we introduce methods to use multi-objective optimization (MOO) in MPC, which we therefore refer to as *dynamic MOO*. First, we motivate the basic principle in the introduction in Section 4.1. Then, we summarize the general field of MOO, how multiple objectives have been handled in MPC so far and which approaches exist to automatize the decision making process in Section 4.2. We present an adapted method to approximate the Pareto front in Section 4.3 and finally our own methods for the automatized decision making, both without preferences in Section 4.4 and with preferences in Section 4.5.

This chapter is based on and has partly been published in the following publications:

[S3] T. Schmitt, T. Rodemann, and J. Adamy. Multi-objective model predictive control for microgrids. *at - Automatisierungstechnik*, 68(8):687 – 702, 2020.

[S8] T. Schmitt, M. Hoffmann, T. Rodemann, and J. Adamy. Incorporating human preferences in decision making for dynamic multi-objective optimization in model predictive control. *Inventions*, 7(3), 2022.

4.1 Introduction

The term *optimal control* refers to the finding of an input trajectory that is optimal to a control objective formulated as a mathematical expression, i. e. a scalar function. Usually, this is a (fixed) compromise between the actuation energy and the deviation of the system's states from a desired point or trajectory. The compromise is defined by weighting matrices, which are usually tuned such that the resulting cost terms are of the same order of

magnitude and simulations show satisfying behavior. As discussed before, with economic MPC, real-world cost terms like monetary costs or CO_2 emissions can be minimized even if they cannot be expressed as quadratic terms of either states or input variables. However, they are much more concrete and thus possibly more meaningful to the control engineer. Here, preferences could be more sophisticated. Furthermore, varying external conditions may influence the possible compromises between non-quadratic objectives stronger, as e. g. with nonlinear peak costs. This might make an adaption of the importance between the objectives, usually expressed as weights, necessary or at least desirable.

Optimizing contradicting objectives simultaneously is the field of MOO. The key element is the *Pareto front*, which is the set of all 'optimal' compromises between objectives. More precisely, it contains all *Pareto optimal* solutions. A solution is Pareto optimal, if there is no other solution which is better in one objective without being worse in at least one other objective. The main challenge in MOO is to numerically derive an approximation of the Pareto front (since an analytical solution is usually impossible, especially for higher dimensional problems). With increasingly available computational resources, the development of computational intelligence methods for this problem has become an important field of research. Applications vary from sensor network design to military mission planning [131]. However, they usually have in common that only a one-time optimization for each problem is necessary. The required decision making process, i. e. choosing a solution from the Pareto front, has experienced less attention – since a so-called (human) decision maker (DM) usually has the last call.

Concluding, the need for optimization of multiple contradicting objectives in economic MPC is evident, but so far this is usually done only by the minimization of a weighted sum of multiple cost functions with fixed weights. An answer to this problem would be MOO, but it has been used mainly for one-time optimization problems so far. The aim of this chapter is to combine both MPC and MOO as suggested in Figure 4.1. Thus, we mainly propose methods to automatize the decision making process. In the following, we first summarize the relevant related work for MOO, the handling of multiple objectives in MPC and which automatized decision making methods exist so far. Then, we present our approaches for the proposed concept of dynamic MOO. Note that our conceptualization of dynamic MOO extends its usual usage in the literature, which considers MOO problems that change over time and how these changes can be best addressed in the optimization with evolutionary strategies [8, 113].

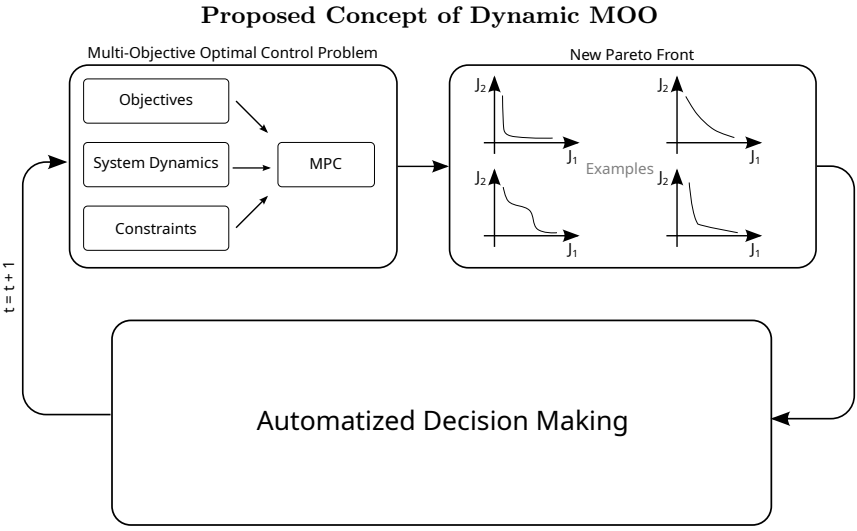

Figure 4.1: General procedure for the use of MOO in MPC. As usual, an OCP is solved at every time step. However, a multi-objective OCP is formulated, to which the solution is the Pareto front (or an approximation of it). Thus, a solution has to be chosen afterwards. Note that each solution on the Pareto front represents a complete control sequence. The first input of the sequence corresponding to the chosen Pareto solution is then applied to the system.

Notation

Decision variables are denoted by z, objective values by J. For vectors, a subscript i as in J_i denotes its i-th value. A superscript j marks the vector as a specific point, e. g. from a set of points such as $J^j \in \mathbb{J}$. For an integer index i, an interval $[1,\, q]$ refers to an interval of integers only, i. e. $i \in [1,\, q] \mathrel{\widehat{=}} i \in \{1, ..., q\}$.

4.2 Related Work

4.2.1 Multi-Objective Optimization

Problem Formulation

A MOO problem can be formulated as

$$\min J(z) = \big(J_1(z), \quad \dots, \quad J_q(z)\big) \tag{4.1a}$$

$$\text{s. t.} \quad g_j(z) \leq 0, \quad j = 1, 2, \dots, m_{\text{ineq}} \tag{4.1b}$$

$$h_l(z) = 0, \quad l = 1, 2, \dots, m_{\text{eq}}, \tag{4.1c}$$

where $z \in \mathbb{Z}$ is the decision variable vector, q the number of objectives and m_{ineq} and m_{eq} the numbers of inequality and equality constraints, respectively. The set of all feasible decision vectors $\mathbb{Z}^{\text{f}} = \{z \mid z \in \mathbb{Z}, (4.1b), (4.1c)\}$ is then called the *feasible decision space* and the set of all possible objective values $\{J(z) \mid z \in \mathbb{Z}^{\text{f}}\}$ the *objective space*. Since there typically is no single solution which minimizes all objectives J_i at the same time, the concept of Pareto optimality is used. A solution z^* is Pareto optimal, if it is not *dominated* by any other solution, i. e. there is no solution z for which $J_i(z) \leq J_i(z^*)\ \forall\, i \in [1, q]$ and $J_k(z) < J_k(z^*)$ for at least one $k \in [1, q]$. All Pareto optimal solutions together form the Pareto front. However, usually only a set of solutions $\mathbb{J} = \{J^1, \dots, J^N\}$ which approximates the Pareto front can be determined. A solution z^* is only *weakly Pareto optimal*, if there is no other solution which is better in *every* objective, i. e. if there is no solution z such that $J_i(z) < J_i(z^*)\ \forall\, i \in [1, q]$. A weakly Pareto optimal solution is thus not part of the Pareto front.

Important points apart from the Pareto front are the *Utopia* and the *Nadir* point. The Utopia point can be constructed from the Pareto front's *extreme points*. An extreme point is the Pareto solution with the minimum values for its corresponding objective, i. e. the extreme point for objective i is

$$J^{\text{extreme},i} = \underset{J^j \in \mathbb{J}}{\arg\min}\, J_i^j. \tag{4.2}$$

The Utopia point then consists of the single minima of all objectives,

$$J^{\text{utopia}} = \big(J_1^{\text{extreme},1}, \dots, J_q^{\text{extreme},q}\big) = \Big(J_1^{\text{utopia}}, \dots, J_q^{\text{utopia}}\Big), \tag{4.3}$$

and is thus generally not attainable.

Similarly, the Nadir point is the combination of all objectives' worst values on the front, i. e.

$$J^{\text{nadir}} = \left(\sup_{J^i \in \mathbb{J}} J_1, \ldots, \sup_{J^i \in \mathbb{J}} J_q\right) = \left(J_1^{\text{nadir}}, \ldots, J_q^{\text{nadir}}\right). \tag{4.4}$$

Figure 4.2 shows an illustration of a Pareto front for two objectives.

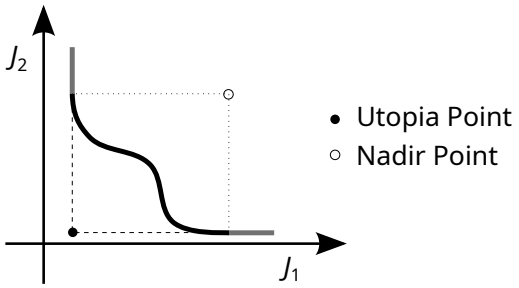

Figure 4.2: Illustrative 2D Pareto front with nonconvex parts and weakly Pareto optimal solutions (in gray).

Solving the MOO Problem

It is important to note that different categorizations of MOO methods exist, and our approach, which we will use throughout this thesis - determining (an approximation of) the entire Pareto front and choosing a solutions from it afterwards - is not the only way to solve (4.1). In their great review paper from 2004, Marler and Arora [86] distinguish between methods with

A1) *a priori articulation of preferences*, which determine only a single solution based on parameters representing the DM's preferences, e. g. the weighted sum method;

A2) *no articulation of preferences*, which also determine only a single solution, but without any input from the DM, e. g. the sum of all objectives without weights or the minimization of the maximum value of all objectives; and

A3) *a posteriori articulation of preferences*, which means that the entire Pareto front is determined and a solution is chosen afterwards – as we do here.

However, today especially due to the rise of evolutionary algorithms since then, a different categorization is more common [136]. It distinguishes between

B1) *a priori* (or *explicit*) methods, which respect preferences or interests of the DM by calculating Pareto solutions on specific areas of the Pareto front;

B2) *interactive* (or *progressive*) methods, which ask the DM for input during the optimization process itself, also to focus on specific areas; and

B3) again *a posteriori* (or *implicit*) methods as before.

In the following, we will limit all descriptions to the a posteriori methods. Thereby, the biggest difference lies in how the Pareto front is approximated: either by meta-heuristic (evolutionary strategies, genetic algorithms, etc.) or deterministic (mathematical programming) methods.

Meta-heuristic methods can be considered the standard choice. Their biggest advantage is that they can be used for any optimization problem, even with black box models, as long as one can evaluate the objective function, e. g. by simulation. However, this comes at the cost of high and possibly unpredictable computation times and the uncertainty whether a global (or even local) optimum has been found. Since all models used in this thesis are expressed by (linear) ODEs, the use of deterministic methods is sufficient and thus appropriate. Therefore, we omit any further descriptions of meta-heuristic methods here and refer the interested reader to [50, 152].

Approximating the Pareto front with deterministic methods means to repeatedly solve a single-objective optimization problem of type A1). Thereby, the parameters are varied iteratively such that a different point of the Pareto front is determined each time. Combining the objectives into a single scalar objective function (instead of the objective vector as in (4.1a)) is called *scalarization*. Two groups of scalarization methods are commonly used for the above purpose. The first utilizes weighted sums, possibly with exponential expressions of the objectives. The second we will – due to the lack of a better term – call *intersection methods*, since they aim at finding the intersection of the Pareto front with some geometric entity, usually a vector. In the following, we present a candidate from both groups and discuss their strengths and weaknesses.

A Weighted Sum Method: Adaptive Weight Determination Scheme

Weighted sum methods generally have two weaknesses. First, with a regular weighted sum, only convex parts of the Pareto front can be obtained. This can be overcome by the use of an exponential weighted sum, i. e.

$$\min J(z) = \left[\sum_{i=1}^{q} (w_i J_i)^p \right]^{\frac{1}{p}}, \tag{4.5}$$

with $p \in \mathbb{N}$, $p \geq 2$. However, this increases the optimization problem's complexity significantly, even if the $(\cdot)^{\frac{1}{p}}$ is omitted. The second weakness is that it is hard to choose the weights such that (approximately) equidistant points on the Pareto front are obtained, which is generally not achieved by equidistant variation of the weights [32, 121].

An approach that tackles the second problem in particular is the adaptive weight determination scheme (AWDS) [121]. It uses a geometric interpretation and adjusts the weights for (4.5) iteratively. In the following, we will assume a regular weighted sum, i. e. $p = 1$, which is the standard case and used throughout this thesis since we only minimize convex cost functions. For non-convex cost functions, $p \geq 2$ would be necessary.

The main principle of AWDS is the following. After q samples of the Pareto front are found, they are used to determine new weights w_i. With $q = 2$, this is equivalent to drawing a straight line through both points and interpreting its gradient m as the ratio between both weights. Having found two solutions $\left(J_1^{\mathrm{A}},\ J_2^{\mathrm{A}}\right)$ and $\left(J_1^{\mathrm{B}},\ J_2^{\mathrm{B}}\right)$, new weights $w_{\mathrm{mon}}^{\mathrm{C}}$ and $w_{\mathrm{comf}}^{\mathrm{C}}$ are determined by solving

$$\begin{bmatrix} J_1^{\mathrm{A}} & J_2^{\mathrm{A}} \\ J_1^{\mathrm{B}} & J_2^{\mathrm{B}} \end{bmatrix} \begin{bmatrix} w_{\mathrm{mon}}^{\mathrm{C}} \\ w_{\mathrm{comf}}^{\mathrm{C}} \end{bmatrix} = \begin{bmatrix} 1 \\ 1 \end{bmatrix}. \tag{4.6}$$

Then, the optimization is redone with the new weights $w_{\mathrm{mon}}^{\mathrm{C}}, w_{\mathrm{comf}}^{\mathrm{C}}$. This can be interpreted as shifting a straight line with the gradient m to the origin until it is tangential to the Pareto front[1], as is illustrated in Figure 4.3. (Note that this characteristic of minimizing the weighted sum is not new, but has been described before, e. g. in [32, 35].) As a result, we obtain a

[1] This interpretation fails for non-convex Pareto fronts. In that case, it would be more accurate to imagine the hyperplane moving from the origin towards the Pareto front until they touch.

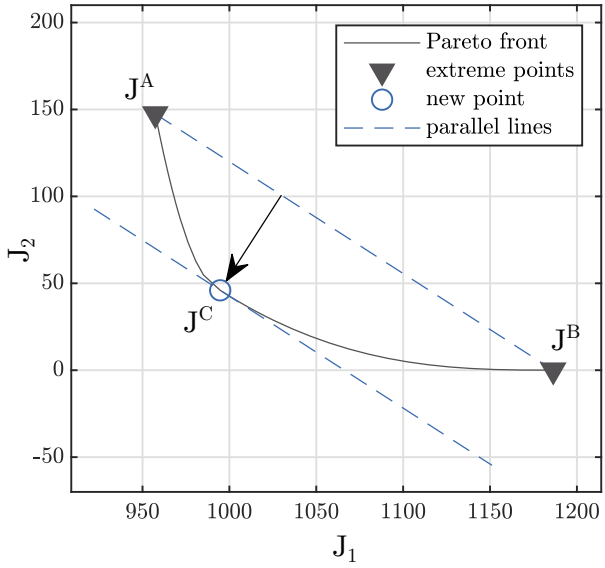

Figure 4.3: Illustration of the AWDS in the first step. The gradient of the connection between Pareto front extreme points is used to determine new weights, with which the 'new point' is determined next. The tangent of the Pareto front in the new point is parallel to the line connecting the extreme points.

new Pareto optimal solution $\left(J_1^{\mathrm{C}}, J_2^{\mathrm{C}}\right)$ which lies between $\left(J_1^{\mathrm{A}}, J_2^{\mathrm{A}}\right)$ and $\left(J_1^{\mathrm{B}}, J_2^{\mathrm{B}}\right)$. Moreover, the new solution J^{C} is more or less in the middle between J^{A} and J^{B}. For a circular Pareto front, it would be exactly in the middle. Next, $J^{\mathrm{A}} \leftrightarrow J^{\mathrm{C}}$ and $J^{\mathrm{B}} \leftrightarrow J^{\mathrm{C}}$ are used to derive new pairs of weights, respectively, in the same fashion by solving equations such as (4.6). This is repeated until the distance between two solutions is below a chosen threshold Δd^{awds}. As starting points, the Pareto front's extreme points are used. Possible ways of determining the extreme points follow below on page 81.

An Intersection Method: Normal Boundary Intersection

The idea to scalarize a MOO problem by, for example, maximizing the length of a vector, dates back to the 1970's [48] and has been varied since then [109]. In general, a geometrization of the objective space is used to reformulate the optimization problem such that the actual objective

function appears in the constraints only. The normal boundary intersection (NBI) was then introduced as a method of systematically varying the scalarizations to obtain a reasonable approximation of the Pareto front [33]. The procedure is as follows. First, the extreme points have to be determined. Second, a simplex connecting the extreme points is constructed, called the convex hull of individual minima (CHIM). Then, this simplex is sampled evenly. This can be expressed with the $q \times q$ matrix Φ, whose i-th column is

$$\Phi(:,i) = J^{\text{extreme},i} - J^{\text{utopia}}. \tag{4.7}$$

The CHIM is sampled by $\Phi\beta^{\text{NBI}}$ with a varying $(q \times 1)$-vector β^{NBI}, s. t.

$$\sum_{i=1}^{q} \beta_i^{\text{NBI}} = 1, \quad \beta_i^{\text{NBI}} > 0. \tag{4.8}$$

A Pareto solution is then obtained by maximizing the length κ of the CHIM's normal vector $\hat{n}$ pointing towards the Pareto front, with the constraint that the vector's tip ends at the Pareto solution itself. For a combination β^{NBI}, the MOO problem (4.1) is then replaced by

$$\begin{aligned} & \min\ (-\kappa) && \text{(4.9a)} \\ \text{s. t.}\quad & \Phi\beta^{\text{NBI}} + \kappa\hat{n} = J(z) - J^{\text{utopia}} && \text{(4.9b)} \\ & (4.1\text{b}), (4.1\text{c}). && \text{(4.9c)} \end{aligned}$$

Figure 4.4 gives an illustration of the geometric interpretation. Note that (4.9) is the same if (4.9a) is replaced by $\max(\kappa)$. Furthermore, the optimization problem's solvability might be changed, since all possible nonlinearities are shifted to the constraints instead of the objective function, which is one of its disadvantages, next to its susceptibility to weakly Pareto optimal solutions. However, intersection methods showed to be numerically more robust for $q \geq 3$ objectives in the simulation studies conducted throughout this thesis and presented in Chapter 5. The original NBI as described here has been modified in different ways since then [49, 90, 94, 96] and we also use a modified version which will be described in Section 4.3.

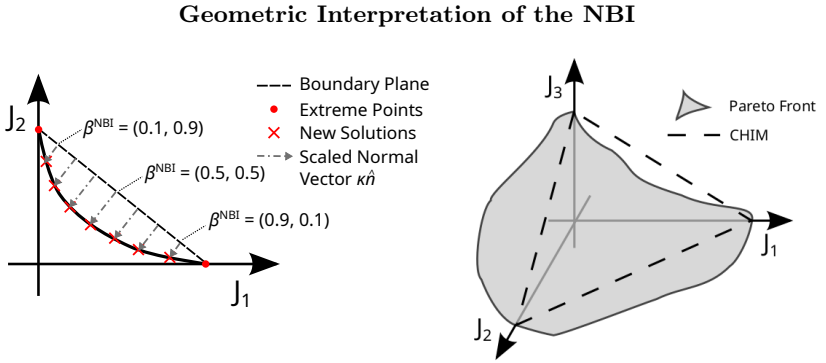

(a) NBI for 2 Objectives

(b) Simplex (CHIM) for 3 Objectives

Figure 4.4: Illustration of the NBI method.

(a) Different values for β^{NBI} from (4.8) lead to different starting points on the simplex, from which the normal vector $\hat{n}$ point onto the Pareto front.

(b) For 3 objectives, it becomes clear that the simplex (CHIM) does not necessarily cover neither the entire nor only the Pareto front, which is why not all Pareto solutions are necessarily obtainable and weak Pareto solutions are possible with the NBI method.

Determining the Extreme Points

The knowledge of the extreme points is a prerequisite for most deterministic methods approximating the Pareto front, including the ones described before and used in this thesis. However, determining the extreme points is not trivial and in general hard to do [14, 36]. A straightforward approach to approximating $J^{\text{extreme},j}$ is to minimize the weighted sum

$$\sum_{i=1}^{q} w_i J_i \tag{4.10}$$

with $w_j = 1$ and all other weights $w_{i\neq j} = w_{\text{th}}$ with a threshold value $0 < w_{\text{th}} \ll 1$, e. g. 10^{-5}. Note that for $w_{\text{th}} = 0$, the absolute minimum of J_j would be obtained, but the solution would (most likely) only be weakly Pareto optimal in terms of all other objectives. $w_{\text{th}} > 0$ will lead to a real Pareto solution, but inevitably to a value of J_j larger than the real J_j^{utopia}.

A more sophisticated approach is the *lexicographic method* [86, 128]. $J^{\text{extreme},j}$ can be determined by first minimizing J_j only, and then subsequently minimizing every other objective, but with the constraint(s) that J_j and the other already minimized objectives are not larger than before. In total, q optimizations are necessary for each extreme point. Note that the order in which the objectives $i \neq j$ are minimized can be relevant. Assuming an order $\mathcal{O}$ is used, e. g. $\mathcal{O} = [j, 1, 2, \ldots, j-1, j+1, \ldots, q]$, the i-th optimization would write

$$z^{*,i} = \arg\min \; J_i(z) \tag{4.11a}$$

$$\text{s. t.} \quad J_k(z) \leq J_k(z^{*,i-1}) \quad \forall\, k = \mathcal{O}(1), \ldots, \mathcal{O}(i),\ i > 1 \tag{4.11b}$$

$$(4.1\text{b}), (4.1\text{c}). \tag{4.11c}$$

The extreme point of objective j is then defined as $J^{\text{extreme},j} = J(z^{*,q})$. In practice, the constraints (4.11b) can make the optimization problem significantly harder to solve, since they are of the same type as the actual objective functions, e. g. quadratic or worse. In addition, it might be necessary to add a positive threshold on the right side to avoid numerical issues.

4.2.2 A Posteriori Decision Making Strategies

Various types of a posteriori methods exist. *Fuzzy logic* can be used, e. g., for uncertain objectives, constraints or decision variables [91], or to

incorporate preferences from linguistic values [66], or (without preferences) on top of the concept of k-optimality to loosen the crisp definition of Pareto optimality [41]. Overall, the literature on different Fuzzy approaches is rich. Another concept is the use of *Shannon Entropy* [79]. For each objective, the solutions' entropy is calculated, which depends on their diversity. From these, weights for all objectives are derived. Then, the (normalized) solution which fits the weights best is selected. *Evidential Reasoning* is a method for decision making in the presence of uncertainties [141]. Multiple attributes are weighted according to their importance. For each attribute, possible grades are defined and the likelihood of a solution's attribute to match them is assessed, e. g. a likelihood of 0.3 to be 'good' and 0.6 to be 'very good'. Then, a single overall score of the solution can be derived and all Pareto solutions are ranked accordingly. *Euclidean distance based metrics* are widely used, e. g. LINMAP, which minimizes the weighted distance to the Utopia point [127]. Frequently, the unweighted but normalized distance is minimized instead [144, S1]. TOPSIS is an algorithm which considers both distances to the Utopia and the Nadir point [62]. ϵ-dominance describes which constant offset ϵ one would have to add to all objectives of a solution z^* such that the resulting point would be dominated [17, 152]. Thus, the higher the necessary ϵ is, the more preferable the solution is.

However, possibly the most popular aim is the selection of a *knee point*, which in general is a solution on the Pareto front from which a small improvement in one direction (objective) would lead to a large(r) deterioration in all others. Thus, the shape of the Pareto front is essential. Different possibilities to define (or find) a knee point exist. Multiple approaches do so based on the point's angle to other parts of the front, e. g. the reflex angle [24], the bend angle [35], the extended angle dominance [25] or the angle utility [25]. Utility-based methods generally define a knee by the best trade-off, i. e. the best ratio of improvements vs. deteriorations compared to all other solutions [14, 35, 112]. This approach is extended to multiple regions of the Pareto front in [18], i. e. the best trade-off for each region is determined. In [143], knee points are identified by mapping the Pareto front onto a hyperplane. Then, a solution is considered to be a knee point if the other solutions are densely located around it. According to [24], a point is a knee point if it is the result of the optimization of a weighted sum for multiple (different) weight combinations. In an early work, Das [31] characterizes the point with the largest distance to the convex hull of individual minima as the knee.

Since there is no way of defining a clear knee point for every Pareto front,

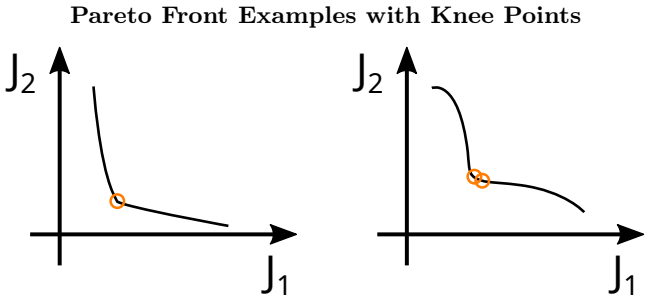

Figure 4.5: 2D Pareto fronts (black lines) with knee points (orange circles). The left Pareto front has a sharp bend at which its derivative is discontinuous, which is considered to be a knee point. The right Pareto front has a convex bulge, which constitutes a knee point. However, which point exactly is to be considered the knee depends on the definition.

a subset or multiple subsets of the front which show knee-like or other properties of interest are often determined and presented to the DM. If their definition is based on a metric as explained above, they are usually called *knee region*, e. g. a trade-off based knee region [35] or the bulge of points with the largest distance to the convex hull of individual minima [77]. If their definition is based on a DM's preference, they might be called *region of interest*. In [92], the DM defines a cost reference point, i. e. an arbitrary chosen $J^{\text{ref}} = \left(J_1^{\text{ref}}, \ldots, J_n^{\text{ref}}\right)$, either infeasible or feasible. Then, imagining a coordinate plane with J_{ref} at its origin, the part of the Pareto front which dominates J_{ref} (if feasible) or which is dominated by J_{ref} (if infeasible) is considered as the region of interest. However, it does not provide the DM with a final choice and, more importantly, it is neither clear how large the region of interest will be, nor does it indicate whether it will contain possible knee points or not. In [59], the DM defines a starting point and a preference direction. Then, the part of the Pareto front which lies within a pre-defined preference radius around the preference direction is defined as the region of interest. Again, no final solution is provided and possible knee points are ignored.

In summary, there are many ways of choosing a solution (compromise) to the MOO problem (4.1) once an approximation of the Pareto front has been determined. However, in the context of dynamic MOO, important problems are still unsolved. First, it is mostly unclear what kind of compromises are selected with each method in a repeating (but slightly changing) process.

Second, methods to automatize this process while both incorporating the preferences of a DM in a comprehensible way and preferring solutions with knee-like behavior are missing. This is the main gap we try to fill with our approaches presented in Sections 4.4 and 4.5. Before that, we review how multiple objectives have been addressed specifically in the context of MPC so far.

4.2.3 Multiple Objectives in MPC

The interest in MPC has been rising significantly throughout the last decades. However, despite its optimization nature, no unifying framework for MOO in MPC is available so far. Considering regular MPC with its quadratic objective function, i. e.

$$\min \sum_{k=0}^{N_\mathrm{p}-1} x(k)^\intercal Q x(k) + u(k)^\intercal R u(k) + V_\mathrm{f}(x(N_\mathrm{p})), \tag{4.12}$$

where V_f is the terminal cost function, the challenge of weight tuning Q and R could be considered an optimization of two competing objectives, i. e. between state control (with Q as its 'weights') and actuator energy (with R as its 'weights'). Literature about this general problem of weight tuning is rich (see [47] and the references therein). However, in most auto-tuning methods, only the system's step or impulse responses are used and evaluated by a different metric, which is insufficient for complex systems such as microgrids.

In [34], a MOO MPC scheme for general nonlinear systems is defined. They consider a finite number of objectives and show that, given some mild assumptions in addition to the usual, the max() of all objectives as costs can be used as a Lyapunov function to guarantee stability. In [15], a weighted sum is used. However, the weights are updated in every time step, thus choosing different Pareto solutions. It is shown that, under some conditions on the objectives, e. g. joint convexity, closed-loop stability can be guaranteed. However, for the updating of the weights, a linear programming problem which is not jointly convex in general has to be solved in every time step. An economic MPC scheme with a compromise solution is formulated in [145]. Namely, the authors directly minimize the (unweighted) distance to the Utopia point. However, they only consider steady-state control and show that, if the objectives satisfy a Lipschitz continuity property and strong duality, stability can be guaranteed.

In [53, 54], nonlinear discrete-time systems with an arbitrary number of (contradicting) objectives and without disturbances are considered. Given some assumptions of the system (e. g. an equilibrium point), terminal costs and a local feedback control law in the terminal region, the authors propose a stabilizing MPC algorithm for which they show that the infinite-horizon closed loop performance has an upper bound defined by a Pareto optimal control sequence chosen at the beginning of the algorithm. For economic stage costs and similar assumptions, they show that the average closed-loop performance is bounded above. While they are able to give statements on the performance of Pareto optimal sequences, the trade-off between the multiple objectives seems to rely on the choice of their algorithms' initialization. Thus, changing conditions over time cannot be respected.

A goal programming method for regular (quadratic) MPC is used in [40]. They define goals for arbitrary objective functions and minimize the (weighted) distance to the goals. However, this is done offline, i. e. it is a one-time weight tuning (and does not further consider Pareto optimality).

In [102], a linear wind turbine model is controlled with regular MPC. Thereby, one weight of Q and R each are varied contradictory, i. e. proportional to ρ and $(1-\rho)$ with $\rho \in (0,1)$. Then, the system is simulated for different input velocities. The resulting state trajectories are evaluated for 5 different objectives and some Pareto solutions in dependence of ρ are plotted. However, the objectives are not directly considered in this weight tuning approach and there is no systematic selection from the set of Pareto solutions.

Evolutionary algorithms are used as optimization methods for an economic MPC scheme with a weighted sum of a finite number of objectives in [10]. Furthermore, Smith dynamics are used to dynamically tune the weights such that the solution lies in a pre-defined region of the Pareto front. This so-called *management region* is defined by the objectives' ratio in a normalized space.

Concluding, while there are some theoretical approaches to establish stability in MPC with multiple objectives and some practical simulation studies in which different possible compromises between objectives have been observed, systematic methods and analyses how the concept of Pareto optimization can be beneficially incorporated into MPC are missing. Possible methods to do so are presented in the rest of this chapter, while extensive analyses with long-term simulations are discussed in Chapter 5.

4.3 Pareto Front Determination

The method described in this chapter has been derived within the supervision of a Master's thesis [56]. It builds on the NBI method, but is more apt for the purpose of dynamic MOO. Namely, due to varying conditions, objectives may correlate sometimes. This would lead to a degenerate Pareto front [60]. Even if they do not correlate perfectly, some extreme points may end up very close to each other. If this is the case for 2 out of 3 objectives, the resulting simplex (i. e. the CHIM) is a very narrow triangle. Then, in combination with the search direction being strictly orthogonal to the simplex, this might lead to almost no real Pareto solutions being found.

Thus, we propose the focus point boundary intersection (FPBI) method. In contrast to the NBI, it 1) constructs a hyperplane which depends less on the extreme points and 2) enables the DM to define a search direction to increase the probability of finding solutions in the area of interest. If no specific goal is available, we use the Utopia point.

The procedure of the proposed FPBI method is as follows. We assume that the Pareto front's extreme points $\{J^{\text{extreme},1}, \ldots, J^{\text{extreme},q}\}$ are known. Moreover, all further calculations are done after a (dynamic) normalization of the solutions, $J \to \tilde{J}$, such that each objective lies within [0, 1] in the normalized space $\tilde{\mathbb{J}}$. Details are explained in the next section and are not relevant for the understanding of the rest of the procedure.

First, we determine the extreme point indices $(a,\ b)$ between which the distance is the longest,

$$(a,\ b) = \underset{i,\,j \in [1,\ q]}{\arg\max} \left\| \tilde{J}^i - \tilde{J}^j \right\|_2. \tag{4.13}$$

With $(a,\ b)$ known, we determine the center point between them,

$$\tilde{J}^{\text{center}} = \frac{1}{2}(\tilde{J}^a + \tilde{J}^b). \tag{4.14}$$

The search direction is then defined from $\tilde{J}^{\text{center}}$ to the *focus point*,

$$n^{\text{f}} = \tilde{J}^{\text{focus}} - \tilde{J}^{\text{center}}. \tag{4.15}$$

If no specific focus point is given, $\tilde{J}^{\text{focus}} = \tilde{J}^{\text{utopia}}$ is used, which usually gives good results.

The main idea is to use a hyperplane between the farthest extreme points (a, b), sample it equidistantly in every direction and to then solve an

optimization problem similar as in the NBI method, i. e. maximizing the length of a vector with the direction n^{f} from the hyperplane to the Pareto front. $\tilde{J}^{\mathrm{center}}$ is used as the base vector of the hyperplane. Thus, we further need $q-1$ (orthonormal) direction vectors to describe it. For $q=2$ objectives, the connection between the two extreme points already constitutes the hyperplane and

$$ {}^{\mathrm{F}}d^{1} = \frac{\tilde{J}^{b} - \tilde{J}^{a}}{\left\| \tilde{J}^{b} - \tilde{J}^{a} \right\|_2} \tag{4.16} $$

is its only direction vector. For $q=3$ objectives, the necessary second direction vector can directly be determined as the cross product of the search direction and the first direction vector,

$$ {}^{\mathrm{F}}d^{2} = \frac{n^{\mathrm{f}} \times {}^{\mathrm{F}}d^{1}}{\left\| n^{\mathrm{f}} \times {}^{\mathrm{F}}d^{1} \right\|_2} \quad (\text{for } q=3 \text{ only!}). \tag{4.17} $$

For $q \geq 4$ objectives, we have additional degrees of freedom. For ease of representation, assume that $a=1, b=2$. This is no limitation, but can be achieved by simple (temporary) re-ordering. Then, we first construct $q-2$ auxiliary direction vectors

$$ {}^{\mathrm{F}}\hat{d}^{\ell} = \tilde{J}^{\mathrm{extreme},\ell+1} - \tilde{J}^{\mathrm{center}} \quad \forall\, \ell \in [2,\ \ldots,\ q-1]. \tag{4.18} $$

Note that we use the extreme points since we can assume that the resulting vectors are linearly independent.

The direction vectors are then determined in increasing order by subsequently calculating the cross product of the search direction vector n^{f}, the already known direction vectors ${}^{\mathrm{F}}d^{i}$ and the auxiliary direction vectors ${}^{\mathrm{F}}\hat{d}^{j}$ for all other directions. To increase readability, we borrow the $\bigwedge$ symbol for the cross product of multiple vectors in the following, with which the ℓ-th direction vector is determined by

$$ {}^{\mathrm{F}}d^{\ell} = \frac{n^{\mathrm{f}} \times \bigwedge_{i=1}^{\ell-1} {}^{\mathrm{F}}d^{i} \times \bigwedge_{j=\ell+1}^{q-1} {}^{\mathrm{F}}\hat{d}^{j}}{\left\| n^{\mathrm{f}} \times \bigwedge_{i=1}^{\ell-1} {}^{\mathrm{F}}d^{i} \times \bigwedge_{j=\ell+1}^{q-1} {}^{\mathrm{F}}\hat{d}^{j} \right\|_2} \quad \forall\, j \in [2,\ \ldots,\ q-1]. \tag{4.19} $$

The generalized cross product of $q-1$ vectors can be calculated as the

determinant of an extended matrix, i. e.

$$\bigwedge_{i=1}^{q-1} v^i = \det \begin{pmatrix} \vec{e}^1 & v_1^1 & v_1^2 & \dots & v_1^{q-1} \\ \vec{e}^2 & v_2^1 & v_1^2 & \dots & v_2^{q-1} \\ \vdots & \vdots & \vdots & \ddots & \vdots \\ \vec{e}^q & v_q^1 & v_q^2 & \dots & v_q^{q-1} \end{pmatrix}. \tag{4.20}$$

Note that we exceptionally use the vector symbol $\vec{e}^i$ here to emphasize that these are the unit vectors, e. g. $\vec{e}^1 = \big(1,\ 0,\ \cdots,\ 0\big)^\intercal$, and not scalar values. (4.20) can be solved by using the Laplace expansion along the first column. In doing so, the purpose of the unit vectors becomes clear, too: they transform the minors into a vector again.

With the hyperplane defined by $\tilde{J}^{\text{center}}$, n^{f} and the direction vectors, we need to sample it to determine starting points for the optimization problem. Hereby, the user can control the resolution by defining a number ${}^{\text{F}}r$ of steps along each direction. Thus, the total number of optimization problems is ${}^{\text{F}}r^{q-1}$. We define a $1 \times {}^{\text{F}}r$ step size vector γ by

$$\Delta s = \frac{\left\| \tilde{J}^b - \tilde{J}^a \right\|_2}{{}^{\text{F}}r}, \tag{4.21}$$

$$\gamma = \big(1 \cdot \Delta s,\quad \cdots,\quad {}^{\text{F}}r \cdot \Delta s\big) - \frac{{}^{\text{F}}r}{2} \Delta s. \tag{4.22}$$

Let ${}^{\text{F}}p_i \in [1,\ \dots,\ {}^{\text{F}}r]$ for $i = 1, \dots q-1$ be the sample indices along the $q-1$ direction vectors. For a combination $({}^{\text{F}}p_1,\ {}^{\text{F}}p_2,\ \dots,\ {}^{\text{F}}p_{q-1})$, the $(q \times 1)$-dimensional starting vector in the optimization problem is then given by

$$\Theta({}^{\text{F}}p_1,\ {}^{\text{F}}p_2,\ \dots,\ {}^{\text{F}}p_{q-1}) = \tilde{J}^{\text{center}} + \sum_{i=1}^{q-1} \gamma({}^{\text{F}}p_i) \cdot {}^{\text{F}}d^i. \tag{4.23}$$

The corresponding optimization problem is described by

$$\begin{aligned} & \min\ -\kappa && \text{(4.24a)} \\ \text{s. t.}\quad & \Theta({}^{\text{F}}p_1,\ {}^{\text{F}}p_2,\ \dots,\ {}^{\text{F}}p_{q-1}) + \kappa n^{\text{f}} \geq \tilde{J}(z) && \text{(4.24b)} \\ & (4.1\text{b}), (4.1\text{c}). && \text{(4.24c)} \end{aligned}$$

Note that we use $\geq$ instead of $=$ in (4.24b) since this led to faster convergence in practice.

4.4 Automatized Metric-Based Decision Making

In this section, we propose the use of metrics in combination with different normalization schemes to automatically select a solution from the Pareto front. First, we describe a dynamic and a fixed normalization of the Pareto solutions. Second, we present three different metrics a decision maker can choose from. The procedure in combination with MPC is illustrated in Figure 4.6.

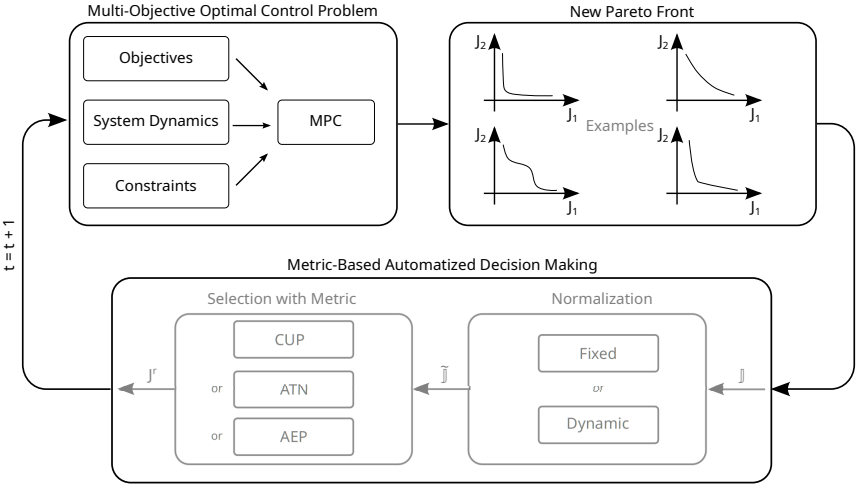

Figure 4.6: Automatized metric-based decision making in multi-objective MPC. At every time step, the approximated Pareto front is first normalized, either with the dynamic or the fixed normalization scheme. Then, all solutions are ranked by one of the three proposed metrics from Section 4.4.2 and the best solution is selected. The first step of the corresponding input trajectory is applied to the system.

4.4.1 Normalizations

We assume to have an approximation $\mathbb{J}$ of the Pareto front and propose two possible transformations; 1) a *dynamic normalization* $\mathbb{J} \to {}^{\mathrm{d}}\tilde{\mathbb{J}}$, also called *upper-lower bound approach* and 2) a *fixed normalization* $\mathbb{J} \to {}^{\mathrm{f}}\tilde{\mathbb{J}}$ using constant values chosen a priori by the DM.

Dynamic Normalization The dynamic normalization can be considered the standard procedure [87]. The i-th component of a Pareto solution $J^r \in \mathbb{J}$ is normalized as

$$^{\mathrm{d}}\tilde{J}_i^r(k) = \frac{J_i^r(k) - J_i^{\mathrm{utopia}}(k)}{J_i^{\mathrm{nadir}}(k) - J_i^{\mathrm{utopia}}(k)}. \tag{4.25}$$

Namely, the Utopia point is moved to the origin and its distance to the Nadir point is scaled to 1 for every objective. Note that this dynamic normalization respects that both the Utopia point and Nadir point change over time.

Fixed Normalization In dynamic MOO, changing conditions can lead to significantly different extreme points of the Pareto front. An example in microgrid control are the possible peak costs, which can vary from 0 to over 20,000 €. Thus, single objectives may overly dominate in the dynamic normalization. To overcome this issue, we propose the so-called fixed normalization,

$$^{\mathrm{f}}\tilde{J}_i^r(k) = \frac{J_i^r(k) - J_i^{\mathrm{utopia}}(k)}{\Delta J_i^{\mathrm{fix}}}. \tag{4.26}$$

The constant scaling value $\Delta J_i^{\mathrm{fix}}$ has to be chosen once for every objective. This can be done either from experience, or from long-term simulations in which the Pareto front is determined at every time step. In the latter case, the distribution of the Pareto front's widths can be utilized to obtain a representative value. We use this method for our application example in the simulation study in Section 5.3.2.

4.4.2 Metrics

We investigate three different metrics for the selection of a knee point: 1) the Euclidean distance to the Utopia point, i. e. the closest to Utopia point (CUP) solution is chosen; 2) the minimum angle to the neighbor points (ATN) and 3) the minimum angle to the extreme points (AEP) of the Pareto front is considered best. Note that all metrics are determined after the normalization, whether dynamic or fixed. Thus, we will use $\tilde{J}$ instead of $^{\mathrm{d}}\tilde{J}$ or $^{\mathrm{f}}\tilde{J}$ in the following descriptions.

CUP The Euclidean distance of solution r to the Utopia point is given by

$$d_{\text{cup}}(\tilde{J}^r) = \left\| (\tilde{J}_1^r, \ldots, \tilde{J}_q^r) \right\| = \sqrt{(\tilde{J}_1^r)^2 + (\tilde{J}_q^r)^2}. \tag{4.27}$$

ATN To calculate the angle α_{ATN} between a solution $\tilde{J}^r$ and its neighbors for $q = 2$ objectives, we assume that the Pareto set $\tilde{\mathbb{J}}$ is of size n_{samp} and has been ordered with increasing values for objective 1, i. e. $\tilde{J}_i^r \leq \tilde{J}_{i+1}^r$. Then, the ATN is calculated by

$$r_{\text{ATN}}(\tilde{J}^r) = \begin{pmatrix} \tilde{J}_1^r \\ \tilde{J}_2^r \end{pmatrix} - \begin{pmatrix} \tilde{J}_1^{r-1} \\ \tilde{J}_2^{r-1} \end{pmatrix}, \tag{4.28}$$

$$p_{\text{ATN}}(\tilde{J}^r) = \begin{pmatrix} \tilde{J}_1^r \\ \tilde{J}_2^r \end{pmatrix} - \begin{pmatrix} \tilde{J}_1^{r+1} \\ \tilde{J}_2^{r+1} \end{pmatrix}, \tag{4.29}$$

$$\alpha_{\text{ATN}}(\tilde{J}^r) = \frac{r_{\text{ATN}}^\intercal \cdot p_{\text{ATN}}}{\|r_{\text{ATN}}\| \cdot \|p_{\text{ATN}}\|}. \tag{4.30}$$

Note that 1) α_{ATN} is defined only for $i = 2, \ldots, n_{\text{samp}} - 1$, i. e. not for the extreme points; and 2) this calculation is sensitive to the (Euclidean) distance Δd between the samples. Namely, on a continuously differentiable curve, $\lim_{\Delta d \to 0} \alpha_{\text{ATN}} = 180°$. Thus, the Pareto solutions have to be equally distributed at least approximately. While this would be a big constraint for especially meta-heuristic methods, it can be achieved by the use of both the FPBI presented in Section 4.3 and the AWDS. The ATN can also be extended to 3 or more objectives. However, the calculation becomes more complicated; thus the interested reader is referred to [56].

AEP Similar to the ATN, for $q = 2$ the angle of a solution $\tilde{J}^r$ to the extreme points is calculated by

$$r_{\text{AEP}}(\tilde{J}^r) = \begin{pmatrix} \tilde{J}_1^r \\ \tilde{J}_2^r \end{pmatrix} - \begin{pmatrix} \tilde{J}_1^1 \\ \tilde{J}_2^1 \end{pmatrix}, \tag{4.31}$$

$$p_{\text{AEP}}(\tilde{J}^r) = \begin{pmatrix} \tilde{J}_1^r \\ \tilde{J}_2^r \end{pmatrix} - \begin{pmatrix} \tilde{J}_1^{n_{\text{samp}}} \\ \tilde{J}_2^{n_{\text{samp}}} \end{pmatrix}, \tag{4.32}$$

$$\alpha_{\text{AEP}}(\tilde{J}^r) = \frac{r_{\text{AEP}}^\intercal \cdot p_{\text{AEP}}}{\|r_{\text{AEP}}\| \cdot \|p_{\text{AEP}}\|}. \tag{4.33}$$

As the ATN, α_{AEP} is only defined for $i = 2, \ldots, n_{\mathrm{samp}} - 1$. However, in contrast to the ATN, it is not sensitive to the distance Δd between the samples. Again, an extension for $q \geq 3$ can be found in [56].

4.5 Automatized Preference-Based Decision Making

With the metric-based strategies described above, the decision making process can be automatized to either find knee points (AEP and ATN) or a balanced compromise CUP. However, no preferences of a DM on the importance of the objectives are respected. Thus, we present a new preference-based decision making strategy in the following to overcome this issue. The approach allows for representing preferences in an easy to interpret way and at the same time limits their influence in dependence of 1) a design parameter and 2) the shape of the Pareto front itself, thus ensuring that no unreasonable compromise is selected. The approach consists of two steps and as before, we assume that an approximation of the Pareto front is available. First, a knee region of the normalized Pareto front is determined, i. e. the set of solutions which would be of the highest interest to the DM. Second, preferences formulated as a relative importance, e. g. 50-20-30, are translated into the orientation of a hyperplane. The solution inside the knee region at which the hyperplane can be placed without interfering with the rest of the knee region is then selected. Figure 4.7 illustrates the approach in the MPC setting.

4.5.1 Knee Region Determination

In all following calculations, we assume that the available approximation $\mathbb{J}$ of the Pareto front has been normalized. Both normalization schemes from Section 4.4.1 are possible. Thus, we again use the general forms $\tilde{\mathbb{J}}$ or $\tilde{J}$.

For the definition of our knee region, we use a metric similar to [31], i. e. for each Pareto solution, we calculate its Euclidean distance to a geometric object at the edge of the Pareto front. However, the individual minima (also called extreme points) are often hard to find [14, 36]. Thus, instead of maximizing the distance from the convex hull of the extreme points, we

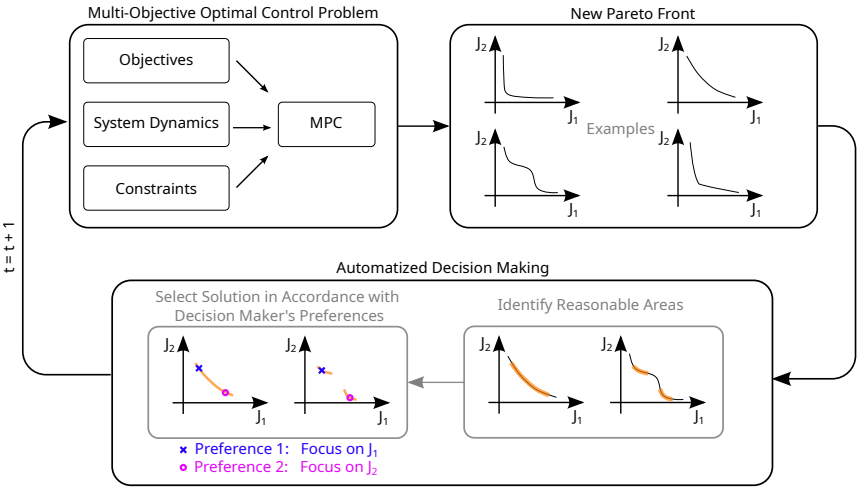

Figure 4.7: Automatized preference-based decision making in multi-objective MPC. First, reasonable areas of the Pareto front are identified as the knee region, i. e. we exclude solutions that are too extreme. Then, we incorporate the decision maker's preferences by a geometric interpretation to finally choose a compromise. The solution represents a control plan which is then applied (at least the first step in case of MPC). Then, the process is repeated for the next time step.

use a hyperplane

$$\mathcal{D} : \{x \mid -\mathbf{1}_{1\times q}(x - \tilde{J}^r) = 0, \quad r = \arg\max_i ||\tilde{J}^i||_2\}, \tag{4.34}$$

which we refer to as the *distance plane* in the following. Note that $\tilde{J}^r \in \tilde{\mathbb{J}}$ is the point of the (normalized) Pareto front with the largest Euclidean distance to the normalized Utopia point $\tilde{J}^{\text{utopia}} = \big(0, \dots, 0\big)$ and that we use the negative vector of ones $-\mathbf{1}_{1\times q}$ as the distance plane's normal vector to avoid sensitivity to possibly unreliable extreme points. Then, the distance of every solution $\tilde{J}^i \in \tilde{\mathbb{J}}$ to $\mathcal{D}$ is calculated as

$${}^{\mathcal{D}}\delta(\tilde{J}^i) = \frac{1}{\sqrt{q}}(-\mathbf{1}_{1\times q})(\tilde{J}^i - \tilde{J}^r). \tag{4.35}$$

Finally, similarly to [77, 137], we define the knee region $\bar{\mathbb{J}} \subseteq \tilde{\mathbb{J}}$ as

$$\bar{\mathbb{J}} = \{\tilde{J}^i \mid {}^{\mathcal{D}}\delta(\tilde{J}^i) \geq r_{\text{lim}} \cdot \max_{\tilde{J}^j} {}^{\mathcal{D}}\delta(\tilde{J}^j)\}, \tag{4.36}$$

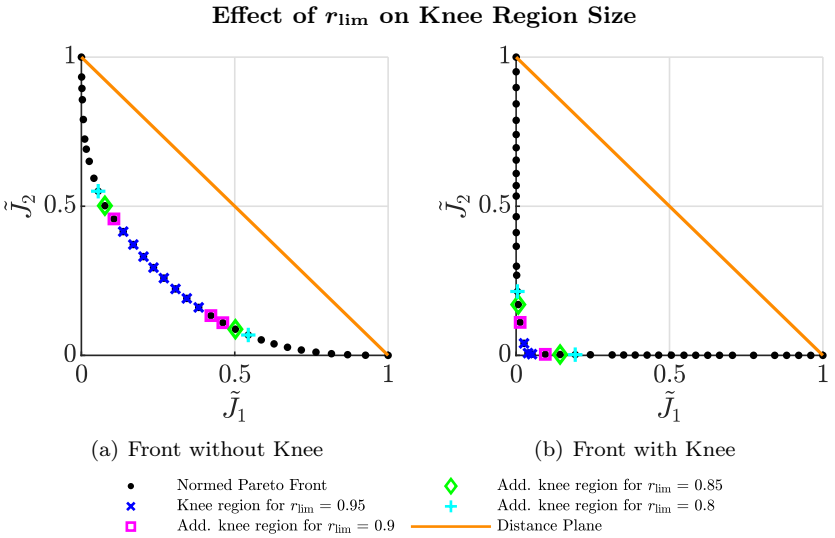

Figure 4.8: Exemplary knee regions in 2D for different r_{lim}. For fronts without a knee point (a), the knee region is larger than for fronts with a knee point (b) for any r_{lim}. Note that for convex 2D fronts, the distance plane is equivalent to the convex hull of the minima from [31] (if normalized).

where $r_{\text{lim}} \in [0, 1]$ is a design parameter with which the influence of the DM's preferences can be adjusted. Furthermore, $\bar{\mathbb{J}}$ can be understood as a bulge of the Pareto front in the direction of the Utopia point, whose size depends on the Pareto front's shape, as illustrated in Figure 4.8. Note that, in contrast to the commentary in [77], while the bulge is hard to comprehend in more than 3 dimensions, this is not necessary for our approach, since the final decision making is automatized, too.

4.5.2 Choosing a Solution

After the knee region $\bar{\mathbb{J}}$ has been determined, one of its solutions has to be chosen. First, the preferences of the decision maker are formulated as the preference vector $p \in \mathbb{R}^q_+$ for all q objectives. Since we work in the normalized space, the objectives' possibly different magnitudes can be ignored. Then, p can be interpreted as the normal vector of a hyperplane

$$\mathcal{P}(\tilde{J}^{\text{b}}) : \{x \mid p^{\intercal}(x - \tilde{J}^{\text{b}}) = 0\} \tag{4.37}$$

where $\tilde{J}^{\mathrm{b}} \in \bar{\mathbb{J}}$ is the hyperplane's base point. In the following, we will refer to $\mathcal{P}$ as the *preference plane*.

As the base point $\tilde{J}^{\mathrm{b}}$, we choose the knee region's solution to which the preference plane is 'tangent', i. e. the $\tilde{J}^{\mathrm{b}} = \tilde{J}^{i} \in \bar{\mathbb{J}}$ that builds a halfspace with the preference plane which is below all other solutions, such that

$$p^{\intercal}(\tilde{J}^{j} - \tilde{J}^{\mathrm{b}}) \geq 0 \;\forall\; \tilde{J}^{j} \in \bar{\mathbb{J}}. \tag{4.38}$$

In 2D, this halfspace is the area below a line, and the line which passes through $\tilde{J}^{\mathrm{b}}$ and is orthogonal to p. In the unlikely event that multiple solutions on the knee region fulfill (4.38), any of them can be selected. Figure 4.9 illustrates different preference planes and the resulting selections for a 2D front.

4.5.3 Discussion of the Preference for Knee Points

As stated in Section 4.2.2, [24] defines the knee point of a 2D MOO problem as the point which is the solution for the most λ_i in the weighted sum

$$\min_{x}(\lambda_i \cdot J_1(x) + (1 - \lambda_i) \cdot J_2(x)) \tag{4.39}$$

where λ_i is chosen from a large but finite set $\subseteq [0, 1]$. However, as illustrated in [35, Figure 1] and explained in [32], the minimization of (4.39) can be interpreted as shifting a plane with an angle $\alpha(\lambda_i)$ to the origin until it is tangent to the Pareto front. Furthermore, this interpretation is also applicable with q-dimensional hyperplanes, see e. g. [121]. Thus, our approach of constructing a hyperplane a posteriori and choosing the solution at which it is tangent to the Pareto front inherently prefers knee points, since multiple preferences p (and thus preference planes) will satisfy (4.38) for the same $\tilde{J}^{i}$ if it is a knee point (as the small illustration in Figure 4.9(b) suggests). However, note that this does not admit the conclusion that our approach could be replaced by solving a weighted sum with the according weights instead. First, the reduction of possible decisions to a knee region prevents point which are too extreme (and thus uninteresting) to be selected, independently of the formulated preferences. Second, our approach allows us to use an approximation of the Pareto front which can be derived from any method, not just from the minimization of a weighted sum.

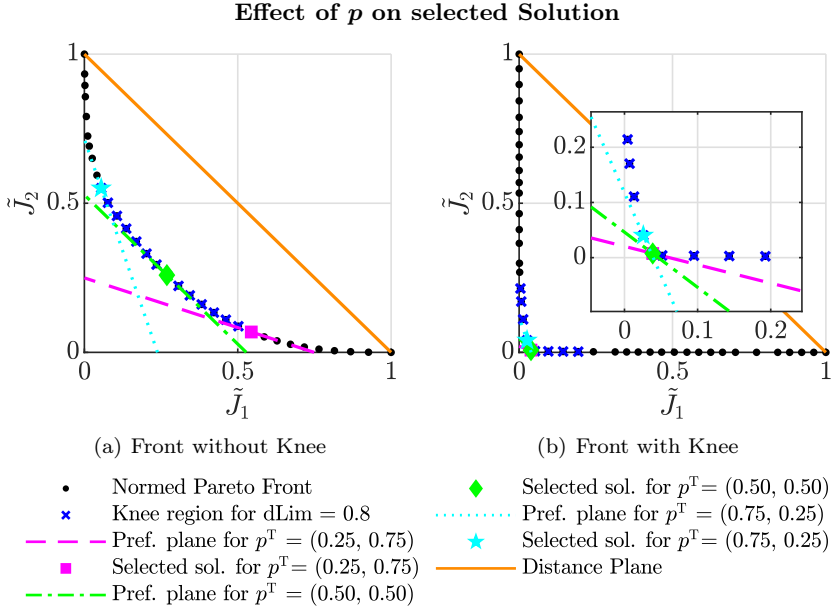

(a) Front without Knee (b) Front with Knee

Figure 4.9: Exemplary preference planes (4.37) for the Pareto fronts from Figure 4.8 and the selected solutions (i. e. base points $\tilde{J}^b$) with $r_{\text{lim}} = 0.8$. For example, for the green preference plane with $p^\intercal = \big(0.50,\ 0.50\big)$, the base point $\tilde{J}^b$ is marked as a green diamond. Note that for the front without a knee in (a), the different preferences lead to solutions far apart from each other. For the front with a knee in (b), two of the three preferences choose the knee itself. Even for $p^\intercal = \big(0.75,\ 0.25\big)$, the selected solution is close to the knee point, despite the large knee region (with solutions a human DM would not consider to be interesting).

4.6 Summary

In this chapter, we combine multi-objective optimization (MOO) with (economic) MPC by formulating the optimal control problem as a multi-objective optimization problem. Namely, all constraints from the system dynamics etc. are respected as usual, but the solution to the multi-objective optimal control problem is the Pareto front representing all possible Pareto optimal compromises of the objectives. Then, a solution from the Pareto front is chosen and the first step of the underlying control sequence is applied to the system. We refer to this procedure as *dynamic MOO*. Furthermore, we present the focus point boundary intersection (FPBI) method, a new approach to sample higher dimensional Pareto fronts in the dynamic MOO setting with varying conditions in a robust fashion.

Besides the determination of the Pareto front itself, the most crucial task is to automatize the decision making process, since it would be too tedious for a human decision maker (DM) to manually choose a compromise, which is the usual procedure in regular MOO, in every time step. Thus, we present two different strategies to automatize the decision making process; 1) a metric-based strategy, which first normalizes the Pareto front and then selects the solution with the best value of a pre-defined metric. We propose 2 different normalization schemes and 3 different metrics, resulting in 6 possible combinations. And 2), a preference-based strategy, which is the main methodological contribution of this thesis. In a first step, it determines a knee region of the Pareto front which would be most interesting to the DM. In a second step, it uses easy to interpret preferences of the DM, e. g. 50-20-30, to finally choose a solution by interpreting them as the normal vector of a hyperplane. Its advantages are that it 1) ensures that only good compromises can be selected by limiting possible choices to the knee region, which 2) depends on the Pareto front's shape, 3) gives the DM a design parameter with which he can comprehensibly choose how strong his influence should be a priori, and 4) has a built-in proclivity for knee points, if they exist.

5 Building Energy Management with Multi-Objective MPC

In this chapter, we build upon the models and simulations from Chapter 2 and apply the dynamic MOO strategies from Chapter 4. First, we motivate why multi-objective MPC is necessary for the control of building energy management systems in Section 5.1. Then, we review how multiple objectives have been handled in microgrid control so far in Section 5.2. We analyze the effect of both the metric-based and preference-based decision making strategies to our exemplary building in long-term simulation studies in Section 5.3 and end with a summary in Section 5.4.

This chapter is based on and has partly been published in the following publications:

[S3] T. Schmitt, T. Rodemann, and J. Adamy. Multi-objective model predictive control for microgrids. *at - Automatisierungstechnik*, 68(8):687 – 702, 2020.

[S4] T. Schmitt, J. Engel, M. Hoffmann, and T. Rodemann. PARODIS: One MPC framework to control them all. Almost. In *2021 IEEE Conference on Control Technology and Applications (CCTA)*, 2021.

[S8] T. Schmitt, M. Hoffmann, T. Rodemann, and J. Adamy. Incorporating human preferences in decision making for dynamic multi-objective optimization in model predictive control. *Inventions*, 7(3), 2022.

5.1 Introduction

In Section 2.3.2, we introduced 5 different objectives which we used in the subsequent simulation studies: monetary costs, temperature comfort, ecological costs (CO_2 emissions), battery degradation and EV charging satisfaction. This list of possible objectives is incomplete and could be

extended, but is already sufficient to illustrate that compromises inevitably have to be made in the control of an energy management system. All objectives are of both different units and scales, which makes it hard for a DM to compare them. Furthermore, the changing environment during long-term control, e. g. weather seasons, renewable energy production and possible peak costs can lead to changing conditions in the optimization problems over time such that a compromise (or weighting) decided on before may not represent the DM's intention anymore. Thus, the systematic incorporation of (dynamic) MOO in the control of building energy management systems is necessary and, due to the slow system dynamics, possible, too.

5.2 Related Work

As explained in Section 2.1, the two main approaches in microgrid control are either ODE modeling in combination with deterministic optimizers, which we use, or BPS-based modeling in combination with meta-heuristic optimizers. Since the majority of the MOO community uses meta-heuristic methods, these also constitute a large part of the microgrid control literature which considers multiple objectives. Thus, studies following both approaches are covered in the following literature review.

Examples for complex models based on a BPS and meta-heuristic optimization are [7, 78, 118], which all consider monetary costs and thermal comfort as objectives. The authors of [78] use a combination of GenOpt [138] and EnergyPlus to optimize temperature set points of three building models in an MPC scheme over a time period of 5 days. As the optimization strategy, they use Hooke-Jeeves Particle Swarm Optimization. However, they do not construct a dense Pareto front for the two objectives, but determine five Pareto solutions by running their simulation with five different weights on the monetary costs. In [7], a three-room building is modeled with EnergyPlus. MATLAB is used to derive optimal control sequences with genetic algorithms in an MPC framework. The optimization is repeated only once every 24 h with $T_\mathrm{s} = 1\,\mathrm{h}$, possibly due to the long optimization time required ($> 1\,\mathrm{h}$), which makes this approach not applicable in real-time. In [118], again the combination of EnergyPlus and genetic algorithms is used to control the model of a residential building with 6 temperature zones. As decision variables, hourly set points are used. However, the fitness of a population within the optimization process is not evaluated by simulating the model in EnergyPlus, but by an artificial neural network

surrogate model. It is trained for every temperature zone to reproduce simulation results such as energy consumption and indoor temperature in dependence of forecasted exogenous factors such as outdoor temperature, relative humidity and solar irradiance. Artificial neural networks are used both for determining a population's fitness as well as for approximating solutions from the genetic algorithms to reduce optimization time, which allows for online optimization with $\Delta t = 1\,\mathrm{h}$. However, thermal comfort is only defined by being in a certain temperature range in occupied times. If this is violated, a penalty function is applied in the genetic algorithm. Thus, no trade-offs in form of a MOO problem are considered.

Examples for modeling based on ODEs and MPC using deterministic optimization are [57, 106, 126, 144]. The authors of [57] model a simple linear microgrid model with a stationary battery as the only state. As the objective function, they use the unweighted sum of monetary costs and battery lifetime degradation. A time horizon of 12 h with a time step $\Delta t = 20\,\mathrm{min}$ is chosen. However, the battery lifetime is a nonlinear function and it is not clear how the resulting optimization problem has been solved (other than with the MATLAB optimization toolbox). In [144], a simplified building model with 4 ODEs including an air-handling unit is used. Energy consumption and thermal comfort are considered as objectives. The distance to the Utopia point is directly minimized, which leads to an NLP problem. However, only one optimization problem per day with $\Delta t = 1\,\mathrm{h}$ is solved. In [126], a microgrid in island mode with diesel generators and shiftable loads is considered. The prediction horizon is 24 h. However, to reduce computational expenses, the sampling time varies, i. e. increases from 5 min in the first half hour to 1 h for the last 22 h of the horizon. Fuel and emission costs are minimized. The authors compare two different strategies for this MOO problem, namely taking a (fixed) weighted sum and directly minimizing the distance to the Utopia point, which results in a mixed-integer nonlinear programming (MINLP) problem and took on average 8.12 s to solve. However, the results of the one day simulation for the scenario without demand response show that the compromise solution is outperformed by the weighted sum solution. This might be due to non-global optima found for the MINLP. In [106], stochastic MPC with chance constraints and uncertain weather forecasts is used. Namely, constraints for the building temperature are not violated with a likelihood of $1 - \alpha$. Samples of the Pareto front (energy use vs. number of constraint violations) are derived by varying α. However, no systematic choice of a trade-off is conducted.

Concluding, applying sophisticated MOO methods within a MPC framework to microgrid models with increasing complexity generally is a challenging problem. Furthermore, there is a lack of research as to how compromises between contradicting objectives are selected best.

5.3 Simulation Studies

In the following, we analyze the effect of the dynamic MOO methods from Chapter 4 to the microgrid models derived in Chapter 2 in simulation. After a short overview of the Pareto functionalities of our MATLAB framework PARODIS in Section 5.3.1, we first apply the decision making strategies with fixed metrics in Section 5.3.2 and then the preference-based knee region approach in Section 5.3.3.

5.3.1 Pareto Functionalities in PARODIS

We presented the basic functionalities of our new MATLAB MPC framework PARODIS in Section 2.4.2. Here, we shortly describe its functionalities for the use of dynamic MOO.

Pareto optimization in PARODIS is used by simply defining the `Controller` to be of type `ParetoController` (instead of `SymbolicController` or `ExplicitController`). Then, the user can choose from the different pre-implemented methods for

1) determining the extreme points (called *extreme point method*),
2) calculating the rest of the Pareto front (called *front determination scheme*) and
3) choosing a solution from the Pareto front (called *metric function*).

Note that, alternatively to 3), a solution could be chosen by hand. The method to be used for each type is defined in the `config` of the controller, e. g.

```
controller.config.extremePointFunction='LEX';
controller.config.frontDeterminationScheme='NBI';
controller.config.metricFunction='CUP';
```

Table 5.1 summarizes the currently available options.

Table 5.1: List of extreme point functions, front determination schemes and metric functions in PARODIS. The string for selecting a method is given in parentheses.

Extreme Point Methods	
Lexicographic Approach	(`'LEX'`) Optimization in lexicographic order as in (4.11).
Miniscule Weight Approximation	(`'MWA'`) Approximation of the extreme points with weights $w_i = 1$ and $w_{j\neq i} = 10^{-5}$ as described in Section 4.2.1, page 81.
Normalized Miniscule Weight Approximation	(`'MWAN'`) Miniscule Weight Approximation with prior (dynamic) normalization as in (4.25) for a better conditioning of the optimization problem.
Front Determination Schemes	
Normal Boundary Intersection	(`'NBI'`) NBI method as described in Section 4.2.1, page 78.
Focus Point Boundary Intersection	(`'FPBI'`) FPBI method from Section 4.3, page 86.
Adaptive Weight Determination Scheme	(`'AWDS'`) AWDS method as described in Section 4.2.1, page 77.
Metric Functions	
Closest-to-Utopia-point	(`'CUP'`) Distance-based CUP metric, see (4.27).
Angle to extreme points	(`'AEP'`) Angle-based AEP metric, see (4.31)-(4.33)
Angle to neighbors	(`'ATN'`) Angle-based ATN metric, see (4.28)-(4.30)
(Approximated) radius of curvature	(`'RoC'`) In 2D, the radius of curvature is the radius of the circle which connects a point on the Pareto front with its two neighbors. See [71] for a formal definition and [56] for the implemented approximation.

5.3.2 Fixed Metrics

In this section, we analyze all possible combinations of the 2 normalization schemes (dynamic or fixed) and 3 metrics (CUP, ATN or AEP) from Section 4.4.2. To this end, we first summarize the simulation setting, then we derive the scaling values for the fixed normalization scheme, show selections for all combinations on exemplary Pareto fronts and finally compare their long-term effects in 1-year simulations. Note that parts of this simulation study have been published in [S3].

Simulation Setting

The simulation conditions are the same as in Section 2.4.3, i. e. we use the standard model HL-1, data from 2018 and monetary and comfort costs as the two objectives. For the monetary costs, both the industry and the intraday pricing scenarios are simulated. For the industry scenario, the optimization problem is as in (2.62). For the intraday scenario, it is defined by

$$\begin{aligned} \mathcal{O}_{\mathrm{HL}-1}^{\mathrm{Mon.(Intra)},\mathrm{Comf.}}(k)\colon \min_{\boldsymbol{u}} \; & w_{\mathrm{mon}} \cdot J_{\mathrm{mon}}^{\mathrm{intra}}(k) + w_{\mathrm{comf}} \cdot J_{\mathrm{comf}}(k), \\ \text{s. t. } & (2.8\mathrm{b}), \\ & (2.46), (2.48), (2.49). \end{aligned} \tag{5.1}$$

AWDS is used to determine the Pareto front. Furthermore, if either CUP or AEP are used as metrics, the area around the first determined solution has been sampled again with a smaller distance ratio Δd^{awds} to increase precision. For ATN, this is not done because the result is sensitive to the distance between solutions, as discussed in Section 4.4.2.

Determining Constant Scaling Values for Fixed Normalization

To use the fixed normalization scheme (4.26), we have to choose fixed scaling values $\Delta J_i^{\mathrm{fix}}$. Note that, in the following, we use the notation $\left(J_{\mathrm{mon}},\, J_{\mathrm{comf}}\right)$ instead of $\left(J_1,\, J_2\right)$ to refer to the individual objectives for better readability.

As motivated before, the widths of the Pareto fronts can vary significantly, especially for the monetary costs. Thus, instead of relying on expert knowledge, we simulate the system with the dynamic normalization scheme

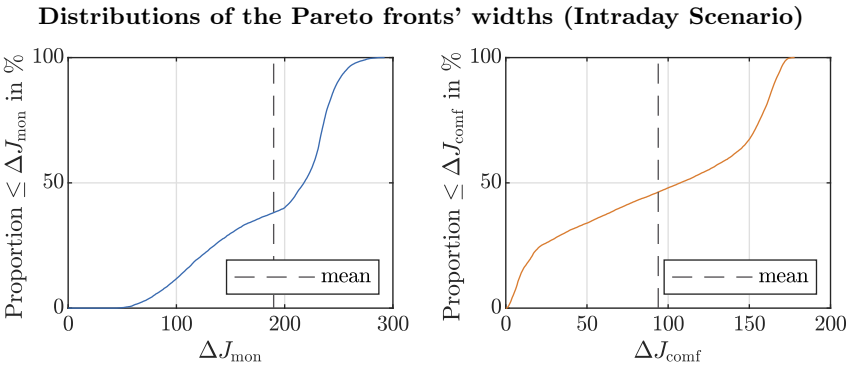

(a) Monetary Costs (b) Comfort Costs

Figure 5.1: Frequency distributions of (a) ΔJ_{mon} and (b) ΔJ_{comf} in a one year simulation for the intraday scenario (dynamic normalization, CUP metric). For example, $\Delta J_{\text{mon}}(k)$ has been ≤ 189.82 (which is the mean value) in 38.13 % of all cases. The maximum value for ΔJ_{mon} has been 290.64.

and CUP as the metric for one year. Then, we determine the frequency distributions of the (unnormalized) Pareto fronts' widths for both objectives, i. e.

$$\Delta J_{\text{mon}}(k) = J_{\text{mon}}^{\text{nadir}}(k) - J_{\text{mon}}^{\text{utopia}}(k), \tag{5.2}$$
$$\Delta J_{\text{comf}}(k) = J_{\text{comf}}^{\text{nadir}}(k) - J_{\text{comf}}^{\text{utopia}}(k) \tag{5.3}$$

at time step k. Afterwards, we can derive appropriate $\left(\Delta J_{\text{mon}}^{\text{fix}}, \Delta J_{\text{comf}}^{\text{fix}}\right)$ from the frequency distributions.

Figure 5.1 shows the distributions for a 1-year simulation of the *intraday* scenario. Note that these distributions would vary if different metrics were used for the selection, but are similar enough for the purpose of determining representative values. For the intraday scenario, the mean values are taken, which cover 38.13 % of all ΔJ_{mon} and 46.32 % of all ΔJ_{comf}.

The resulting distributions for the industry scenario are presented in Figure 5.2. Figure 5.2(a) shows that the mean value of all ΔJ_{mon} is drastically shifted to the right in comparison to the mean of all ΔJ_{comf} in Figure 5.2(b). This is due to the possibly occurring new peaks. Thus, taking the means as $\Delta J_{\text{mon}}^{\text{fix}}$ and $\Delta J_{\text{comf}}^{\text{fix}}$ is not appropriate. Instead, we make use of the bend in the distribution of Figure 5.2(a). It corresponds to $\Delta J_{\text{mon}}^{\text{fix}} = 272$

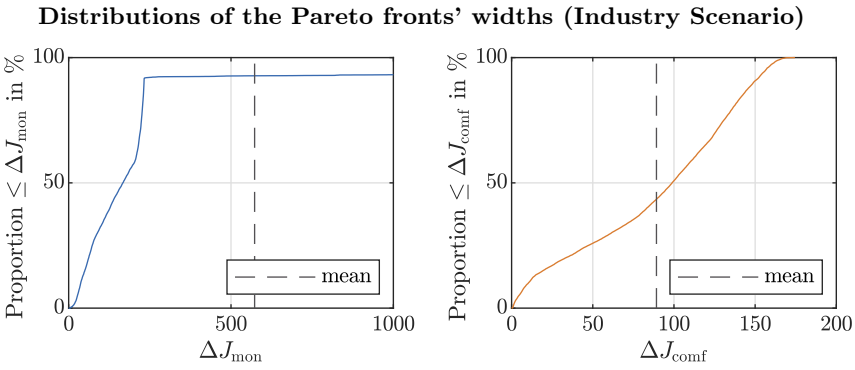

(a) Monetary Costs (b) Comfort Costs

Figure 5.2: Frequency distributions of (a) ΔJ_{mon} and (b) ΔJ_{comf} in a one year simulation for the industry scenario (dynamic normalization, CUP metric).

and lies above 91.80 % of all occuring ΔJ_{mon}. Accordingly, we choose $\Delta J_{\text{comf}}^{\text{fix}} = 153.5$, which covers 91.82 % of all ΔJ_{comf}. Table 5.2 summarizes the constant scaling values for the fixed normalization.

Table 5.2: Scaling values for fixed normalization.

	Intraday Scenario	Industry Scenario
$\Delta J_{\text{mon}}^{\text{fix}}$	189.82	272
$\Delta J_{\text{comf}}^{\text{fix}}$	93.90	153.5

Comparison of Selections on Real Pareto Fronts

To gain insights on the different selections with each normalization and metric, three typical Pareto fronts in the industry scenario are examined. Figure 5.3(a) shows a setting in winter, when heating is necessary. Due to a low ΔJ_{comf}, the fixed normalization shifts all selections to the right. Thereby, the ATN solution is affected less in comparison to CUP and AEP.

Figure 5.3(b) shows the selections for a cooling scenario in summer without possible peak costs. For the dynamic normalization, both angle-based metrics (ATN and AEP) select the same point which could be considered a knee point. If fixed normalization is used, ΔJ_{mon} is scaled stronger than

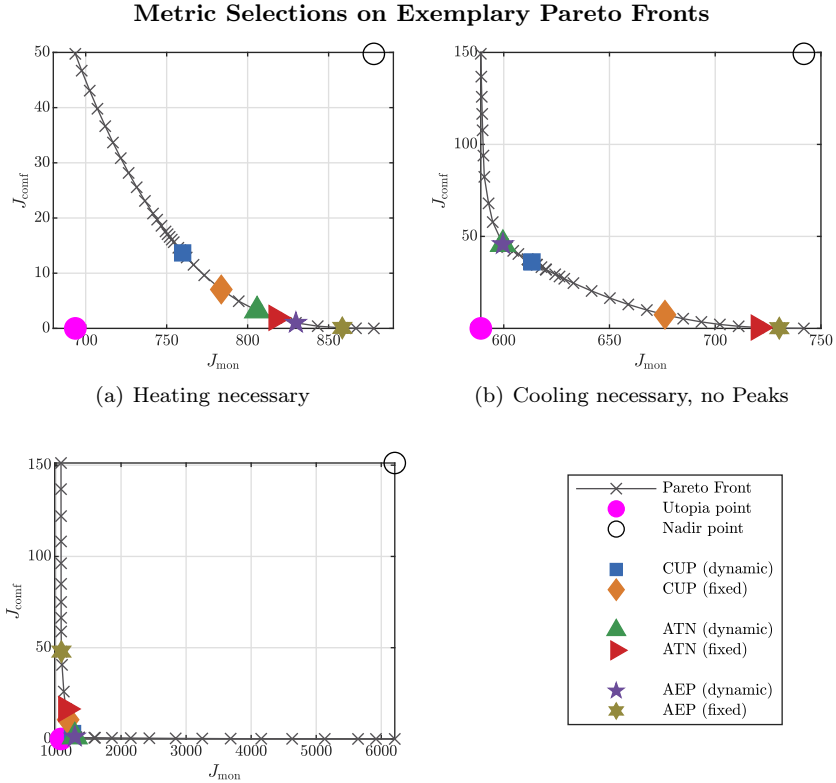

(a) Heating necessary

(b) Cooling necessary, no Peaks

(c) Cooling necessary, possible Peaks

Figure 5.3: Exemplary Pareto fronts in the industry scenario and the selections for the different combinations of metrics and normalization schemes.

(a) $\vartheta_{\text{air}} \approx 8.59°\text{C} < 21°\text{C}$, i. e. heating is necessary. Since $\frac{\Delta J_{\text{comf}}}{\Delta J^{\text{fix}}_{\text{comf}}} < \frac{\Delta J_{\text{mon}}}{\Delta J^{\text{fix}}_{\text{mon}}}$, all knee selections are shifted to the right when fixed normalization is used.

(b) $\vartheta_{\text{air}} > 21°\text{C}$, i. e. cooling is necessary. Since $\Delta J_{\text{comf}} \approx \Delta J^{\text{fix}}_{\text{comf}}$ and $\Delta J_{\text{mon}} < \Delta J^{\text{fix}}_{\text{mon}}$, the CUP and AEP selection are shifted to the right when fixed normalization is used.

(c) $\vartheta_{\text{air}} > 21°\text{C}$ and high demand, i. e. cooling is necessary and (high) peak costs are possible. Thus, $\Delta J_{\text{mon}} >> \Delta J^{\text{fix}}_{\text{mon}}$ and the selections for all metrics are shifted to the left.

ΔJ_{comf}. Thus, again all solutions are shifted to the right. However, the CUP is shifted significantly less than the ATN and AEP.

In Figure 5.3(c), a Pareto front with high peak costs is shown. Here, a clear knee point can be deducted. However, only for the dynamic normalization all metrics find it. For the fixed normalization, all selections are shifted to the left due to $\Delta J_{\text{mon}} >> \Delta J_{\text{mon}}^{\text{fix}}$. This results in trajectories with higher J_{comf}. Again, the CUP is shifted the least.

Despite the last setting with peak costs, the Pareto fronts and the knee selections for the intraday scenario look similar and are thus omitted. The examples show that metrics based on an angle, i. e. ATN or AEP, are more sensitive to the front's curvature than the CUP. The fixed normalization mainly shifts the solutions to one side, depending on the relation of $\frac{\Delta J_{\text{comf}}}{\Delta J_{\text{comf}}^{\text{fix}}}$ to $\frac{\Delta J_{\text{mon}}}{\Delta J_{\text{mon}}^{\text{fix}}}$, i. e. whether it is greater or smaller. In summary, the CUP metric seems to be the most robust one. However, long time simulations are necessary to evaluate the resulting trajectories and assess whether the shifting from the fixed normalization is beneficial or not.

Simulation Results

Determining the 2D Pareto front takes $\approx 0.4\,\text{s}$ in PARODIS on a single core of an Intel Xeon CPU E5-1607 v4 with 3.10 GHz, a 1-year simulation takes $\approx 105\,\text{min}$. Note that in the following, we refer to the summed costs over the 1-year simulation as $(J_{\text{mon}}^{\text{year}}, J_{\text{comf}}^{\text{year}})$.

Intraday Scenario Figure 5.4 illustrates the results for the intraday scenario and simulation with data from 2018. Note that, to support interpretation, the model has been simulated with $w_{\text{mon}} = 1$, $w_{\text{comf}} \approx 0$, i. e. with a focus only on monetary costs to obtain a lower limit on how much money has to be spent only on fulfilling P_{dem} (while making use of the stationary battery). This value of 98,341 € has been substracted from all other simulation results for Figure 5.4. All numerical values without this adaption can be found in the Appendix in Table A.2. Note that, due to numerical reasons and to ensure Pareto optimality (and not only weak Pareto optimality), w_{comf} has actually been set to a very small value (10^{-5}). However, the effect on $J_{\text{mon}}^{\text{year}}$ is negligible.

In addition to the three metrics for both dynamic and fixed normalization, we also simulated the entire year with fixed weights (i. e. without Pareto

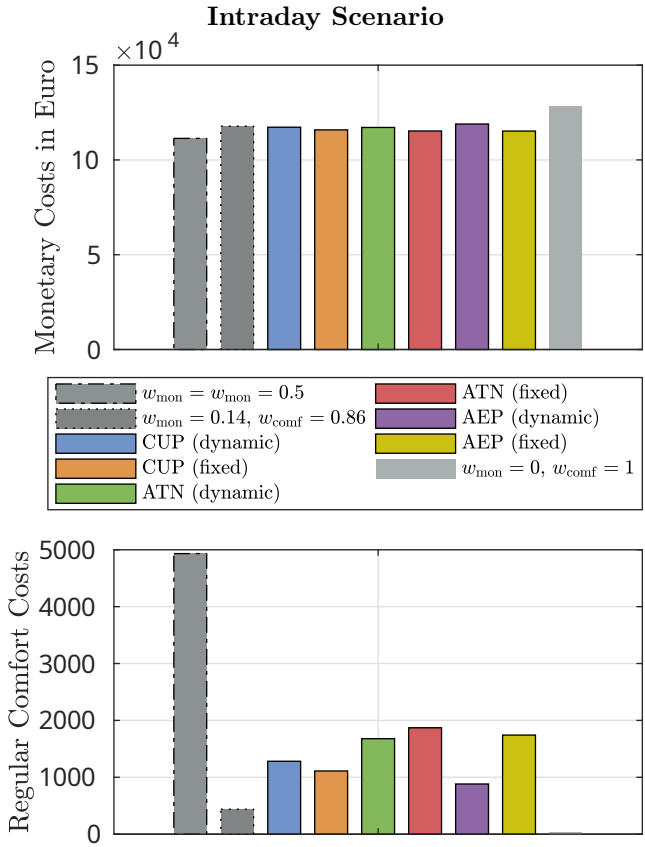

Figure 5.4: 2018 results for the intraday scenario. Note that the minimum possible value for $J_{\text{mon}}^{\text{year}}$ has been subtracted.

front construction and knee point selection). First, $w_{\mathrm{mon}} = w_{\mathrm{comf}} = 0.5$ is the setting for no weighting between the objectives and can be considered a baseline result. Second, the mean weights from the CUP (dynamic) simulation have been used as fixed weights, i. e. $w_{\mathrm{mon}} = 0.14$, $w_{\mathrm{comf}} = 0.86$. Note that this setting can also be considered a comparison baseline. However, this (sophisticated) weighting could not have been done a priori. Last, we focused on comfort only, i. e. $w_{\mathrm{mon}} \approx 0$, $w_{\mathrm{comf}} = 1$. Again, due to the reasons described before, $w_{\mathrm{mon}} = 10^{-5}$ for this setting.

In comparison to the unweighted setting ($w_{\mathrm{mon}} = w_{\mathrm{comf}} = 0.5$), all dynamic MOO settings significantly reduce $J_{\mathrm{comf}}^{\mathrm{year}}$ (≈ 60 to $80\,\%$) with only a slight increase of $J_{\mathrm{mon}}^{\mathrm{year}}$ (≈ 4 to $8\,\%$). The same applies for the fixed weighting with $w_{\mathrm{mon}} = 0.14$, $w_{\mathrm{comf}} = 0.86$, which results in an even lower $J_{\mathrm{comf}}^{\mathrm{year}}$ but higher $J_{\mathrm{mon}}^{\mathrm{year}}$ than any knee point setting. However, as has been stated before, these weights could not have been chosen a priori. Surprisingly, when the CUP is chosen as the metric, the fixed normalization outperforms the dynamic normalization.

If the knee point is chosen by an angle metric (either ATN or AEP), the fixed normalization leads to a stronger focus on costs, i. e. a lower $J_{\mathrm{mon}}^{\mathrm{year}}$ and higher $J_{\mathrm{comf}}^{\mathrm{year}}$. Note that this behavior might change with different normalization scales, which have been derived from a one-year simulation with CUP (dynamic) as described in Section 4.4.1.

Industry Scenario The results for the industry scenario are illustrated in Figure 5.5. Again, for ease of interpretation, the minimum monetary costs have been subtracted and all numerical results are given in the Appendix, Table A.3. Note that the (unadapted) $J_{\mathrm{mon}}^{\mathrm{year}}$ is higher overall due to the higher grid (and peak) costs.

Furthermore, if no focus is set on comfort ($w_{\mathrm{mon}} = 1$, $w_{\mathrm{comf}} \approx 0$), J_{comf} is less than half as high as for the intraday scenario. This is due to the stronger use of the CHP, whose electricity is cheaper than energy from the grid for the industry scenario. However, for the other settings, the comfort costs are generally higher, since a stronger focus on minimizing the monetary costs is set due to the higher grid costs. In contrast to the intraday scenario, the fixed normalization always leads to a lower $J_{\mathrm{mon}}^{\mathrm{year}}$ and higher $J_{\mathrm{comf}}^{\mathrm{year}}$ here. This is more severe if an angle-based metric is used (both ATN and AEP).

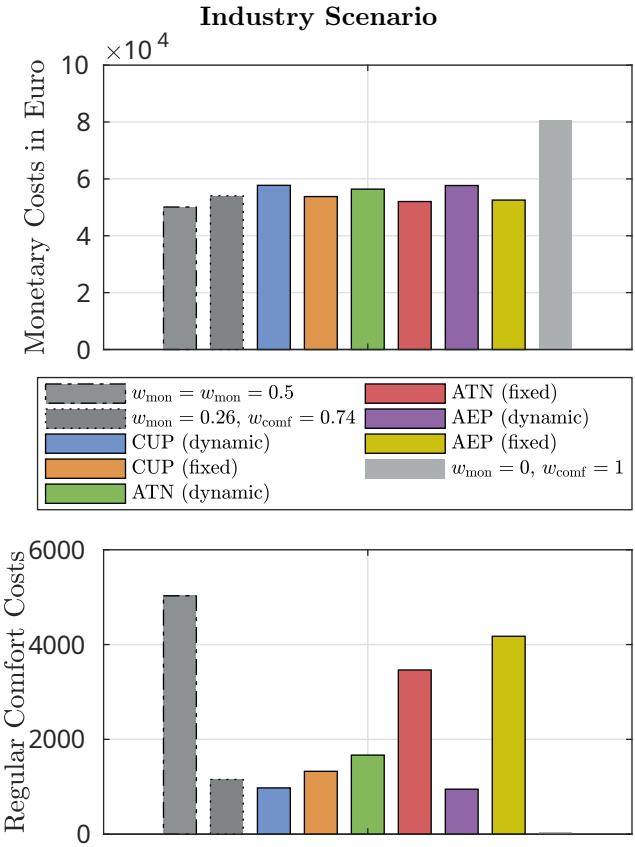

Figure 5.5: 2018 results for the industry scenario. Note that the minimum possible value for $J_{\text{mon}}^{\text{year}}$ has been subtracted.

Note that the CUP (dynamic) setting is the only one (besides $w_{\text{mon}} = 1$, $w_{\text{comf}} \approx 0$) which 'voluntarily' accepts new peak costs. Namely, in all other settings, the maximum peak is 384.6 kW and it is dictated by a high $P_{\text{dem}}(k = 1081) = -630.55\,\text{kW}$ on the 23$^{\text{rd}}$ of January. However, the CUP in the dynamic normalized space is associated with new peak costs twice within three time steps on the 23$^{\text{rd}}$ of June and goes up to 394.62 kW. This results in 875.35 € higher peak costs and leads to the CUP (dynamic) setting being slightly outperformed by the AEP (dynamic) solutions.

Conclusion

In summary, the results suggest that using the CUP is the most robust metric. For the angle based metrics, the fixed normalization shifts the focus further on reducing monetary costs at the expense of a lower thermal comfort. This effect is more severe for the industry than for the intraday scenario. The most promising combination seems to be the CUP metric together with the fixed normalization, since in the intraday scenario it even outperforms the CUP with dynamic normalization and in the industry scenario it avoids unnecessary peak costs (in comparison to the dynamic normalization). Alternatively, mean weights resulting from the knee point selections can be used a posteriori.

5.3.3 Preference-Based Knee Region Approach

In this section, we analyze how effectively the long-term costs can be varied with the preference-based decision making strategy from Section 4.5. We first summarize the simulation setting, then describe a simpler approach to respect preferences as a baseline comparison, and finally present the results for 30-day simulations with different preferences for both 2 and 3 objectives.

Simulation Setting

We again use the standard model HL-1, but data from July 2018 only and assume the intraday pricing scenario. First, we use only monetary and comfort costs as the two objectives. Then, in contrast to the simulation study before, we additionally respect the battery degradation costs (2.32)

as a third objective, which would result in the optimization problem

$$\begin{aligned} \mathcal{O}_{\mathrm{HL}-1}^{\mathrm{Mon.(Intra),Comf.,Bat.}}(k)\colon \min_{\boldsymbol{u}} \; & w_{\mathrm{mon}} \cdot J_{\mathrm{mon}}^{\mathrm{intra}}(k) + w_{\mathrm{comf}} \cdot J_{\mathrm{comf}}(k) \ldots \\ & + w_{\mathrm{bat}} \cdot J_{\mathrm{bat}}^{\mathrm{stat}}(k), \\ \text{s. t. } & (2.8\mathrm{b}), \\ & (2.46), (2.48), (2.49). \end{aligned} \tag{5.4}$$

However, since we use the FPBI method to determine a Pareto front approximation in the 3D case, this optimization problem is transformed as in (4.24).

For the 3D MOO problem, it formulates 378 single optimization problems in every time step. Overall, one simulation in PARODIS with data from July 2018 and its $30 \cdot 48 = 1440$ time steps takes about 2.5 h on a single core of an Intel Xeon CPU E5-1607 v4 with 3.10 GHz. The 2D problem takes only 9 min.

Baseline Comparison

To compare the effectiveness of our proposed approach, we present a simpler strategy as a baseline. Assume $q = 3$ objectives and $p^\intercal = [20\,\%, 70\,\%, 10\,\%]$. The preferences determine the order in which the objectives are considered in the following. For the above example, all Pareto solutions would be ranked by J_2 first. Then, the worst 70 % (in terms of J_2) are removed from the set of possible solutions. Next, the remaining solutions are ranked by J_1, from which the worst 20 % (in terms of J_1) are then removed. Finally, the remaining solutions are ranked by J_3 and the solution which is better than the worst 10 % (in terms of J_3) is selected.

In the simulation results presented below, we optionally combine this simple approach with the limitation to a knee region as in our proposed approach from Section 4.5. If so, the knee region $\bar{\mathbb{J}}$ is determined first as usual, and then we select a solution from $\bar{\mathbb{J}}$ by the rules described above (instead of using the preference plane).

Note that the preferences might have to be normalized first, such that $\sum_{i=1}^{q} p_i = 100\,\%$. If only $q = 2$ objectives are considered, the solution which splits the set in terms of the preferences can be selected directly.

Simulation Results

For all results presented in the following, the minimum possible costs for each objective have been subtracted. Namely, we run the simulations with each objective separately (e. g. $w_{\text{mon}} = 1, w_{\text{comf}} = 0, w_{\text{bat}} = 0$ if only monetary costs are to be minimized) to obtain the lowest values which cannot be avoided. In this way, the effect of the preferences can be interpreted appropriately.

2 Objectives For the 2D simulations, we vary p_{mon} from 0 to 100 while $p_{\text{mon}} + p_{\text{comf}} = 100$. The results are shown in Figure 5.6.

Figures 5.6(a) and 5.6(b) show the monetary and comfort costs for the simple baseline approach. The preferences are respected, i. e. every increase in p_{mon} leads to a decrease in monetary costs and consequently to an increase in comfort costs. However, the trade-offs for higher preference values are extreme, especially the resulting comfort costs for $p_{\text{mon}} \geq 80$.

This can be overcome by limiting all possible selections to the knee region, as we propose. If so, even the simple selection shows good results in the 2D case, see Figures 5.6(c) and 5.6(d). The highest comfort costs are limited to ≈ 100, instead of more than 4000. Note that for $p_{\text{mon}} = \{0, 10, 20\}$ and $p_{\text{mon}} = \{80, 90, 100\}$, respectively, the results are (nearly) the same, because the knee region sizes have been so small that the extremes are (nearly) almost chosen by rounding. This would be different for denser samplings.

The proposed approach (Figures 5.6(e) and 5.6(f)) incorporates the preferences in the long term costs as expected, too. Furthermore, the knee region limitation leads to the same results for $p_{\text{mon}} = \{0, 10\}$ and $p_{\text{mon}} = \{80, 90, 100\}$ only. However, here this is not due to the sampling density and rounding, but intended behavior. Namely, the resulting preference planes are so steep that they choose the extreme points of the knee region every time. Note that this would change for increasing knee region sizes, i. e. for $r_{\text{lim}} < 0.85$.

Concluding, in the 2D case, the simple baseline approach is inappropriate for the dynamic decision making due choices and trade-offs which are too extreme if the preferences are not set cautiously. The limitation of possible selections to a knee region, i. e. the first step of our two-step approach, can overcome this problem even in combination with a simpler selection

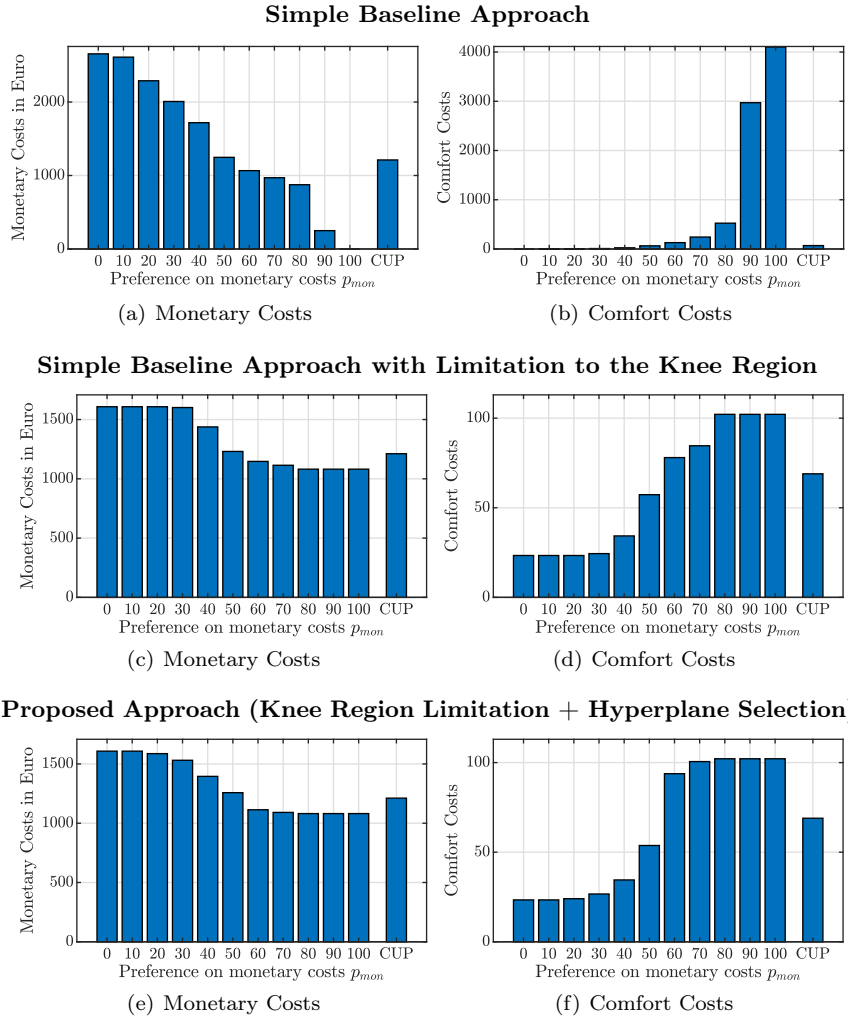

Figure 5.6: Monetary and comfort costs for the 30 days 2D simulations with different preferences p_{mon} and p_{comf} for (a)+(b) the simple baseline approach, (c)+(d) the simple baseline approach but with limitation to the knee region, and (e)+(f) the proposed preference-based decision making approach, with $r_{\text{lim}} = 0.85$ for the latter two cases. Results from using the CUP metric are plotted for comparison.

technique than the proposed preference hyperplane (the second step of our proposed approach). However, most likely this only holds because the occurring Pareto fronts are all convex. Furthermore, in the following we will see that the selection based on the preference hyperplane is superior if 3 objectives are considered.

3 Objectives The battery degradation costs are now considered as an additional third objective. Since only the relationship between the elements of the preference vector $p^\intercal = (p_{\text{mon}}, p_{\text{comf}}, p_{\text{bat}})$ is relevant, we vary both p_{mon} and p_{comf} by $\{25, 50, 75, 100\}$ while we keep $p_{\text{bat}} = 50$ constant.

Figures 5.7 (a) – (c) show the simulation results for the simple baseline approach. As in the 2D case, the costs for higher differences in the preferences become extreme, especially the comfort costs in Figure 5.7(b). Furthermore, in contrast to the 2D case, the resulting long term costs do not follow the preferences as expected. For example, in Figure 5.7(a) the monetary costs are reduced by half first if preferences are changed from $\big(p_{\text{mon}}, p_{\text{comf}}, p_{\text{bat}}\big) = \big(25, 100, 50\big)$ to $\big(50, 100, 50\big)$, but then *increase* for $\big(75, 100, 50\big)$. Note that these considerable jumps and changes in direction can partly be explained by the necessary ordering in the algorithm. Namely, the order in which the objectives are considered in removing parts of the Pareto front is relevant. For equal preferences of two objectives, J_{mon} is respected before J_{comf}, which is respected before J_{bat}.

However, this does not explain all of the unwanted behavior. Consider the row for $p_{\text{comf}} = 50$ in Figure 5.7(a). The monetary costs increase instead of decreasing if p_{mon} is increased from 50 to both 75 or 100, although the order in which the objectives are considered is the same, i. e. first J_{mon}, then J_{comf} and then J_{bat}.

The battery costs in Figure 5.7(c) are even more turbulent. They decrease instead of increase for increasing p_{mon} and $p_{\text{comf}} = 25$ and have drastic jumps in general.

Figures 5.7 (d) – (f) show the simulation results for the simple baseline approach if the selection is limited to the knee region. As expected, the extreme solutions are avoided, i. e. the maximum comfort costs are reduced from 4040.14 to 271.12 and for the battery costs from 387.56 to 86.49. However, the unwanted behavior is mostly the same otherwise. In contrast to the 2D case, the limitation to the knee region is not sufficient in combination with the simple baseline approach for an appropriate representation

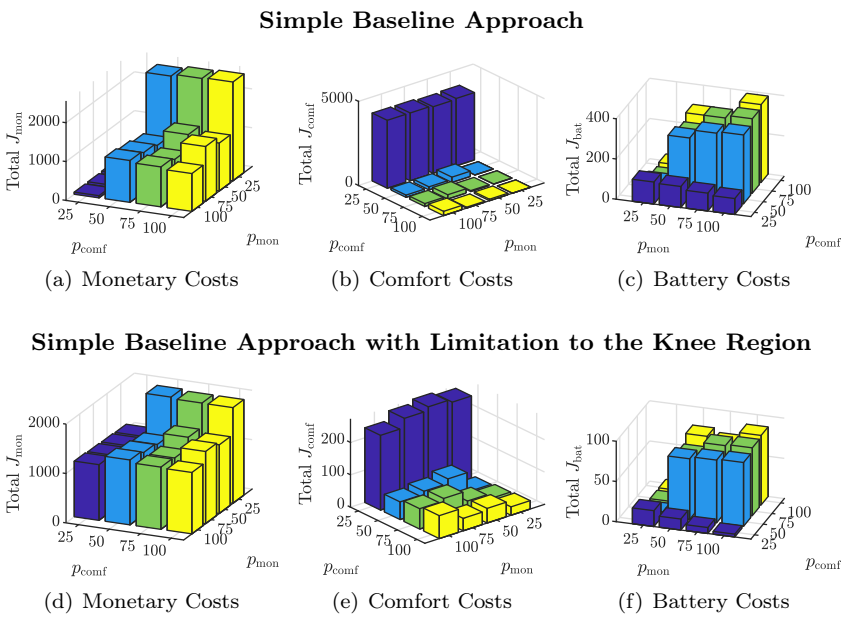

(a) Monetary Costs (b) Comfort Costs (c) Battery Costs

(d) Monetary Costs (e) Comfort Costs (f) Battery Costs

Figure 5.7: Monetary, comfort and battery degradation costs for the 30 days 3D simulations with different preferences p_{mon} and p_{comf} and $p_{\text{bat}} = 50$ for (a)-(c) the simple baseline approach and (d)-(f) the simple baseline approach but with limitation to the knee region; $r_{\text{lim}} = 0.85$. Note the different camera angles for better readability and especially the inverted axis for p_{comf} in (c) and (f). Subtracted minimum costs for each objective have been determined by single-objective optimizations.

of the preferences in the long term simulation costs.

Figure 5.8 shows the simulation results for our proposed approach. In contrast to the baseline approach, the long term costs for the monetary and comfort objective differ when varying p_{mon} and p_{comf} just as expected. The jumps between the different preference settings are smaller and more evenly distributed. Every increase in a preference leads to a decrease in the long term costs and vice versa.

For the battery costs, some simulations still show unexpected results, e. g. the total J_{bat} is slightly lower for $p^{\intercal} = \big(100,\ 50,\ 50\big)$ than for $p^{\intercal} = \big(100,\ 75,\ 50\big)$. However, this can be explained by the weak influence of

Proposed Approach (Knee Region Limitation + Hyperplane Selection)

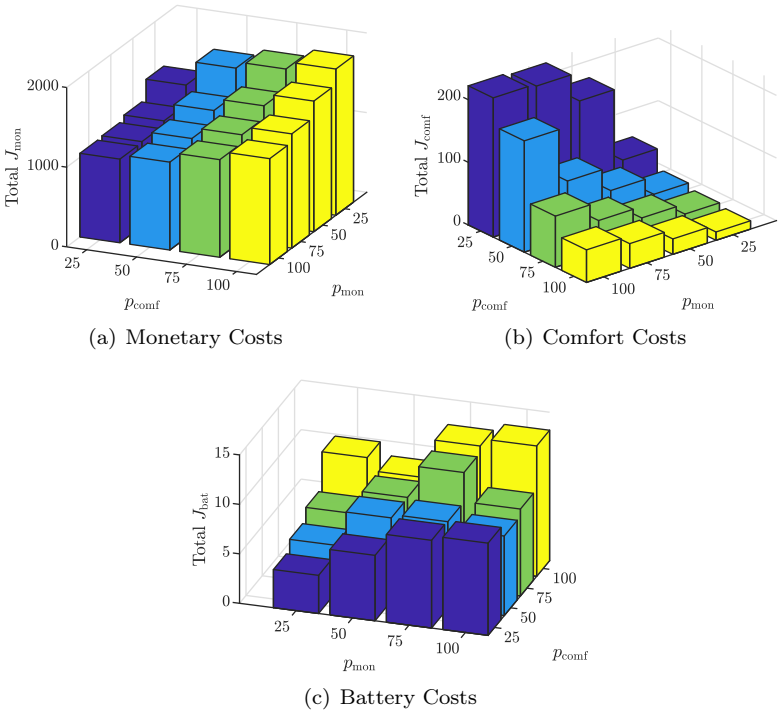

(a) Monetary Costs

(b) Comfort Costs

(c) Battery Costs

Figure 5.8: Total (i. e. summed) monetary (a), comfort (b) and battery (c) costs for the 30 days simulations with different preferences p_{mon} and p_{comf}, while $p_{\text{bat}} = 50$ is kept constant. The knee region size is set to $r_{\text{lim}} = 0.85$. Note the different camera angles for better readability and especially the inverted axis for p_{comf} in (c). Minimum costs for each objective have been determined by single-objective optimizations and subtracted.

J_{bat}. Battery and comfort costs are nearly independent and only implicitly linked via the monetary costs or possibly if P_{grid} would be at its limit. The monetary costs are in direct conflict with the battery costs because they can be reduced by buying energy at lower prices, storing it temporarily and selling it at higher prices. However, the assumed battery capacity and charging power are so low that the vast majority of possible monetary costs are due to the possible (but not necessary) cooling and heating of the building. Thus, the Pareto fronts become extremely steep, as Figure 5.9 shows exemplary. The Pareto fronts are almost degenerate [60].

However, our approach still handles this problem sufficiently well, as Figure 5.8(c) shows a clear trend of increasing costs J_{bat} from $p_{\text{mon}} = p_{\text{comf}} = 25$ to $p_{\text{mon}} = p_{\text{comf}} = 100$. Furthermore, in contrast to the baseline approach (even with the limitation to the knee region), the battery costs are significantly lower with a maximum of 13.18 instead of 86.49 overall. The long term results can actually be considered better overall, as our approach outperforms both the simple approach (e. g. $\big(25,\ 25,\ 50\big)$ vs. $\big(75,\ 100,\ 50\big)$ and the simple approach with prior limitation to the knee region (e. g. $\big(75,\ 25,\ 50\big)$ vs. $\big(55,\ 25,\ 50\big)$) for some preference combinations. The numerical values for the 3D simulations can be found in the appendix, see Tables A.4, A.5 and A.6.

Figure 5.10 shows how r_{lim} affects the possible influence of the DM. For every r_{lim}, we simulated the three possible extremes $p^1 = \big(1,\ 0,\ 0\big)^\intercal$, $p^2 = \big(0,\ 1,\ 0\big)^\intercal$ and $p^3 = \big(0,\ 0,\ 1\big)^\intercal$ and calculated the maximum difference for each objective, e. g.

$$\Delta J_{\text{mon}}(r_{\text{lim}}) = \max_{p \in \{p^2, p^3\}} \big(J_{\text{mon}}(r_{\text{lim}}, p)\big) - J_{\text{mon}}(r_{\text{lim}}, p^1). \tag{5.5}$$

The difference in monetary costs shown in Figure 5.10(a) is nearly (anti)proportional to r_{lim}. The possible differences in ΔJ_{comf} seem to decrease quadratically with an increasing r_{lim} in (b), which is probably due to its quadratic form (2.23). The battery costs in (c) again have an outlier for $r_{\text{lim}} = 0.75$, which can be explained by its weak influence and the steep Pareto fronts as discussed before. However, the trend of the decrease in ΔJ_{bat} with an increasing r_{lim} is clear, too. The average number of Pareto points which are determined as part of the knee region is nearly linear to r_{lim}, as (d) shows. However, this depends on the shapes of the Pareto fronts and cannot be generalized.

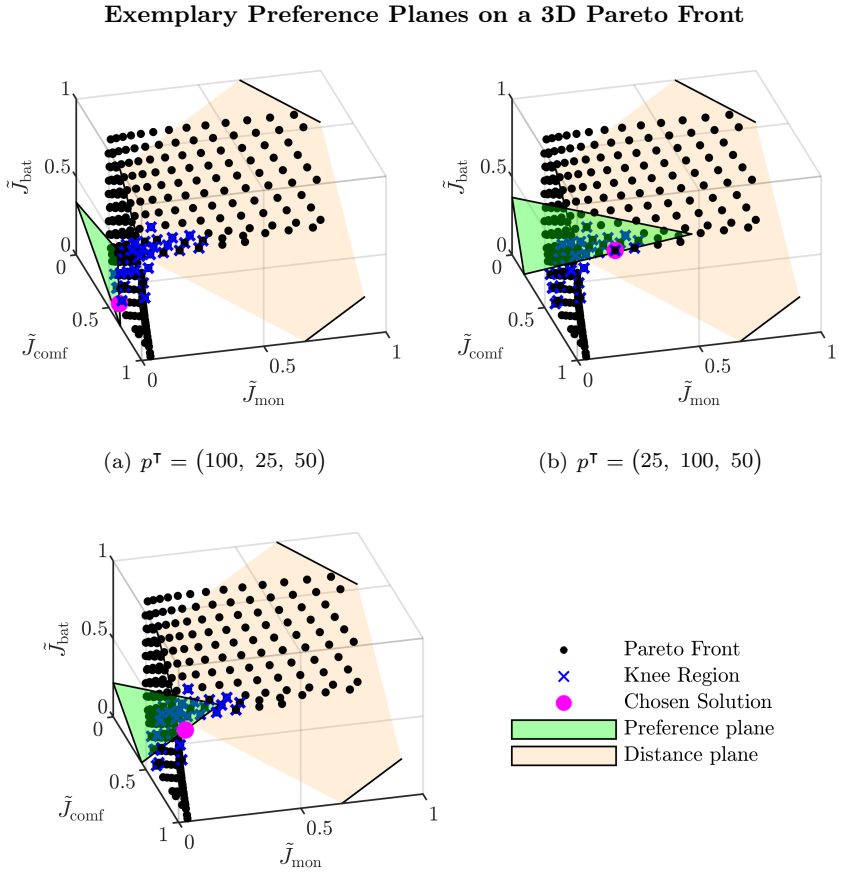

(a) $p^\intercal = (100,\ 25,\ 50)$

(b) $p^\intercal = (25,\ 100,\ 50)$

(c) $p^\intercal = (25,\ 25,\ 50)$

Figure 5.9: Single Pareto front from simulation with its knee region ($r_{\text{lim}} = 0.85$) and different preference planes with focus on (a) monetary, (b) comfort and (c) battery costs. Note that the different preferences are set according to the extreme cases from Figure 5.8.

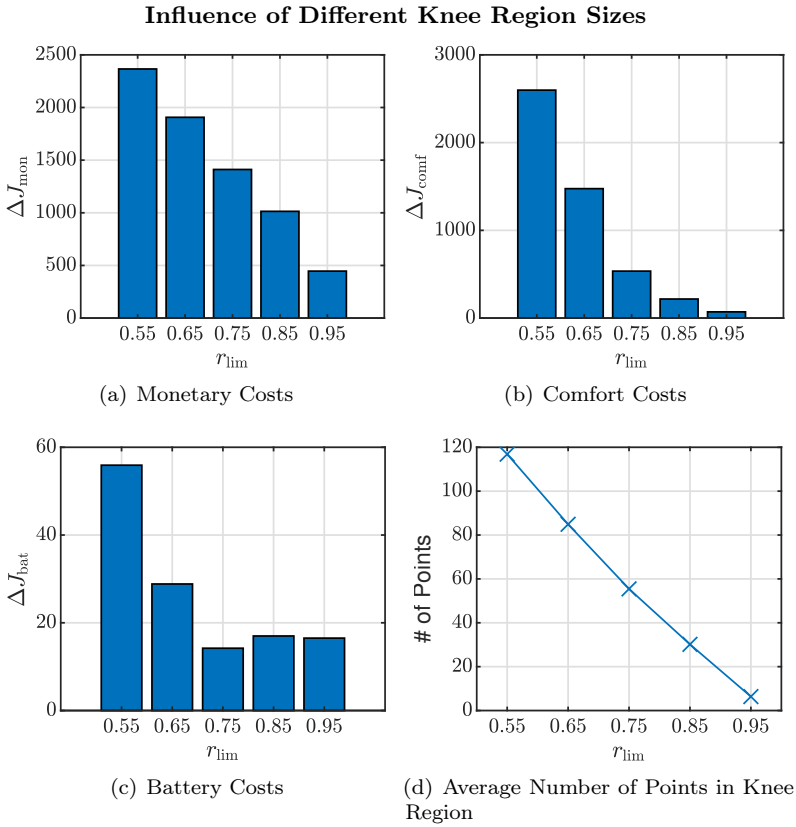

(a) Monetary Costs

(b) Comfort Costs

(c) Battery Costs

(d) Average Number of Points in Knee Region

Figure 5.10: Maximum difference in total monetary (a), comfort (b) and battery (c) costs and the average number of points considered to be part of the knee region (d) for different r_{lim}; calculated according to (5.5).

Conclusion

The results show that the determination of the Pareto front at every time step is feasible even for 3 objectives. Furthermore, our proposed preference-based decision making strategy from Section 4.5 successfully respects the DM's preferences in the long-term costs and shows superior results compared to a simpler baseline strategy, especially for 3 objectives. The results of this one-month simulation could be shown to a DM to help him choose his preference values for the building energy management system, while all intrinsic advantages of the method as discussed in Section 4.6 remain.

5.4 Summary

In this section, we apply the dynamic MOO methods developed in Chapter 4 to the standard microgrid model from Chapter 2.

We analyze the different combinations of normalization schemes and metrics from Section 4.4 in a 1-year simulation of the microgrid with real-world data for both the intraday and the industry pricing scenarios. The distance-based metric (CUP) showed to be the most stable and especially promising in combination with the fixed normalization scheme for both scenarios.

The preference-based decision making strategy from Section 4.5 as the main contribution of this thesis showed to successfully represent preferences formulated by a DM not only in the selection of a single Pareto solution, but also in the accumulated long-term costs. For 3 objectives, it even outperforms a proposed simpler baseline strategy for the selection of a Pareto solution due to its better handling of steep and nearly degenerate Pareto fronts. The selection of a solution by the preference plane shows to be very reliable and the knee region sizes can be effectively controlled with the design parameter r_{lim}.

6 Conclusions

In this final chapter, we summarize this thesis shortly and put it in a larger context. Afterwards, we finish with a short outlook on possible future directions for multi-objective building energy management.

6.1 Summary

So far, MOO and MPC have rarely been considered in combination. In part, reasons for this are probably that it is hard to derive analytical properties, since the optimization only covers the prediction horizon, but the long-term costs are relevant. And even empirically, large obstacles exist in general. In comparison to single-objective MPC, the computational costs are at least significantly and possibly a lot higher, depending on the number of objectives. This makes MOO in MPC unsuitable for most applications.

However, BEM systems present a first real-world application which is both suitable and promising for the use of MOO in MPC. First, the system dynamics, at least on the secondary level, are slow enough to allow for sampling times of minutes, which offers enough time for the determination of sufficiently dense approximations of the Pareto front for multiple objectives. Second, the objectives in BEM control are diverse and contradicting enough to justify the use of MOO. For example, it is hard to express the building occupants' comfort, the satisfaction with an EV's battery status or the degradation of batteries with all its ecological impacts by monetary terms without losing parts of their meaning. Third, current policies force the need for significant adaption in energy usage and production, as explained in the motivation for this thesis. Thus, enough attention and monetary interest from both the public and industrial sector exist to drive further developments, which also becomes evident in the extensive investigation of this topic throughout current literature.

In this thesis, we have presented a methodological framework for how MOO can systematically be incorporated into MPC and called it *dynamic MOO*.

The main idea is to formulate the OCP in MPC as a multi-objective OCP, i. e. as a MOO problem. As its solution, (an approximation of) the Pareto front is derived and then a solution is automatically chosen, for which different methods are presented.

The optimization problem has to be sufficiently well-behaved to solve the necessary number of different variations quickly enough to determine the Pareto front's approximation within a time step. To this end, we have presented different linear state space models for the most important entities of a medium-sized company building in Chapter 2. In addition, we have made use of reformulation techniques to derive a convex representation of e. g. peak costs in the objective function. We also have proposed models of different complexity for the thermal zones of a building or EV charging stations, with which computational burdens can be lowered by using a hierarchical setup. Pareto optimization could be used at the highest level only, while more complex models follow predetermined aggregated power flows on the lower levels.

In Chapter 3, we have made a small digression to the importance and influence of prediction accuracy in BEM with MPC, since this has not yet been covered sufficiently. Empirical analysis has shown that real-world weather forecasts can already be used successfully to lower peak costs, but that every improvement at the beginning of the prediction horizon would be beneficial.

The main methodological contributions have been introduced in Chapter 4. First, we presented a new algorithm to determine an approximation of the Pareto front more suitable for dynamic MOO, since it is more robust to imperfect extreme points and possibly non-contradicting objectives. For the decision making process, we have presented two main strategies, which we then evaluated in long-term simulations in Chapter 5. The use of fixed metrics in combination with a normalization of the Pareto solutions showed good long-term results. The Euclidean distance-based CUP metric has been the most promising, especially in combination with the proposed fixed normalization scheme. However, its disadvantage is that the balance between objectives cannot be influenced and is hard to anticipate a priori. This is overcome by our second strategy, the knee region approach from Section 4.5. It successfully maps preferences from a DM to long-term costs, as simulations for both 2 and 3 objectives show. Thus, we consider it the superior decision making strategy.

6.2 Future Directions

Conceptually, a key challenge in the future will be to investigate how a DM can be included in the control process. Although the decision making process evidently has to be automatized, the acceptance for such control systems will most likely depend on whether the DM not only has the feeling that his preferences are respected, but that he is still *in control* of the type of decisions being made. This could e. g. be done by presenting the last decisions to him on demand and asking him whether he is satisfied, or if he wants to change the parameters of the decision making process.

On the more technical end, we see two major challenges. First, the appropriate hierarchization and communication between the different levels is a non-trivial problem. The hierarchy possibly includes a digital twin and ends at the lowest level with the real-world actuators and sensors. Modeling differences between levels may lead to unforeseen instabilities which have to be prevented in a systematic way. This leads to the second major technical challenge. So far, the models for BEM systems are usually derived with expert knowledge for the specific building. The design of control schemes, especially in a hierarchical setup, then depends on further expertise from control engineers. However, to successfully establish BEM systems for a wide variety of buildings and users, both the modeling as well as the subsequent control design has to be modularized.

A Appendix: Numerical Results from Simulation Studies

A.1 Electric Vehicle Charging, Section 2.4.5

Table A.1: Total results for the 1-year EV charging simulation study. The numerical values are the same as shown in Figure 2.13.

	MPC/MPC	MPC/RBC	RBC/RBC
Monetary Costs in 1000 €	243.0369	242.2289	293.0400
Avg. Temp Deviation in K	0.0553	0.0553	0.0162
Avg. Charge Satisfact. in %	100.6987	98.9551	110.8549
EV Capacity Degr. in %	5.4059	4.1773	3.4017
Stat. Capacity Degr. in %	0.6613	0.7293	0.0071

A.2 Metric-Based Decision Making, Section 5.3.2

Table A.2: Results for the 1-year simulations with data from 2018 in the *intraday* scenario. Note that these are the complete costs. The minimum possible monetary costs, which have been subtracted for the representation in Figure 5.4, are stated below for $w_{\text{mon}} = 1$, $w_{\text{comf}} \approx 0$.

	J_{mon} in €	J_{comf}
$w_{\text{mon}} = 1$, $w_{\text{comf}} \approx 0$	98341.66	2211587.11
$w_{\text{mon}} = w_{\text{mon}} = 0.5$	209709.19	4932.82
$w_{\text{mon}} = 0.14$, $w_{\text{comf}} = 0.86$	216148.36	438.71
CUP (dynamic)	215593.36	1281.63
CUP (fixed)	214209.20	1110.64
ATN (dynamic)	215480.22	1678.42
ATN (fixed)	213606.31	1869.77
AEP (dynamic)	217274.28	881.78
AEP (fixed)	213570.40	1741.81
$w_{\text{mon}} \approx 0$, $w_{\text{comf}} = 1$	226940.76	35.16

Table A.3: Results for the 1-year simulations with data from 2018 in the *industry* scenario. Note that these are the complete costs. The minimum possible costs, which have been subtracted for the representation in Figure 5.5, are stated below for $w_{\text{mon}} = 1$, $w_{\text{comf}} \approx 0$.

	J_{mon} in €	J_{comf}
$w_{\text{mon}} = 1$, $w_{\text{comf}} \approx 0$	297114.09	1031189.72
$w_{\text{mon}} = w_{\text{mon}} = 0.5$	347226.94	5028.78
$w_{\text{mon}} = 0.26$, $w_{\text{comf}} = 0.74$	351185.20	1153.58
CUP (dynamic)	354854.43	975.78
CUP (fixed)	350899.90	1325.99
ATN (dynamic)	353513.58	1667.77
ATN (fixed)	349152.45	3463.39
AEP (dynamic)	354785.96	948.41
AEP (fixed)	349662.53	4175.14
$w_{\text{mon}} \approx 0$, $w_{\text{comf}} = 1$	377954.87	35.24

A.3 Preference-Based Decision Making, Section 5.3.3

Table A.4: Numerical results from the simulation study in Section 5.3.3 for the simple baseline approach. The results are the same as presented in Figures 5.7 (a) – (c). Note that all values are presented unitless and as one vector for $[J_{\text{mon}}, J_{\text{comf}}, J_{\text{bat}}]$ and the minimum possible values [10866.84, 0.049, 53.73] have been subtracted. $p_{\text{bat}} = 50$ applies for all settings.

	$p_{\text{comf}} = 25$	$p_{\text{comf}} = 50$
$p_{\text{mon}} = 25$	[59.13, 4007.62, 109.43]	[2463.87, 3.020, 54.5]
$p_{\text{mon}} = 50$	[69.79, 3960.26, 104.60]	[942.62, 315.50, 292.75]
$p_{\text{mon}} = 75$	[60.38, 4033.94, 88.68]	[1018.12, 183.82, 334.03]
$p_{\text{mon}} = 100$	[56.68, 4040.14, 79.14]	[1077.26, 134.70, 342.53]

	$p_{\text{comf}} = 75$	$p_{\text{comf}} = 100$
$p_{\text{mon}} = 25$	[2519.38, 4.73, 24.59]	[2543.40, 2.10, 34.13]
$p_{\text{mon}} = 50$	[1336.79, 57.04, 264.52]	[1233.47, 87.13, 298.36]
$p_{\text{mon}} = 75$	[957.82, 254.47, 356.61]	[1407.25, 57.16, 286.11]
$p_{\text{mon}} = 100$	[1028.29, 172.83, 370.16]	[973.59, 252.07, 387.56]

Table A.5: Numerical results from the simulation study in Section 5.3.3 for the simple baseline approach with prior limitation to the knee region. The results are the same as presented in Figures 5.7 (d) – (f). Note that all values are presented unitless and as one vector for $[J_{\text{mon}}, J_{\text{comf}}, J_{\text{bat}}]$ and the minimum possible values [10866.84, 0.049, 53.73] have been subtracted. $p_{\text{bat}} = 50$ applies for all settings.

	$p_{\text{comf}} = 25$	$p_{\text{comf}} = 50$
$p_{\text{mon}} = 25$	[1090.24, 261.50, 19.69]	[1967.86, 17.52, 4.99]
$p_{\text{mon}} = 50$	[1102.22, 271.12, 13.65]	[1215.26, 77.65, 75.30]
$p_{\text{mon}} = 75$	[1111.35, 259.55, 7.39]	[1257.98, 63.57, 78.01]
$p_{\text{mon}} = 100$	[1127.13, 230.96, 3.52]	[1313.43, 54.59, 79.34]
	$p_{\text{comf}} = 75$	$p_{\text{comf}} = 100$
$p_{\text{mon}} = 25$	[1938.58, 23.12, 4.65]	[1936.68, 25.97, 4.90]
$p_{\text{mon}} = 50$	[1451.70, 38.63, 66.44]	[1389.81, 45.17, 76.72]
$p_{\text{mon}} = 75$	[1238.53, 70.54, 82.72]	[1461.27, 38.51, 71.79]
$p_{\text{mon}} = 100$	[1260.10, 63.04, 84.33]	[1242.50, 70.82, 86.49]

Table A.6: Numerical results from the simulation study in Section 5.3.3 for our proposed approach. The results are the same as presented in Figure 5.8. Note that all values are presented unitless and as one vector for $[J_{\text{mon}}, J_{\text{comf}}, J_{\text{bat}}]$ and the minimum possible values [10866.84, 0.049, 53.73] have been subtracted. $p_{\text{bat}} = 50$ applies for all settings.

	$p_{\text{comf}} = 25$	$p_{\text{comf}} = 50$
$p_{\text{mon}} = 25$	[1360.69, 55.79, 3.86]	[1664.16, 25.25, 4.92]
$p_{\text{mon}} = 50$	[1117.64, 172.63, 6.61]	[1338.79, 53.60, 8.41]
$p_{\text{mon}} = 75$	[1063.37, 218.72, 8.87]	[1193.50, 91.22, 8.76]
$p_{\text{mon}} = 100$	[1050.14, 222.33, 9.32]	[1103.01, 177.78, 8.05]
	$p_{\text{comf}} = 75$	$p_{\text{comf}} = 100$
$p_{\text{mon}} = 25$	[1744.27, 17.76, 6.16]	[1835.29, 13.23, 9.79]
$p_{\text{mon}} = 50$	[1489.06, 33.99, 8.49]	[1639.04, 24.56, 8.52]
$p_{\text{mon}} = 75$	[1331.20, 52.23, 11.75]	[1433.75, 39.41, 12.44]
$p_{\text{mon}} = 100$	[1225.23, 81.69, 8.79]	[1328.93, 51.88, 13.18]

List of Own Publications

[S1] T. Schmitt, J. Engel, T. Rodemann, and J. Adamy. Application of Pareto optimization in an economic model predictive controlled microgrid. In *2020 28th Mediterranean Conference on Control and Automation (MED)*, pages 868–874. IEEE, 2020.

[S2] T. Schmitt and B. Ritter. Data-based identifiability and observability assessment for nonlinear control systems using the profile likelihood method. In *21th IFAC World Congress 2020*, 2020.

[S3] T. Schmitt, T. Rodemann, and J. Adamy. Multi-objective model predictive control for microgrids. *at - Automatisierungstechnik*, 68(8):687 – 702, 2020.

[S4] T. Schmitt, J. Engel, M. Hoffmann, and T. Rodemann. PARODIS: One MPC framework to control them all. Almost. In *2021 IEEE Conference on Control Technology and Applications (CCTA)*, 2021.

[S5] T. Schmitt, T. Rodemann, and J. Adamy. The cost of photovoltaic forecasting errors in microgrid control with peak pricing. *Energies*, 14(9), 2021.

[S6] T. Schmitt, T. Rodemann, and J. Adamy. Application of Pareto frontiers in an economic model predictive controlled microgrid. In *GMA Fachausschuss 1.40 Systemtheorie und Regelungstechnik*, Anif, Österreich, September 2019. Presentation on 23.09.2019.

[S7] T. Schmitt, T. Rodemann, and J. Adamy. Automatized decision making in multi-objective MPC with preferences. In *GMA Fachausschuss 1.40 Systemtheorie und Regelungstechnik*, Anif, Österreich, September 2021. Presentation on 20.09.2021.

[S8] T. Schmitt, M. Hoffmann, T. Rodemann, and J. Adamy. Incorporating human preferences in decision making for dynamic multi-objective optimization in model predictive control. *Inventions*, 7(3), 2022.

[S9] J. Engel, T. Schmitt, T. Rodemann, and J. Adamy. Hierarchical economic model predictive control approach for a building energy management system with scenario-driven EV charging. *IEEE Transactions on Smart Grid*, 13(4):3082–3093, 2022.

[S10] M. Hoffmann and T. Schmitt. I'll tell you what I want: Categorization of Pareto fronts for better preference inclusion. In *2022 18th IFAC Workshop on Control Applications of Optimization*. IFAC, 2022. *Accepted.*

Bibliography

[1] A. Afram and F. Janabi-Sharifi. Theory and applications of HVAC control systems – a review of model predictive control (MPC). *Building and Environment*, 72:343–355, 2014.

[2] A. Agüera-Pérez, J. C. Palomares-Salas, J. J. González de la Rosa, and O. Florencias-Oliveros. Weather forecasts for microgrid energy management: Review, discussion and recommendations. *Applied Energy*, 228:265 – 278, 2018.

[3] A. Ahmadian, M. Sedghi, A. Elkamel, M. Fowler, and M. Aliakbar Golkar. Plug-in electric vehicle batteries degradation modeling for smart grid studies: Review, assessment and conceptual framework. *Renewable and Sustainable Energy Reviews*, 81(2):2609–2624, 2018.

[4] C. Aichberger and G. Jungmeier. Environmental life cycle impacts of automotive batteries based on a literature review. *Energies*, 13(23):6345, Jan. 2020.

[5] R. Amrit, J. B. Rawlings, and D. Angeli. Economic optimization using model predictive control with a terminal cost. *Annual Reviews in Control*, 35(2):178–186, 2011.

[6] D. Angeli, R. Amrit, and J. B. Rawlings. On average performance and stability of economic model predictive control. *IEEE transactions on automatic control*, 57(7):1615–1626, 2012.

[7] F. Ascione, N. Bianco, C. D. Stasio, G. M. Mauro, and G. P. Vanoli. CASA, cost-optimal analysis by multi-objective optimisation and artificial neural networks: A new framework for the robust assessment of cost-optimal energy retrofit, feasible for any building. *Energy and Buildings*, 146:200 – 219, 2017.

[8] R. Azzouz, S. Bechikh, and L. Ben Said. *Dynamic Multi-objective Optimization Using Evolutionary Algorithms: A Survey*, pages 31–70. Springer International Publishing, Cham, 2017.

[9] D. A. Babayev. Piece-wise linear approximation of functions of two variables. *Journal of Heuristics*, 2(4):313–320, 1997.

[10] J. Barreiro-Gomez, C. Ocampo-Martinez, and N. Quijano. Evolutionary game-based dynamical tuning for multi-objective model predictive control. In *Developments in model-based optimization and control*, pages 115–138. Springer, 2015.

[11] F. A. Bayer, M. Lorenzen, M. A. Müller, and F. Allgöwer. Improving performance in robust economic MPC using stochastic information. *IFAC-PapersOnLine*, 48(23):410 – 415, 2015. 5th IFAC Conference on Nonlinear Model Predictive Control NMPC 2015.

[12] F. A. Bayer, M. Lorenzen, M. A. Müller, and F. Allgöwer. Robust economic model predictive control using stochastic information. *Automatica*, 74:151 – 161, 2016.

[13] F. A. Bayer, M. A. Müller, and F. Allgöwer. Tube-based robust economic model predictive control. *Journal of Process Control*, 24(8):1237 – 1246, 2014. Economic nonlinear model predictive control.

[14] S. Bechikh, L. B. Said, and K. Ghédira. Searching for knee regions of the Pareto front using mobile reference points. *Soft Computing*, 15(9):1807–1823, 2011.

[15] A. Bemporad and D. M. de la Peña. Multiobjective model predictive control. *Automatica*, 45(12):2823–2830, 2009.

[16] D. Bertsimas and M. Sim. The price of robustness. *Operations research*, 52(1):35–53, 2004.

[17] K. S. Bhattacharjee, H. K. Singh, and T. Ray. A study on performance metrics to identify solutions of interest from a trade-off set. In *Australasian conference on artificial life and computational intelligence*, pages 66–77. Springer, 2016.

[18] K. S. Bhattacharjee, H. K. Singh, M. Ryan, and T. Ray. Bridging the gap: Many-objective optimization and informed decision-making. *IEEE Transactions on Evolutionary Computation*, 21(5):813–820, 2017.

[19] J. Bisschop. *AIMMS optimization modeling*. Lulu.com, 2006.

[20] BMVI. Förderrichtlinie Elektromobilität vom 14. Dezember 2020. `https://www.bundesanzeiger.de/pub/publication/`

7BgfAWccBSjmOKWHcLw/content/7BgfAWccBSjmOKWHcLw/BAnz%20AT%2024.12.2020%20B3.pdf, 2020. Accessed on 22.11.2021.

[21] BMWi. Energieeffizienzstrategie Gebäude (Langfassung). https://www.bmwi.de/Redaktion/DE/Publikationen/Energie/energieeffizienzstrategie-gebaeude.html, 2015. Accessed on 22.11.2021.

[22] G. Box. Robustness in the strategy of scientific model building. In R. L. LAUNER and G. N. WILKINSON, editors, *Robustness in Statistics*, pages 201–236. Academic Press, 1979.

[23] S. Boyd and L. Vandenberghe. *Convex optimization*. Cambridge university press, 2004.

[24] J. Branke, K. Deb, H. Dierolf, and M. Osswald. Finding knees in multi-objective optimization. In *International conference on parallel problem solving from nature*, pages 722–731. Springer, 2004.

[25] M. Braun, P. Shukla, and H. Schmeck. Angle-based preference models in multi-objective optimization. In H. Trautmann, G. Rudolph, K. Klamroth, O. Schütze, M. Wiecek, Y. Jin, and C. Grimme, editors, *Evolutionary Multi-Criterion Optimization*, pages 88–102, Cham, 2017. Springer International Publishing.

[26] G. Bruni, S. Cordiner, V. Mulone, V. Rocco, and F. Spagnolo. A study on the energy management in domestic micro-grids based on model predictive control strategies. *Energy Conversion and Management*, 102:50–58, 2015. Clean, Efficient, Affordable and Reliable Energy for a Sustainable Future.

[27] J. Cai, D. Kim, R. Jaramillo, J. E. Braun, and J. Hu. A general multi-agent control approach for building energy system optimization. *Energy and Buildings*, 127:337–351, 2016.

[28] E. F. Camacho and C. B. Alba. *Model predictive control*. Springer science & business media, 2013.

[29] J. Cigler, S. Prívara, Z. Váňa, E. Žáčeková, and L. Ferkl. Optimization of predicted mean vote index within model predictive control framework: Computationally tractable solution. *Energy and Buildings*, 52:39–49, 2012.

[30] V. N. Coelho, M. Weiss Cohen, I. M. Coelho, N. Liu, and F. G. Guimarães. Multi-agent systems applied for energy systems integra-

tion: State-of-the-art applications and trends in microgrids. *Applied Energy*, 187:820–832, 2017.

[31] I. Das. On characterizing the "knee" of the Pareto curve based on normal-boundary intersection. *Structural optimization*, 18(2-3):107–115, 1999.

[32] I. Das and J. E. Dennis. A closer look at drawbacks of minimizing weighted sums of objectives for Pareto set generation in multicriteria optimization problems. *Structural optimization*, 14(1):63–69, 1997.

[33] I. Das and J. E. Dennis. Normal-boundary intersection: A new method for generating the pareto surface in nonlinear multicriteria optimization problems. *SIAM journal on optimization*, 8(3):631–657, 1998.

[34] D. De Vito and R. Scattolini. A receding horizon approach to the multiobjective control problem. In *2007 46th IEEE Conference on Decision and Control*, pages 6029–6034. IEEE, 2007.

[35] K. Deb and S. Gupta. Understanding knee points in bicriteria problems and their implications as preferred solution principles. *Engineering optimization*, 43(11):1175–1204, 2011.

[36] K. Deb, K. Miettinen, and D. Sharma. A hybrid integrated multi-objective optimization procedure for estimating nadir point. In *International conference on evolutionary multi-criterion optimization*, pages 569–583. Springer, 2009.

[37] Z. Dong and D. Angeli. Tube-based robust economic model predictive control on dissipative systems with generalized optimal regimes of operation. In *2018 IEEE Conference on Decision and Control (CDC)*, pages 4309–4314. IEEE, 2018.

[38] J. Drgoňa, J. Arroyo, I. Cupeiro Figueroa, D. Blum, K. Arendt, D. Kim, E. P. Ollé, J. Oravec, M. Wetter, D. L. Vrabie, and L. Helsen. All you need to know about model predictive control for buildings. *Annual Reviews in Control*, 50:190 – 232, 2020.

[39] J. Engel. Integration of electric vehicles into a model predictive control building energy system. Master's thesis. Technische Universität Darmstadt, 2020.

[40] V. Exadaktylos and C. J. Taylor. Multi-objective performance optimi-

sation for model predictive control by goal attainment. *International Journal of Control*, 83(7):1374–1386, 2010.

[41] M. Farina and P. Amato. A fuzzy definition of "optimality" for many-criteria optimization problems. *IEEE Transactions on Systems, Man, and Cybernetics - Part A: Systems and Humans*, 34(3):315–326, 2004.

[42] A. H. Fathima and K. Palanisamy. Optimization in microgrids with hybrid energy systems – a review. *Renewable and Sustainable Energy Reviews*, 45:431–446, 2015.

[43] T. Faulwasser, L. Grüne, and M. A. Müller. Economic nonlinear model predictive control. *Foundations and Trends® in Systems and Control*, 5(1):1–98, 2018.

[44] A. Ferramosca, J. B. Rawlings, D. Limon, and E. F. Camacho. Economic MPC for a changing economic criterion. In *49th IEEE Conference on Decision and Control (CDC)*, pages 6131–6136, Dec 2010.

[45] F. García and C. Bordons. Optimal economic dispatch for renewable energy microgrids with hybrid storage using model predictive control. In *IECON 2013 - 39th Annual Conference of the IEEE Industrial Electronics Society*, pages 7932–7937, Nov 2013.

[46] K. Garifi, K. Baker, B. Touri, and D. Christensen. Stochastic model predictive control for demand response in a home energy management system. In *2018 IEEE Power Energy Society General Meeting (PESGM)*, pages 1–5, 2018.

[47] J. L. Garriga and M. Soroush. Model predictive control tuning methods: A review. *Industrial & Engineering Chemistry Research*, 49(8):3505–3515, 2010.

[48] F. Gembicki and Y. Haimes. Approach to performance and sensitivity multiobjective optimization: The goal attainment method. *IEEE Transactions on Automatic Control*, 20(6):769–771, Dec. 1975.

[49] A. Ghane-Kanafi and E. Khorram. A new scalarization method for finding the efficient frontier in non-convex multi-objective problems. *Applied Mathematical Modelling*, 39(23):7483–7498, Dec. 2015.

[50] A. Ghosh and S. Dehuri. Evolutionary algorithms for multi-criterion

optimization: A survey. *International Journal of Computing & Information Sciences*, 2(1):38, 2004.

[51] D. Görges and S. Liu. Energy management in smart grids with electric vehicles based on pricing. *IFAC Proceedings Volumes*, 46(27):182–189, 2013.

[52] L. Grüne. Economic receding horizon control without terminal constraints. *Automatica*, 49(3):725–734, 2013.

[53] L. Grüne and M. Stieler. Performance guarantees for multiobjective model predictive control. In *2017 IEEE 56th Annual Conference on Decision and Control (CDC)*, pages 5545–5550. IEEE, 2017.

[54] L. Grüne and M. Stieler. Multiobjective model predictive control for stabilizing cost criteria. *Discrete & Continuous Dynamical Systems-B*, 24(8):3905, 2019.

[55] Gurobi Optimization, LLC. Gurobi Optimizer Reference Manual. `https://www.gurobi.com`, 2021.

[56] M. K. Hoffmann. Pareto optimization in model predictive control: Finding trade-offs for microgrids. Master's thesis. Technische Universität Darmstadt, 2020.

[57] A. Hooshmand, B. Asghari, and R. Sharma. A novel cost-aware multi-objective energy management method for microgrids. In *2013 IEEE PES Innovative Smart Grid Technologies Conference (ISGT)*, pages 1–6. IEEE, 2013.

[58] M. Hosseinzadeh and F. R. Salmasi. Robust optimal power management system for a hybrid AC/DC micro-grid. *IEEE Transactions on Sustainable Energy*, 6(3):675–687, 2015.

[59] J. Hu, G. Yu, J. Zheng, and J. Zou. A preference-based multi-objective evolutionary algorithm using preference selection radius. *Soft Computing*, 21(17):5025–5051, 2017.

[60] Y. Hua, Q. Liu, K. Hao, and Y. Jin. A survey of evolutionary algorithms for multi-objective optimization problems with irregular Pareto fronts. *IEEE/CAA Journal of Automatica Sinica*, 8(2):303–318, 2021.

[61] G. Huang. Model predictive control of VAV zone thermal systems

concerning bi-linearity and gain nonlinearity. *Control Engineering Practice*, 19(7):700–710, 2011.

[62] C.-L. Hwang and K. Yoon. *Multiple Attribute Decision Making: Methods and Applications*. Lecture Notes in Economics and Mathematical Systems 186. Springer-Verlag Berlin Heidelberg, 1st edition, 1981.

[63] P. Icha and G. Kuhs. Entwicklung der spezifischen Kohlendioxid-Emissionen des deutschen Strommix in den Jahren 1990-2019. techreport, Umweltbundesamt, Feb. 2020.

[64] L. Igualada, C. Corchero, M. Cruz-Zambrano, and F. J. Heredia. Optimal energy management for a residential microgrid including a vehicle-to-grid system. *IEEE Transactions on Smart Grid*, 5(4):2163–2172, 2014.

[65] Z. Ji, X. Huang, C. Xu, and H. Sun. Accelerated model predictive control for electric vehicle integrated microgrid energy management: A hybrid robust and stochastic approach. *Energies*, 9(11), 2016.

[66] Y. Jin and B. Sendhoff. Incorporation of fuzzy preferences into evolutionary multiobjective optimization. In *GECCO*, volume 2, page 683, 2002.

[67] C. Ju, P. Wang, L. Goel, and Y. Xu. A two-layer energy management system for microgrids with hybrid energy storage considering degradation costs. *IEEE Transactions on Smart Grid*, 9(6):6047–6057, Nov 2018.

[68] F. Kennel, D. Görges, and S. Liu. Energy management for smart grids with electric vehicles based on hierarchical MPC. *IEEE Transactions on Industrial Informatics*, 9(3):1528–1537, 2013.

[69] A. A. Khan, M. Naeem, M. Iqbal, S. Qaisar, and A. Anpalagan. A compendium of optimization objectives, constraints, tools and algorithms for energy management in microgrids. *Renewable and Sustainable Energy Reviews*, 58:1664 – 1683, 2016.

[70] A. Khodaei, S. Bahramirad, and M. Shahidehpour. Microgrid planning under uncertainty. *IEEE Transactions on Power Systems*, 30(5):2417–2425, 2015.

[71] H. Kishan. *Differential Calculus*. Atlantic Publishers & Distributors (P) Ltd., 2007.

[72] C. D. Korkas, S. Baldi, I. Michailidis, and E. B. Kosmatopoulos. Occupancy-based demand response and thermal comfort optimization in microgrids with renewable energy sources and energy storage. *Applied Energy*, 163:93–104, 2016.

[73] P. Kou, D. Liang, L. Gao, and F. Gao. Stochastic coordination of plug-in electric vehicles and wind turbines in microgrid: A model predictive control approach. *IEEE Transactions on Smart Grid*, 7(3):1537–1551, may 2016.

[74] D. Lazos, A. B. Sproul, and M. Kay. Optimisation of energy management in commercial buildings with weather forecasting inputs: A review. *Renewable and Sustainable Energy Reviews*, 39:587–603, 2014.

[75] Z. J. Lee, T. Li, and S. H. Low. ACN-Data: Analysis and applications of an open EV charging dataset. *e-Energy 2019 - Proceedings of the 10th ACM International Conference on Future Energy Systems*, pages 139–149, 2019.

[76] V. Lenzi, A. Ulbig, and G. Andersson. Impacts of forecast accuracy on grid integration of renewable energy sources. In *2013 IEEE Grenoble Conference*, pages 1–6, 2013.

[77] W. Li, R. Wang, T. Zhang, M. Ming, and K. Li. Reinvestigation of evolutionary many-objective optimization: Focus on the Pareto knee front. *Information Sciences*, 522:193–213, 2020.

[78] X. Li and A. Malkawi. Multi-objective optimization for thermal mass model predictive control in small and medium size commercial buildings under summer weather conditions. *Energy*, 112:1194–1206, 2016.

[79] Y. Li, S. Liao, and G. Liu. Thermo-economic multi-objective optimization for a solar-dish Brayton system using NSGA-II and decision making. *International Journal of Electrical Power & Energy Systems*, 64:167–175, 2015.

[80] J. Löfberg. Approximations of closed-loop minimax MPC. In *42nd IEEE International Conference on Decision and Control (IEEE Cat. No. 03CH37475)*, volume 2, pages 1438–1442. IEEE, 2003.

[81] J. Löfberg. YALMIP : A toolbox for modeling and optimization

in MATLAB. In *In Proceedings of the CACSD Conference*, Taipei, Taiwan, 2004.

[82] J. Ma, J. Qin, T. Salsbury, and P. Xu. Demand reduction in building energy systems based on economic model predictive control. *Chemical Engineering Science*, 67(1):92–100, 2012. Dynamics, Control and Optimization of Energy Systems.

[83] Y. Ma, J. Matuško, and F. Borrelli. Stochastic model predictive control for building HVAC systems: Complexity and conservatism. *IEEE Transactions on Control Systems Technology*, 23(1):101–116, 2015.

[84] M. Maasoumy, M. Razmara, M. Shahbakhti, and A. S. Vincentelli. Handling model uncertainty in model predictive control for energy efficient buildings. *Energy and Buildings*, 77:377–392, 2014.

[85] M. Maasoumy and A. Sangiovanni-Vincentelli. Optimal control of building HVAC systems in the presence of imperfect predictions. In *Dynamic Systems and Control Conference*, volume 45301, pages 257–266. American Society of Mechanical Engineers, 2012.

[86] R. T. Marler and J. S. Arora. Survey of multi-objective optimization methods for engineering. *Structural and multidisciplinary optimization*, 26(6):369–395, 2004.

[87] R. T. Marler and J. S. Arora. Function-transformation methods for multi-objective optimization. *Engineering Optimization*, 37(6):551–570, 2005.

[88] S. Mazzola, C. Vergara, M. Astolfi, V. Li, I. Perez-Arriaga, and E. Macchi. Assessing the value of forecast-based dispatch in the operation of off-grid rural microgrids. *Renewable Energy*, 108:116 – 125, 2017.

[89] L. Meng, E. R. Sanseverino, A. Luna, T. Dragicevic, J. C. Vasquez, and J. M. Guerrero. Microgrid supervisory controllers and energy management systems: A literature review. *Renewable and Sustainable Energy Reviews*, 60:1263–1273, 2016.

[90] A. Messac, A. Ismail-Yahaya, and C. A. Mattson. The normalized normal constraint method for generating the Pareto frontier. *Structural and multidisciplinary optimization*, 25(2):86–98, 2003.

[91] K. Miettinen. *Nonlinear multiobjective optimization*, volume 12. Springer Science & Business Media, 1999.

[92] J. Molina, L. V. Santana, A. G. Hernández-Díaz, C. A. Coello Coello, and R. Caballero. g-dominance: Reference point based dominance for multiobjective metaheuristics. *European Journal of Operational Research*, 197(2):685–692, 2009.

[93] P.-D. Moroşan, R. Bourdais, D. Dumur, and J. Buisson. Building temperature regulation using a distributed model predictive control. *Energy and Buildings*, 42(9):1445–1452, 2010.

[94] R. d. S. Motta, S. M. Afonso, and P. R. Lyra. A modified NBI and NC method for the solution of N-multiobjective optimization problems. *Structural and Multidisciplinary Optimization*, 46(2):239–259, 2012.

[95] W. Mrozik, M. A. Rajaeifar, O. Heidrich, and P. Christensen. Environmental impacts, pollution sources and pathways of spent lithium-ion batteries. *Energy & Environmental Science*, Oct. 2021.

[96] D. Mueller-Gritschneder, H. Graeb, and U. Schlichtmann. A successive approach to compute the bounded Pareto front of practical multiobjective optimization problems. *SIAM Journal on Optimization*, 20(2):915–934, 2009.

[97] M. A. Müller. *Distributed and economic model predictive control: beyond setpoint stabilization*. PhD thesis, Universität Stuttgart, 2014.

[98] M. A. Müller, D. Angeli, and F. Allgöwer. On necessity and robustness of dissipativity in economic model predictive control. *IEEE Transactions on Automatic Control*, 60(6):1671–1676, 2015.

[99] M. A. Müller, D. Angeli, and F. Allgöwer. Transient average constraints in economic model predictive control. *Automatica*, 50(11):2943 – 2950, 2014.

[100] A.-T. Nguyen, S. Reiter, and P. Rigo. A review on simulation-based optimization methods applied to building performance analysis. *Applied Energy*, 113:1043–1058, 2014.

[101] NPM. Ergebnisbericht der Nationalen Plattform Zukunft der Mobilität – Ergebnisse aus drei Jahren NPM (2018-2021). `https://www.plattform-zukunft-mobilitaet.de/2download/mobilitaet-von-morgen-ganzheitlich-gestalten-ergebnisse%`

2Daus-drei-jahren-npm-2018-2021/, 2021. Accessed on 22.11.2021.

[102] P. F. Odgaard, L. F. Larsen, R. Wisniewski, and T. G. Hovgaard. On using Pareto optimality to tune a linear model predictive controller for wind turbines. *Renewable Energy*, 87:884–891, 2016.

[103] Y. Ogata and T. Namerikawa. Energy management of smart home by model predictive control based on EV state prediction. *2019 12th Asian Control Conference, ASCC 2019*, pages 410–415, 2019.

[104] L. Olatomiwa, S. Mekhilef, M. Ismail, and M. Moghavvemi. Energy management strategies in hybrid renewable energy systems: A review. *Renewable and Sustainable Energy Reviews*, 62:821–835, 2016.

[105] F. Oldewurtel, C. N. Jones, A. Parisio, and M. Morari. Stochastic model predictive control for building climate control. *IEEE Transactions on Control Systems Technology*, 22(3):1198–1205, 2014.

[106] F. Oldewurtel, A. Parisio, C. N. Jones, D. Gyalistras, M. Gwerder, V. Stauch, B. Lehmann, and M. Morari. Use of model predictive control and weather forecasts for energy efficient building climate control. *Energy and Buildings*, 45:15–27, 2012.

[107] D. E. Olivares, J. D. Lara, C. A. Cañizares, and M. Kazerani. Stochastic-predictive energy management system for isolated microgrids. *IEEE Transactions on Smart Grid*, 6(6):2681–2693, 2015.

[108] D. E. Olivares, A. Mehrizi-Sani, A. H. Etemadi, C. A. Cañizares, R. Iravani, M. Kazerani, A. H. Hajimiragha, O. Gomis-Bellmunt, M. Saeedifard, R. Palma-Behnke, et al. Trends in microgrid control. *IEEE Transactions on smart grid*, 5(4):1905–1919, 2014.

[109] A. Pascoletti and P. Serafini. Scalarizing vector optimization problems. *Journal of Optimization Theory and Applications*, 42(4):499–524, Apr. 1984.

[110] N. R. Patel, J. B. Rawlings, M. J. Wenzel, and R. D. Turney. Design and application of distributed economic model predictive control for large-scale building temperature regulation. *International High Performance Buildings Conference*, 2016.

[111] F. Petrakopoulou, A. Robinson, and M. Olmeda-Delgado. Impact of climate change on fossil fuel power-plant efficiency and water use. *Journal of Cleaner Production*, 273:122816, 2020.

[112] L. Rachmawati and D. Srinivasan. Multiobjective evolutionary algorithm with controllable focus on the knees of the Pareto front. *IEEE Transactions on Evolutionary Computation*, 13(4):810–824, 2009.

[113] C. Raquel and X. Yao. Dynamic multi-objective optimization: A survey of the state-of-the-art. In *Evolutionary computation for dynamic optimization problems*, pages 85–106. Springer, 2013.

[114] J. B. Rawlings, D. Angeli, and C. N. Bates. Fundamentals of economic model predictive control. In *CDC*, pages 3851–3861, 2012.

[115] J. B. Rawlings, D. Q. Mayne, and M. Diehl. *Model Predictive Control: Theory, Computation, and Design*. Nob Hill Publishing, 2017.

[116] J. B. Rawlings, N. R. Patel, M. J. Risbeck, C. T. Maravelias, M. J. Wenzel, and R. D. Turney. Economic MPC and real-time decision making with application to large-scale HVAC energy systems. *Computers & Chemical Engineering*, 114:89 – 98, 2018. FOCAPO/CPC 2017.

[117] J. Rehrl and M. Horn. Temperature control for HVAC systems based on exact linearization and model predictive control. In *2011 IEEE International Conference on Control Applications (CCA)*, pages 1119–1124, Sep. 2011.

[118] J. Reynolds, Y. Rezgui, A. Kwan, and S. Piriou. A zone-level, building energy optimisation combining an artificial neural network, a genetic algorithm, and model predictive control. *Energy*, 151:729 – 739, 2018.

[119] M. J. Risbeck, C. T. Maravelias, J. B. Rawlings, and R. D. Turney. A mixed-integer linear programming model for real-time cost optimization of building heating, ventilation, and air conditioning equipment. *Energy and Buildings*, 142:220 – 235, 2017.

[120] D. Romero-Quete and C. A. Cañizares. An affine arithmetic-based energy management system for isolated microgrids. *IEEE Transactions on Smart Grid*, 10(3):2989–2998, 2019.

[121] N. Ryu and S. Min. Multiobjective optimization with an adaptive weight determination scheme using the concept of hyperplane. *International Journal for Numerical Methods in Engineering*, 118(6):303–319, 2019.

[122] H. Scherer, M. Pasamontes, J. Guzmán, J. Álvarez, E. Camponogara, and J. Normey-Rico. Efficient building energy management using

distributed model predictive control. *Journal of Process Control*, 24(6):740–749, 2014. Energy Efficient Buildings Special Issue.

[123] S. Schlömer, T. Bruckner, L. Fulton, E. Hertwich, A. McKinnon, D. Perczyk, J. Roy, R. Schaeffer, R. Sims, P. Smith, et al. Annex III: Technology-specific cost and performance parameters. *Climate change*, pages 1329–1356, 2014.

[124] I. Sharma, J. Dong, A. A. Malikopoulos, M. Street, J. Ostrowski, T. Kuruganti, and R. Jackson. A modeling framework for optimal energy management of a residential building. *Energy and Buildings*, 130:55–63, 2016.

[125] E. Skoplaki and J. Palyvos. On the temperature dependence of photovoltaic module electrical performance: A review of efficiency/power correlations. *Solar Energy*, 83(5):614–624, 2009.

[126] B. V. Solanki, K. Bhattacharya, and C. A. Cañizares. A sustainable energy management system for isolated microgrids. *IEEE Transactions on Sustainable Energy*, 8(4):1507–1517, 2017.

[127] V. Srinivasan and A. D. Shocker. Linear programming techniques for multidimensional analysis of preferences. *Psychometrika*, 38(3):337–369, 1973.

[128] W. Stadler. Fundamentals of multicriteria optimization. In *Multicriteria Optimization in Engineering and in the Sciences*, pages 1–25. Springer, 1988.

[129] M. Tavakoli, F. Shokridehaki, M. Marzband, R. Godina, and E. Pouresmaeil. A two stage hierarchical control approach for the optimal energy management in commercial building microgrids based on local wind power and pevs. *Sustainable Cities and Society*, 41:332–340, 2018.

[130] D. Thomas, O. Deblecker, and C. S. Ioakimidis. Optimal operation of an energy management system for a grid-connected smart building considering photovoltaics' uncertainty and stochastic electric vehicles' driving schedule. *Applied Energy*, 210:1188–1206, 2018.

[131] L. Thu Bui and S. Alam. *Multi-Objective Optimization in Computational Intelligence: Theory and Practice: Theory and Practice*. IGI global, 2008.

[132] C. R. Touretzky and M. Baldea. Integrating scheduling and control for economic MPC of buildings with energy storage. *Journal of Process Control*, 24(8):1292–1300, 2014. Economic nonlinear model predictive control.

[133] J. Vasilj, S. Gros, D. Jakus, and M. Zanon. Day-ahead scheduling and real-time economic MPC of CHP unit in microgrid with smart buildings. *IEEE Transactions on Smart Grid*, 10(2):1992–2001, 2019.

[134] P. Velarde, J. M. Maestre, C. Ocampo-Martínez, and C. Bordons. Application of robust model predictive control to a renewable hydrogen-based microgrid. In *2016 European Control Conference (ECC)*, pages 1209–1214. IEEE, 2016.

[135] A. Villalón, M. Rivera, Y. Salgueiro, J. Muñoz, T. Dragičević, and F. Blaabjerg. Predictive control for microgrid applications: A review study. *Energies*, 13(10), 2020.

[136] H. Wang, M. Olhofer, and Y. Jin. A mini-review on preference modeling and articulation in multi-objective optimization: current status and challenges. *Complex & Intelligent Systems*, 3(4):233–245, Dec. 2017.

[137] Y. Wang, S. Limmer, M. Olhofer, M. Emmerich, and T. Bäck. Automatic preference based multi-objective evolutionary algorithm on vehicle fleet maintenance scheduling optimization. *Swarm and Evolutionary Computation*, page 100933, 2021.

[138] M. Wetter. GenOpt - A generic optimization program. In *Seventh International IBPSA Conference, Rio de Janeiro*, pages 601–608, 2001.

[139] D. Wu, H. Zeng, C. Lu, and B. Boulet. Two-stage energy management for office buildings with workplace EV charging and renewable energy. *IEEE Transactions on Transportation Electrification*, 3(1):225–237, mar 2017.

[140] B. Xu, A. Oudalov, A. Ulbig, G. Andersson, and D. S. Kirschen. Modeling of lithium-ion battery degradation for cell life assessment. *IEEE Transactions on Smart Grid*, 9(2):1131–1140, 2018.

[141] J.-B. Yang and D.-L. Xu. On the evidential reasoning algorithm for multiple attribute decision analysis under uncertainty. *IEEE*

Transactions on Systems, Man, and Cybernetics-Part A: Systems and Humans, 32(3):289–304, 2002.

[142] S. Yang, M. P. Wan, W. Chen, B. F. Ng, and D. Zhai. An adaptive robust model predictive control for indoor climate optimization and uncertainties handling in buildings. *Building and Environment*, 163:106326, 2019.

[143] G. Yu, Y. Jin, and M. Olhofer. A method for a posteriori identification of knee points based on solution density. In *2018 IEEE Congress on Evolutionary Computation (CEC)*, pages 1–8, 2018.

[144] V. M. Zavala. Real-time optimization strategies for building systems. *Industrial & Engineering Chemistry Research*, 52(9):3137–3150, 2013.

[145] V. M. Zavala and A. Flores-Tlacuahuac. Stability of multiobjective predictive control: A utopia-tracking approach. *Automatica*, 48(10):2627–2632, 2012.

[146] X. Zhang, G. Schildbach, D. Sturzenegger, and M. Morari. Scenario-based MPC for energy-efficient building climate control under weather and occupancy uncertainty. In *2013 European Control Conference (ECC)*, pages 1029–1034, 2013.

[147] Y. Zhang, N. Gatsis, and G. B. Giannakis. Robust energy management for microgrids with high-penetration renewables. *IEEE Transactions on Sustainable Energy*, 4(4):944–953, 2013.

[148] Y. Zhang, B. Liu, T. Zhang, and B. Guo. An intelligent control strategy of battery energy storage system for microgrid energy management under forecast uncertainties. *Int. J. Electrochem. Sci*, 9(8):4190–4204, 2014.

[149] Y. Zhang, R. Wang, T. Zhang, Y. Liu, and B. Guo. Model predictive control-based operation management for a residential microgrid with considering forecast uncertainties and demand response strategies. *IET Generation, Transmission & Distribution*, 10:2367–2378, July 2016.

[150] Q. P. Zheng, J. Wang, and A. L. Liu. Stochastic optimization for unit commitment—A review. *IEEE Transactions on Power Systems*, 30(4):1913–1924, 2015.

[151] M. F. Zia, E. Elbouchikhi, and M. Benbouzid. Microgrids energy

management systems: A critical review on methods, solutions, and prospects. *Applied energy*, 222:1033–1055, 2018.

[152] E. Zitzler, M. Laumanns, and S. Bleuler. A tutorial on evolutionary multiobjective optimization. *Metaheuristics for multiobjective optimisation*, pages 3–37, 2004.

[153] J. Široký, F. Oldewurtel, J. Cigler, and S. Prívara. Experimental analysis of model predictive control for an energy efficient building heating system. *Applied Energy*, 88(9):3079–3087, 2011.